

**Structure-function analysis of Cmu1,
the secreted chorismate mutase from *Ustilago maydis***



DISSERTATION

zur

Erlangung des Doktorgrades

der Naturwissenschaften

(Dr. rer. nat.)

Dem Fachbereich Biologie
der Philipps-Universität Marburg

vorgelegt von

Xiaowei Han

aus Weifang/China

Marburg/Lahn im Oktober 2017

Die Untersuchungen zur vorliegenden Arbeit wurden von Oktober 2013 bis Oktober 2017 unter der Betreuung von Frau Prof. Dr. Regine Kahmann in Marburg am Max-Planck-Institut für terrestrische Mikrobiologie in der Abteilung Organismische Interaktionen durchgeführt.

Vom Fachbereich Biologie der Philipps-Universität Marburg
als Dissertation angenommen am:

Erstgutachter/in: Frau Prof. Dr. Regine Kahmann

Zweitgutachter/in: Herr Dr. Gert Bange

Tag der mündlichen Prüfung:

Declaration

I hereby declare that the dissertation entitled “**Structure-function analysis of Cmu1, the secreted chorismate mutase from *Ustilago maydis***” submitted to the Department of Biology, Philipps-Universität Marburg, is the original and independent work carried out by me under the guidance of the PhD committee, and the dissertation is not formed previously on the basis of any award of Degree, Diploma or other similar titles.

(Place/date)

(Xiaowei Han)

Dedicated to the people who I love and those who love me

(致那些我爱的人和爱我的人)

Contents

Abbreviations	I
Summary	II
Zusammenfassung	III
1. Introduction	1
1.1 Plant-fungus interactions.....	1
1.1.1 Plant innate immune system.....	1
1.1.2 Effectors –a versatile armory of plant associated fungi	4
1.1.3 Structural studies of effectors from plant pathogenic fungi	6
1.2 <i>Ustilago maydis</i> -a model for biotrophic plant pathogen	8
1.2.1 The <i>U. maydis</i> - <i>Zea mays</i> pathosystem	8
1.2.2 The life cycle of <i>U. maydis</i>	8
1.2.3 Effectors of <i>U. maydis</i>	10
1.3 Chorismate mutases.....	12
1.4 Overall structure of Cmu1	14
1.5 Aims of the study.....	15
2. Results	16
2.1 Unique features are revealed from the crystal structure of Cmu1	16
2.1.1 The surface exposed acidic patch is dispensable for the function of Cmu1	16
2.1.2 Disruption of disulfide bond does not impair the function of Cmu1.....	20
2.1.3 The abolishment of fatty acid binding has no effect on the function of Cmu1	23
2.1.4 A long loop region is required for the full function of Cmu1	24
2.2 Biochemical characterization of Cmu1 and selected mutants.....	26
2.2.1 The allosteric site of Cmu1 possesses a novel fold	26
2.2.2 The kinetics of Cmu1 purified from <i>E. coli</i>	27
2.2.3 The CM activity of Cmu1 is not activated by tryptophan	29
2.3 Putative interplay between a secreted chorismate mutase, an isochorismatase and a salicylate hydroxylase in promoting virulence of <i>U. maydis</i>	30
2.3.1 An isochorismatase Um12021 is encoded in <i>U. maydis</i>	31
2.3.2 <i>um12021</i> is not induced during the disease development of <i>U. maydis</i>	32
2.3.3 Cmu1, Shy1 and Um12021 might be functionally redundant	32
2.4 Investigation of the localization of Cmu1 in maize mesophyll cells.....	34
2.4.1 Cmu1 localizes in the cytosol of mesophyll cell	34
2.4.2 Fusion of Cmu1 to a cTP does not complement CL13 Δ cmu1	35
2.5 Interaction partners of Cmu1	36

2.5.1 A secreted maize CM does not interact with Cmu1 in Y2H assay	36
2.5.2 Co-IP-MS analysis identified a maize protein Cmi1 which specifically interacts with Cmu1	38
2.5.3 Cmi1 is likely a pathogenesis related protein	38
2.5.4 Verification of the interaction between Cmi1 and Cmu1	40
2.5.5 Purification of Cmi1 ³³⁻¹⁹⁸ -His ₆	42
2.5.6 Cmi1 inhibits the CM activity of Cmu1	43
2.5.7 Identification of the interaction interface between Cmu1 and Cmi1 via HDX/MS	44
2.5.8 The loop region of Cmu1 is necessary for the interaction with Cmi1	46
3. Discussion	47
3.1 Secreted chorismate mutases - universal enzymes but divergent strategies.....	47
3.2 The N-terminal region of Cmu1	48
3.3 The unique disulfide bond in Cmu1 proteins from smut fungi may not contribute to stability	48
3.4 The regulation of the CM activity of Cmu1	49
3.5 SA signaling targeted by <i>U. maydis</i>	52
3.6 The loop region is essential for the biological activity of Cmu1	53
3.7 Interaction partners of Cmu1	53
3.7.1 Maize CMs	53
3.7.2 The interaction of Cmu1 with Cmi1 is likely to occur in the apoplast.....	55
4. Materials and Methods	60
4.1 Materials	60
4.1.1 Chemicals	60
4.1.2 Buffers	60
4.1.3 Enzymes and antibodies	60
4.1.4 Kits.....	60
4.2 Media and cultivation methods for microbes	61
4.2.1 Media and cultivation of <i>E. coli</i> and <i>A. tumefaciens</i> strains.....	61
4.2.2 Media and cultivation of <i>S. cerevisiae</i> strains	62
4.2.3 Media and cultivation of <i>U. maydis</i> strains	62
4.2.4 Determination of cell density	64
4.3 Strains, oligonucleotides and plasmids	64
4.3.1 <i>E. coli</i> strains	64
4.3.2 <i>A. tumefaciens</i> strains	65
4.3.3 <i>S. cerevisiae</i> strains.....	65
4.3.4 <i>U. maydis</i> strains.....	65

4.3.5 Oligonucleotides.....	67
4.3.6 Plasmids.....	71
4.4 Microbiological methods.....	76
4.4.1 Competent cell preparation and transformation of <i>E. coli</i>	76
4.4.2 Protoplast preparation and transformation of <i>U. maydis</i>	77
4.4.3 Competent cell preparation and transformation of <i>A. tumefaciens</i>	78
4.4.4 Competent cell preparation and transformation of <i>S. cerevisiae</i>	79
4.4.5 Spotting assay for <i>S. cerevisiae</i>	79
4.5 Molecular microbiological methods.....	80
4.5.1 Isolation of nucleic acids.....	80
4.5.2 <i>In vitro</i> modification of nucleic acid.....	81
4.5.3 Separation and detection of nucleic acids.....	84
4.6 Protein methods and biochemical assays.....	87
4.6.1 Protein overexpression in <i>E. coli</i> and purification.....	87
4.6.2 Protein extraction from <i>S. cerevisiae</i>	88
4.6.3 Protein extraction from maize or tobacco.....	88
4.6.4 <i>In vitro</i> pull-down assay.....	89
4.6.5 Co-immunoprecipitation of Cmu1-HA ₃ followed by mass spectrometry.....	89
4.6.6 SDS polyacrylamide gel electrophoresis (SDS-PAGE).....	90
4.6.7 Western blot.....	91
4.6.8 Chorismate mutase assay.....	92
4.7 Plant assays.....	92
4.7.1 <i>Z. mays</i> cultivars.....	92
4.7.2 Cultivation of <i>Z. mays</i>	93
4.7.3 Infection of <i>Z. mays</i> with <i>U. maydis</i>	93
4.7.4 Cultivation of <i>N. benthamiana</i>	93
4.7.5 Infiltration of <i>N. benthamiana</i> with <i>A. tumefaciens</i>	94
4.7.6 Biolistic transformation of maize leave cells.....	94
4.8 Live-cell imaging by laser-scanning confocal microscopy.....	94
4.9 Bioinformatics methods.....	95
References	96
Acknowledgements	111
Curriculum Vitae	112
Appendix	113

Abbreviations

AD	activation domain	mg	milligram
Amp	Ampicillin	min	minute(s)
BD	DNA binding domain	mL	millilitre
bp	base pairs	mRNA	messenger RNA
Cbx	Carboxin	MW	molecular weight
cDNA	complementary DNA	Neo	Geneticin G418
CM	chorismate mutase	ng	nanogram
Co-IP	co-immunoprecipitation	nm	nanometer
cTP	chloroplast transit peptide	N-terminal	amino-terminal
C-terminal	carboxyl-terminal	N-terminus	amino-terminus
ddH ₂ O	double-distilled water	OD ₆₀₀	optical density at 600 nm
DNA	deoxyribonucleic acid	PAGE	polyacrylamide gel electrophoresis
dNTP	deoxyribonucleoside triphosphate	PCR	polymerase chain reaction
dpi	days post infection/infiltration	PEG	polyethylene glycol
DTT	dithiothreitol	<i>ppi</i>	peptidyl-prolyl isomerase gene
e.g.	<i>exempli gratia</i> (for example)	PR	pathogenesis related
EDTA	ethylenediaminetetraacetic acid	qRT-PCR	quantitative reverse transcription PCR
EM	electron microscopy	Rif	Rifampicin
et al.	<i>et alii</i> (and others)	RNA	ribonucleic acid
Fig.	figure	rpm	revolutions per minute
GAPDH	glyceraldehyde 3-phosphate dehydrogenase	SA	salicylic acid
gDNA	genomic DNA	SDS	sodium dodecyl sulfate
H ₂ O ₂	hydrogen peroxide	sfGFP	superfold green fluorescent protein
HA	hemagglutinin	SP	signal peptide
HEPES	4-(2-hydroxyethyl)-1-piperazineethanesulfonic acid	TEMED	tetramethylethylenediamine
His	histidine	Tris	trishydroxymethylaminomethane
hpi	hours post-infection	U	unit (enzyme activity)
Hyg	Hygromycin B	v/v	volume fraction
i.e.	<i>id est</i> (that is)	w/v	mass concentration
IPTG	isopropyl β-d-1-thiogalactopyranoside	WT	wildtype
Kan	Kanamycin	Y2H	yeast two-hybrid
kb	kilobase pairs	μg	microgram
kDa	kilodalton	μL	microlitre
LC-MS/MS	liquid chromatography tandem-mass spectrometry	μm	micrometer
M	molar	μM	micromolar
MES	2-(n-morpholino) ethanesulfonic acid	Δ	deletion

Summary

The basidiomycete fungus *Ustilago maydis* is the causative agent for smut disease of maize (*Zea mays*). More than 400 putative secreted proteins are encoded in the genome of *U. maydis*. The secreted chorismate mutase Cmu1 of *U. maydis* is such a translocated virulence promoting effector. The chorismate mutase activity of Cmu1 in the cytosol is proposed to lower the chorismate levels in the chloroplast where it would serve as precursor for the biosynthesis of the plant defense hormone salicylic acid (SA). The crystal structure of Cmu1 revealed several unique features in comparison to the cytoplasmic chorismate mutase Aro7p of *Saccharomyces cerevisiae*, including a surface exposed acidic patch, a disulfide bond, a putative fatty acid binding site and a loop region.

This thesis shows, that site-directed mutagenesis affecting the acidic patch, the disulfide bond and the fatty acid binding site results in functional mutant proteins that can complement the virulence phenotype of CL13 Δ cmu1 strains. Wildtype Cmu1 protein purified after heterologous expression in *E. coli* followed a Michaelis-Menten kinetic in a chorismase mutase activity assay. Mutations in the fatty acid binding site did not alter the observed kinetic. A *U. maydis* triple mutant of *cmu1*, the isochorismatase coding gene *um12021* and *shy1* encoding a salicylate hydroxylase was reduced in virulence compared to any single or double mutants, suggesting an interplay of three *U. maydis* enzymes in suppressing SA pathway.

By performing immunoprecipitation (IP) of Cmu1 from infected leave tissues followed by mass spectrometry, the maize protein Cmi1 (**C**mu1 **i**nteractor 1) could be identified as an interactor. *In vitro* pull-down experiments confirmed the interaction between Cmu1 and Cmi1. Recombinant Cmi1 inhibited the chorismate mutase activity of Cmu1. The expression of *cmi1* is strongly induced upon the infection of *U. maydis*, indicating that it is likely a pathogenesis related (PR) protein. Hydrogen-Deuterium exchange mass spectrometry (HDX/MS) mapped the interaction interface between Cmu1 and Cmi1, which involved the loop region of Cmu1. Truncation of the loop in Cmu1, which abolished the interaction of Cmu1 with Cmi1, showed only partial complementation of CL13 Δ cmu1 mutants, suggesting that the interaction between Cmu1 and Cmi1 may be relevant for the virulence of *U. maydis*.

Zusammenfassung

Der Brandpilz *Ustilago maydis* gehört zu den Basidiomyceten und ist Erreger des Maisbeulenbrandes in *Zea mays*. Das *U. maydis* Genom kodiert für mehr als 400 sekretierte Effektoren Proteine. Die sekretierte *U. maydis* Chorismatmutase Cmu1 ist solch ein translozier Effektor. Dem Modell zufolge soll die Chorismatmutase Aktivität von Cmu1 im pflanzlichen Zytoplasma dazu führen, dass die Chorismatkonzentration in den Chloroplasten, wo Chorismat zur Synthese des pflanzlichen Abwehrhormons Salizylat (SA) herangezogen würde, gesenkt wird. Die Cmu1 Kristallstruktur zeigt, dass dieser Effektor im Vergleich zur zytoplasmatischen Chorismatmutase Aro7p von *Saccharomyces cerevisiae* besondere Merkmale besitzt: einen exponierten Bereich aus sauren Aminosäuren, eine Disulfidbrücke, eine putative Fettsäurebindestelle und eine Loop-Region. Diese Arbeit zeigt, dass durch zielgerichtete Mutagenese der sauren Oberflächenregion, der Disulfidbrücke und der putativen Fettsäurebindestelle funktionellen Proteine erzeugt wurden, die den Virulenzphänotyp des *U. maydis* Stammes CL13 Δ cmu1 komplementieren konnten. Nach Überexpression in *E. coli* gereinigtes Cmu1 Protein folgte in einem Chorismatmutase Aktivitätstest einer Michaelis-Menten Kinetik. Die Mutation der Fettsäurebindestelle hatte keinen Einfluss auf die Enzymkinetik von Cmu1. Ein *U. maydis* Dreifachdeletionsstamm, in welchem *cmu1*, das für die Isochorismatase codierende Gen *um12021* und *shy1*, welches für eine Salizylat Hydroxylase codiert deletiert wurden, zeigte, im Gegensatz zu Stämmen in welchen diese Gene einzeln oder paarweise deletiert wurden, reduzierte Virulenz. Dies deutet darauf hin, dass diese drei Enzyme bei der Unterdrückung des SA Weges zusammenwirken. Durch Immunopräzipitation (IP) von Cmu1 aus infiziertem Gewebe und anschließender massenspektroskopischer Analyse konnte das Mais Protein Cmi1 (**C**mu1 **i**nteractor 1) als Interaktionspartner identifiziert werden. Diese Interaktion konnte durch *in vitro* Pull-down Experimente bestätigt werden. Rekombinantes Cmi1 Protein inhibierte die Chorismatmutase Aktivität von Cmu1. Die Expression von *cmi1* wird nach Infektion mit *U. maydis* stark hochreguliert, was für einen Zusammenhang zwischen Cmi1-Funktion und Pathogenität spricht. Mittels Wasserstoff-Deuterium-Austauschmessungen (HDX/MS) konnte die Loop-Region in Cmu1 als Interaktionsbereich identifiziert werden. Ein *cmu1* Allel mit verkürzter Loop-Region, wodurch die Interaktion zwischen Cmu1 und Cmi1 unterbunden wurde, konnte den Virulenzdefekt von CL13 Δ cmu1 nur teilweise komplementieren. Dies könnte deutet darauf hindeuten, dass die Interaktion zwischen Cmu1 und Cmi1 für die Virulenz von *U. maydis* von Bedeutung ist.

1. Introduction

1.1 Plant-fungus interactions

In the natural ecosystem, terrestrial plants are constantly associated with a large variety of organisms, which belong to various life kingdoms, such as viruses, bacteria, fungi, oomycetes, nematodes and pests. The interactions between fungi and plants can result in beneficial or detrimental effects on the growth of plants, which are due to symbionts and pathogens, respectively. Symbiotic fungi, such as arbuscular mycorrhizal (AM) and ectomycorrhizal (ECM) fungi, promote the growth of plants by facilitating nutrient uptake or increasing the resistance against plant pathogens (Zuccaro et al., 2014). Plant pathogenic fungi are growing threats affecting the yield of crops around the world. It is estimated that nearly 10% of annual agricultural yield losses are caused by fungal plant pathogens (Lo Presti et al., 2015). Plant pathogenic fungi establish distinct types of parasitism with plants, namely biotrophy, necrotrophy and hemibiotrophy (Glazebrook, 2005). Biotrophic pathogens feed on living plant tissues without killing their hosts during infection, whereas necrotrophs secrete toxic molecules to promote cell death of plants and derive nutrients from dead plant debris. Hemibiotrophic pathogens keep the host alive during the early stage of infection and later transit to necrotrophy (Glazebrook, 2005). Despite their different infection strategies, all fungal pathogens are inevitably recognized by the plant immune system and activate multilayered plant defenses.

1.1.1 Plant innate immune system

Plants have evolved sophisticated immunity to defend themselves against a myriad of pathogens, which rely on receptors to activate downstream immune responses (Jones and Dangl, 2006; Boller and Felix, 2009). An overview of plant innate immune system is depicted in **Fig.1**. Pattern recognition receptors (PRRs) are typically surface-localized transmembrane proteins constituting the first line of plant innate immunity (Zipfel, 2014). PRRs are divided into two groups, receptor-like kinases (RLKs) with a ligand-binding ectodomain, a single-pass transmembrane domain and an intracellular kinase domain, and receptor-like proteins (RLPs) which have a similar structural fold but lack an intracellular kinase domain (Macho and Zipfel, 2014; Zipfel, 2014; Couto and Zipfel, 2016). PRRs deploy ectodomains to perceive pathogen or microbe-associated molecular patterns (PAMPs or MAMPs), which are highly conserved molecular signatures in microbial taxa,

leading to the activation of pattern triggered immunity (PTI) (Jones and Dangl, 2006). For instance, the bacterial PAMPs flagellin, elongation factor thermo unstable (EF-Tu) and lipopolysaccharide (LPS) are sensed by *Arabidopsis* RLKs flagellin-sensitive-2 (FLS2), EF-Tu receptor (EFR) and lectin S-domain receptor kinase LORE (lipooligosaccharide-specific reduced elicitation), respectively (Gomez-Gomez and Boller, 2000; Zipfel et al., 2006; Ranf et al., 2015). Likewise, the *Arabidopsis* lysin-motif (LysM) protein CERK1 (chitin elicitor receptor kinase 1) forms complexes with co-receptors LysM-RLKs (such as LYK4 and LYK5) or LysM-RLPs (such as LYM1 and LYM3) to recognize oligosaccharides of the fungal cell wall component chitin or bacterial peptidoglycans (Miya et al., 2007; Willmann et al., 2011; Cao et al., 2014).

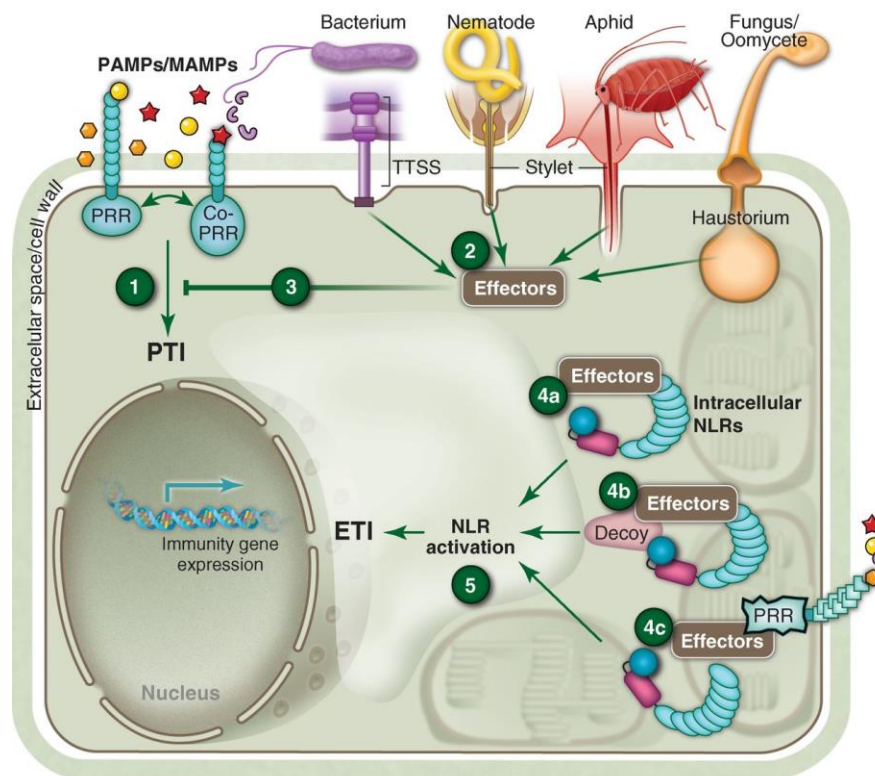


Fig. 1: Schematic overview of the plant innate immune system. Pathogens of all lifestyle classes (color coded and labeled) express PAMPs and MAMPs as they colonize plants. Plants perceive these via extracellular PRRs and initiate PRR-mediated immunity (PTI; step 1). Pathogens deliver virulence effectors to both the plant cell apoplast to block PAMP/MAMP perception (not shown) and to the plant cell interior (step 2). These effectors are addressed to specific subcellular locations where they can suppress PTI and facilitate virulence (step 3). Intracellular NLR receptors can sense effectors in three principal ways: first, by direct receptor ligand interaction (step 4a); second, by sensing effector-mediated alteration in a decoy protein that structurally mimics an effector target, but has no other function in the plant cell (step 4b); and third, by sensing effector-mediated alteration of a host virulence target, like the cytosolic domain of a PRR (step 4c). It is not yet clear whether each of these activation modes proceeds by the same molecular mechanism, nor is it clear whether NLR-dependent effector-triggered immunity, (ETI), proceeds by one or several pathways. [from (Dangl et al., 2013)]

In addition to the detection of microbial derived patterns, plant PRRs also perceive host-derived damage-associated molecular patterns (DAMPs) that are produced upon wounding or attack by pathogens (Couto and Zipfel, 2016). Endogenous plant elicitor peptides (Pep) are the processed products of PROPEP proteins (Yamaguchi et al., 2006). AtPep peptides in *Arabidopsis* function as DAMPs to activate plant immune responses via binding to *Arabidopsis* PRRs PEPR1 and PEPR2 (Huffaker et al., 2006; Yamaguchi et al., 2006; Yamaguchi et al., 2010). Similarly, a plant cell wall associated kinase 1 (WAK1) serves as the receptor for cell wall derived pectin oligogalacturonides (OGs) that are produced due to physical damage or pathogen invasion (Brutus et al., 2010). Furthermore, as a consequence of wounding or pathogen attack, extracellular ATP (eATP) is released from plant cells, which is recognized by a novel class of lectin-domain eATP receptor DORN1/LecRK-I.9 (Choi et al., 2014).

An array of plant defense signaling pathways are elicited after PAMPs or DAMPs are perceived by PRRs. Ca^{2+} and reactive oxygen species (ROS) are commonly regarded as crucial secondary messengers mediating plant defense responses during early stage of PTI (Mazars et al., 2010; Gilroy et al., 2016). Upon PRR recognition, the Ca^{2+} homeostasis is perturbed due to the activation of Ca^{2+} channels in the plant plasma membrane, resulting in the elevation of Ca^{2+} in plant cytosol (Blume et al., 2000; Lecourieux et al., 2002; Qi et al., 2010). Extracellular ROS is generated in response to pathogen attack, which alters the redox status in the plant apoplast (Daudi et al., 2012; O'Brien et al., 2012; Couto and Zipfel, 2016). Ca^{2+} and ROS signaling have been reported to mutually modulate the production of each other, and both are able to activate downstream defense-related mitogen-activated protein kinase (MAPK) cascades (Kovtun et al., 2000; Pei et al., 2000; Kobayashi et al., 2007; Lee et al., 2015; Couto and Zipfel, 2016). In the later stage of PTI, the biosynthesis of plant hormones is changed to regulate the expression of various defense related genes (Pieterse et al., 2012; Berens et al., 2017). In addition, callose deposition in plant cell wall occurs to constrain the invasion of pathogens (Boller and Felix, 2009; Luna et al., 2011; Couto and Zipfel, 2016).

In order to colonize the host, successful plant pathogens secrete an arsenal of effector proteins to avoid triggering PTI (Jones and Dangl, 2006). However, plants have evolved a second line of innate immunity where resistance (R) proteins are utilized to recognize effectors and elicit effector triggered immunity (ETI) (Jones and Dangl, 2006; Dodds and Rathjen, 2010). R proteins are typically intracellular nucleotide-binding leucine-rich-repeat (NLR) receptors, which consist of an

N-terminal Toll–interleukin receptor (TIR) or coiled-coil (CC) domain, a central nucleotide-binding (NB) domain, and a C-terminal leucine-rich repeat (LRR) (Jones and Dangl, 2006; Dodds and Rathjen, 2010). Some plant NLRs directly bind to effectors through the LRR domain, while others indirectly perceive effectors by monitoring the modification of some proteins, which are either host targets (guardee) or mimics of those targets (decoy) for effectors (van der Hoorn and Kamoun, 2008; Jones et al., 2016). Furthermore, several NLRs are equipped with decoys of effectors, detecting paralogous effectors by direct interaction, which has led to the “integrated decoy model” (Le Roux et al., 2015; Sarris et al., 2015). Despite the diversity of NLRs in perceiving effectors, once activated, NLR proteins are believed to undergo a conformational switch from an ADP bound off-state to an ATP bound on-state, accompanied by NLR homodimerization which leads to the activation of ETI (Williams et al., 2014; El Kasmi and Nishimura, 2016; Jones et al., 2016). Consequently, a hypersensitive response (HR) occurs, which is often associated with local cell death, restricting the proliferation of pathogens (Jones et al., 2016).

1.1.2 Effectors –a versatile armory of plant associated fungi

Effectors are proteins potentially secreted by microorganisms to assist parasitism (Chisholm et al., 2006; Jones and Dangl, 2006; Kamoun, 2006). Depending on their functional localization, effectors can be grouped into two families: apoplastic effectors which function in the apoplast between the fungal cell wall and the plant plasma membrane and translocated effectors that are firstly secreted by the microbes and then taken up by the plant cell to exert their functions inside (Kamoun, 2006; Lo Presti et al., 2015). Besides a few exceptions, effectors are normally secreted via the conventional endoplasmic reticulum-Golgi apparatus pathway, which is guided by N-terminal signal peptides (SPs) (Kamoun, 2006; Liu et al., 2014; Petre and Kamoun, 2014; Lo Presti et al., 2015). To identify effectors from fungi, a variety of criteria such as a size smaller than 300 amino acids, cysteine abundance and lack of known functional domains have been used (Duplessis et al., 2011; Gan et al., 2013; Stergiopoulos et al., 2013; Ramachandran et al., 2017). However, some secreted effector proteins from plant associated fungi contain more than 300 amino acids or have functional domains, largely extending the definition of effectors (Catanzariti et al., 2010; Djamei et al., 2011; Mentlak et al., 2012; Liu et al., 2014). Effector genes are often found to reside in dynamic genomic compartments, which are rich in repetitive genes and transposable elements (Dong et al., 2015; Dutheil et al., 2016). The plasticity of these dynamic compartments may in turn drive the evolution of effectors to allow the pathogens to adapt to various host plants or to evade

the recognition of R proteins (Raffaele and Kamoun, 2012; Grandaubert et al., 2014; Rovenich et al., 2014). In addition, genome-wide transcriptomic analyses have promoted the identification of effectors, because effectors encoding genes are often transcriptionally upregulated during the interaction with plants (Mosquera et al., 2009; Zuccaro et al., 2011; Gan et al., 2013; Guyon et al., 2014). The expression of effectors is usually under the control of a variety of transcriptional regulators as well as subject to epigenetic modifications (Santhanam and Thomma, 2013; Soyer et al., 2014; Soyer et al., 2015; Phan et al., 2016).

Plant associated fungi deliver a large arsenal of effectors to overcome plant innate immunity and promote colonization. A multitude of plant processes are targeted by pathogen effectors (Asai and Shirasu, 2015; Toruno et al., 2016). Firstly, chitin, the essential fungal cell wall component, could be hydrolyzed by plant chitinases, releasing chitin oligosaccharides that are recognized by chitin receptors on plant cell wall (Sanchez-Vallet et al., 2015). To avoid eliciting chitin-triggered signaling pathway in plants, plant pathogenic fungi secrete effectors to interfere with the recognition of chitin by cognate receptors. For instance, the tomato pathogen *Cladosporium fulvum* secretes the effector Avr4 possessing a chitin binding domain (van den Burg et al., 2006). Avr4 binds to the fungal cell wall and shields it from attack of plant chitinases (van den Burg et al., 2006; van Esse et al., 2007). The same pathogen utilizes another effector named Ecp6, which possesses LysM motifs, to scavenge soluble chitin fragments (de Jonge et al., 2010). Ecp6 has a high binding affinity to chitin oligosaccharides, aiding in escape from the surveillance of the plant immune system (de Jonge et al., 2010; Sanchez-Vallet et al., 2013). Similarly, the LysM effector Slp1 from the rice blast fungus *Magnaporthe oryzae* suppresses chitin-induced plant immune responses via sequestering chitin oligosaccharides (Mentlak et al., 2012). Secondly, there are numerous plant proteases in the apoplast, which are extremely harmful to plant pathogens. Therefore, adapted plant pathogens deploy strategies to inhibit the activity of plant proteases (Doehlemann and Hemetsberger, 2013). For example, tomato papain-like cysteine proteases (PLCPs) PIP1 and RCR3 are targeted by Avr2 from *C. fulvum* (Rooney et al., 2005; van Esse et al., 2008). Moreover, phytohormone signaling is essential for the regulation of plant immune responses to microorganisms (Pieterse et al., 2012; Berens et al., 2017). The hormone salicylic acid (SA) mediates plant defenses against plant biotrophic pathogens (Glazebrook, 2005). The unconventionally secreted isochorismatase VdIsc1 of the fungal pathogen *Verticillium dahliae* suppresses the biosynthesis of SA through depleting isochorismate, a precursor for SA (Liu et al., 2014). Jasmonic acid (JA) plays a negative role for plant necrotrophic pathogens as well as

mutualistic symbionts (Glazebrook, 2005; Plett et al., 2014b). To downregulate JA signaling, MiSSP7 of the mutualistic fungus *Laccaria bicolor* enters the nucleus of *Populus* cell and suppresses the proteasomal degradation of a repressive regulator JAZ6, thereby maintaining the repression of JA signaling (Plett et al., 2014a; Martin et al., 2016).

1.1.3 Structural studies of effectors from plant pathogenic fungi

The finding that the majority of effectors lack sequence similarity to known proteins poses a challenge to uncover their real functions in the interaction with plants. Structural biology has become a powerful tool to elucidate the molecular mechanisms of effector function. Structural studies have revealed that effectors with low sequence similarity can possess a similar structural fold, which is possibly the result of faster evolution of protein sequences over structures (Illergard et al., 2009; de Guillen et al., 2015; Franceschetti et al., 2017).

The crystal structure of LysM containing effector Ecp6 from *C. fulvum* has allowed to uncover a characteristic $\beta\alpha\alpha\beta$ -fold, which is shared by its three LysM domains (Sanchez-Vallet et al., 2013). Interestingly, the Ecp6 structure revealed a novel pattern for chitin binding: two of the three LysM (LysM1 and LysM3) domains in Ecp6 dimerize to form the binding groove with an ultrahigh affinity for chitin binding to sequester chitin oligosaccharides, while the third one LysM2 with a lower affinity to bind chitin might interfere with chitin-induced immunity by a yet unknown mechanism (Sanchez-Vallet et al., 2013).

Pf-Avr4 from the tomato pathogen *Pseudocercospora fuligena* is the orthologue of Cf-Avr4 in *C. fulvum*, which binds chitin oligosaccharides to inhibit chitin-induced immunity (Kohler et al., 2016). It was presented that Pf-Avr4 displays 10-fold weaker affinity for (GlcNAc)₆ than Cf-Avr4, which is due to the subtle difference in the chitin binding site of Pf-Avr4 compared with Cf-Avr4 (Kohler et al., 2016). In addition to five conserved residues for chitin binding, two tryptophan residues W88 and W94 of Pf-Avr4 were involved in chitin binding (Kohler et al., 2016). Moreover, the structure-based mutagenesis demonstrated that the chitin binding ability of Pf-Avr4 does not directly correlate with the recognition by the cognate resistance protein Cf-4 (Kohler et al., 2016).

The *Magnaporthe* Avr3 and ToxB-like (MAX) family represents a newly discovered effector family in plant pathogenic fungi (de Guillen et al., 2015). The discovery of this effector family relied on the structural studies of two effectors AVR1-CO39 and AVR-Pia from *M. oryzae*. A six-stranded β -sandwich fold is revealed by the structures, which is shared by these two effectors. Surprisingly,

this fold is also shared by sequence-unrelated effector AvrPiz-t from *M. oryzae* and the toxin ToxB from the wheat tan spot pathogen *Pyrenophora tritici-repentis* (Zhang et al., 2013; Nyarko et al., 2014). PSI blast and hidden Markov model (HMM)-based profile search revealed that MAX family effectors are mainly distributed in the *Magnaporthe* species, with a few exceptions in other ascomycetes such as *Colletotrichum* (de Guillen et al., 2015). MAX-effectors in ascomycetes show a similar structural topology but are divergent in molecular properties and activities, indicating that effectors in this family evolved from a common ancestor via duplication but have undergone diversification (de Guillen et al., 2015).

The structure of another effector ToxA from *P. tritici-repentis* is also solved and exhibits a distinct β -sandwich architecture (Manning et al., 2008). An arginyl-glycyl-aspartic (RGD) motif located in a loop region is implicated in recognition by a host receptor and cell entry of this effector (Meinhardt et al., 2002; Manning et al., 2008). Effectors adopting a similar β -sandwich fold are also found in the flax rust fungus *Melampsora lini*, where they comprise the polymorphic AvrL567 family of effectors (Wang et al., 2007). Based on the structures of AvrL567 proteins, several surface exposed residues are mapped which takes part in recognition by respective resistance proteins. The structures also illustrate two interesting positively charged patches on the surface capable of binding nucleic acid *in vitro* (Wang et al., 2007).

The similarity between crystal structures of the C-terminal domains of two different AvrM variants (AvrM-A and avrM) of *M. lini* and oomycete WY-fold effectors illustrates structural resemblance among effectors from different lineages (Ve et al., 2013). A conserved surface-localized hydrophobic patch was shown to be required for the internalization of AvrM into plant cells (Ve et al., 2013).

The avirulence effector AvrLm4-7 of *Leptosphaeria maculans*, the causal agent of stem canker in *Brassica napus* (oilseed rape), is a translocated effector that is recognized by two R proteins Rlm4 and Rlm7 (Parlange et al., 2009). Its three dimensional (3D) structure provides better understanding of the molecular mechanisms by which AvrLm4-7 contributes to the full virulence of *L. maculans* on its host. While a polymorphic residue G120R that is located on a loop mediated the recognition by Rlm4, another three polymorphic residues R100P, F102S and S112R, involved in Rlm7 mediated recognition, are also found on loops of the protein (Blondeau et al., 2015). In addition, motifs RYRE and RAWG on a positively charged patch on the surface are likely involved in the translocation of AvrLm4-7 inside plant cells (Blondeau et al., 2015).

1.2 *Ustilago maydis*-a model for biotrophic plant pathogen

1.2.1 The *U. maydis*-*Zea mays* pathosystem

Maize (*Z. mays* ssp. *mays*) is one of the most important crop plants all over the world. Besides economic traits, in the past 100 years, maize has been extensively studied as a model organism for plant domestication, comparative genomics, genetic transposition and photosynthesis (Strable and Scanlon, 2009; Hake and Ross-Ibarra, 2015).

The basidiomycete fungus *U. maydis* is the causative agent for smut diseases of maize and its wild relative teosinte (*Z. mays* ssp. *parviglumis*) (Banuett and Herskowitz, 1996). Unlike smut diseases of many plants, which only show smutty symptoms in floral organs, *U. maydis* is able to infect aerial parts of a maize plant and induce tumor-like structures (hereafter tumors) (Christensen, 1963; Banuett, 1995). These tumors release dark-colored spores when they rupture (Kahmann et al., 2000). Although the economic significance of *U. maydis* is not as severe as the other devastating fungal pathogens, it is an alternative model to study pathogenicity and biotrophy of fungal plant pathogens (Dean et al., 2012) for the following reasons: the haploid form of *U. maydis* can be propagated in the laboratory in defined media. The haploid cells grow by budding (Christensen, 1963; Banuett and Herskowitz, 1996). *U. maydis* possesses a highly efficient homologous recombination system, which allows PCR-based resistance cassette gene replacements (Kämper, 2004). In addition, the CRISPR-Cas9 system has been adopted and both tools allow to perform reverse genetic studies (Schuster et al., 2016; Schuster et al., 2017). Moreover, to assess the pathogenicity, maize seedlings can be infected and 5-6 days post infection (dpi) disease symptoms can be scored and the entire life cycle is completed in about two weeks under the greenhouse condition (Dean et al., 2012). Last but not the least, the well annotated genome of *U. maydis* combined with transcriptional profiling and proteomics analysis aid in understanding its pathogenic development and aid in finding critical virulence factors (Kämper et al., 2006; Bohmer et al., 2007; Skibbe et al., 2010; Tollot et al., 2016).

1.2.2 The life cycle of *U. maydis*

To colonize the plant, *U. maydis* has to undergo a morphological switch from non-pathogenic haploid cells (sporidia) to the invasive dikaryotic filament (Banuett, 1995; Kahmann et al., 2000). The latter is formed after fusion of two compatible haploid cells (**Fig. 2A**) (Rowell, 1955; Holliday, 1974). The morphological switch from sporidia to filamentous growth is controlled by two distinct

mating loci *a* and *b* (Banuett, 1995; Kahmann et al., 1995; Kahmann et al., 2000). Mating is successful when two mating partners carry compatible alleles at *a* loci (Rowell, 1955; Puhalla, 1969; Kahmann et al., 1995). The bi-allelic *a* locus encodes components for a pheromone-based recognition system, mediating cell recognition, formation of conjugation tubes, cell fusion and maintenance of the filamentous growth (Banuett and Herskowitz, 1989; Bolker et al., 1992; Trueheart and Herskowitz, 1992; Snetselaar et al., 1996). The perception of pheromone activates cyclic AMP (cAMP) signaling as well as MAPK signaling, leading to the activation of pheromone response factor Prf1 (Banuett and Herskowitz, 1994; Kaffarnik et al., 2003; Muller et al., 2003). The transcription factor Prf1 can activate the expression of genes in the *b* mating type locus (Hartmann et al., 1996). The multi-allelic *b* locus encodes two unrelated homeodomain proteins, bE and bW, which heterodimerize and become active when they originate from two different alleles (Kronstad and Leong, 1990; Gillissen et al., 1992; Kämper et al., 1995). The active *b* heterodimer triggers a regulatory cascade of numerous cellular processes that are related to pathogenesis, which makes it a master regulator for virulence (Brachmann et al., 2001; Kahmann and Schirawski, 2007).

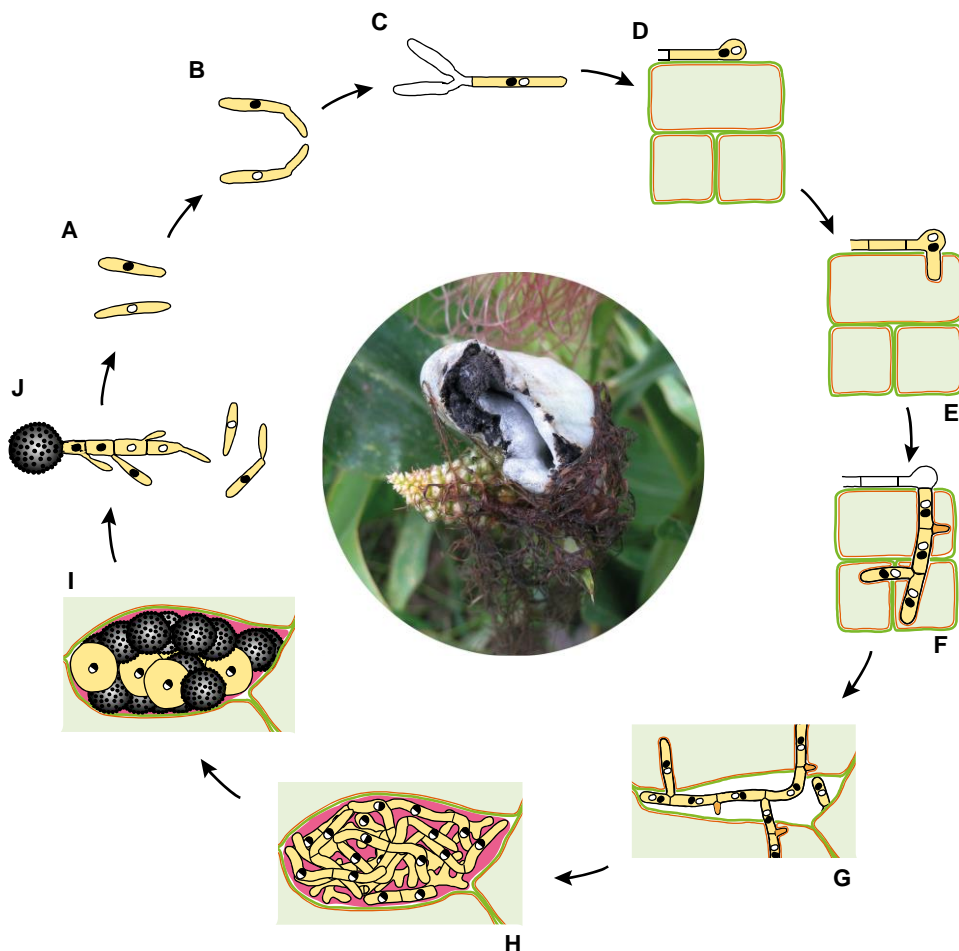


Fig. 2: Schematic representation of the life cycle of *U. maydis*. The biphasic life cycle of *U. maydis* can be divided into a saprophytic phase (A-C) and a biotrophic phase (D-J). The black closed circle and open circle in A-G and J represent haploid nuclei with different mating types. Nuclei in half black and half white in H and I are diploid nuclei produced by the fusion of black and white haploid nuclei. Plant cytoplasm is depicted in light green and the plant plasma membrane is in red. The clamp-like structure is shown in orange in F and G. The pink color in H and I represents the polysaccharide matrix filling the apoplastic space of tumors. The photo in the center of the figure shows a maize cob infected by *U. maydis*. (Figure: modified by S. Reißmann from Lanver et al., 2017; photo: X. Han)

On the leaf surface, polarized growth of the invasive filament is driven by the cytoskeleton (Brefort et al., 2009). The cytoplasm accumulates in the tip cell compartment while the older parts of the filament become vacuolated and segregated by inserted septa (**Fig. 2C, D**) (Steinberg et al., 1998; Brefort et al., 2009). Subsequently, the tip cell differentiates in response to hydroxy-fatty acids and hydrophobicity (Mendoza-Mendoza et al., 2009) into a specialized swollen, non-melanized structure termed appressorium. The appressorium penetrates the plant cuticle (**Fig. 2E**) (Snetselaar and Mims, 1993). After penetration, hyphae of *U. maydis* initially grow intracellularly in the epidermis. During this stage, they are completely encased by the plant plasma membrane (Snetselaar and Mims, 1993). This biotrophic interaction zone is considered to be the site for *U. maydis* to secrete effectors and obtain nutrients from the host (Djamei and Kahmann, 2012). The following proliferation of dikaryotic fungal hyphae in mesophyll cells and vascular bundles is assisted by clamp-like structures (**Fig. 2F**) (Snetselaar and Mims, 1994; Scherer et al., 2006). Several days post infection, tumor tissue begins to develop in the leaf. In tumor tissue, large fungal aggregates form in the intercellular spaces, in which fungal cells are embedded in a mucilaginous matrix (**Fig. 2G-H**) (Snetselaar and Mims, 1994; Banuett and Herskowitz, 1996). Dikaryotic cells within tumors undergo karyogamy followed by fragmentation and sporogenesis (Banuett and Herskowitz, 1996). The diploid melanized teliospores are released when tumors are mature and rupture, which can endure harsh environment (**Fig. 2I**) (Kahmann et al., 2000; Brefort et al., 2009). Ultimately, under favorable conditions, teliospores germinate, undergo meiosis and produce haploid sporidia which can initiate a new round of infection (**Fig. 2J**) (Banuett, 1995; Banuett and Herskowitz, 1996).

1.2.3 Effectors of *U. maydis*

The 20.5 M genome of *U. maydis* is predicted to encode 6,784 proteins and of these more than 400 proteins are putatively secreted (Kämper et al., 2006; Lanver et al., 2017). More than half of these secreted proteins are novel, meaning that they harbor no homology to known functional domains, and many of them contribute to virulence of *U. maydis* (Lanver et al., 2017; Schuster et al., 2017).

However, only five effector proteins of *U. maydis* have been functionally characterized to date (Doehlemann et al., 2009; Djamei et al., 2011; Hemetsberger et al., 2012; Mueller et al., 2013; Tanaka et al., 2014; Redkar et al., 2015).

The first characterized effector is Pep1, an apoplastic effector which is crucial for the virulence *U. maydis*. *U. maydis* mutants lacking *pep1* induce strong host defense responses during penetration, which blocks entry of hyphae in the epidermis (Doehlemann et al., 2009). Pep1 inhibits the accumulation of ROS by inhibiting the maize peroxidase POX12 which is responsible for producing ROS in the apoplast (Hemetsberger et al., 2012).

The first translocated effector described in *U. maydis* is Cmu1, a secreted chorismate mutase that is required for full virulence of the pathogen (Djamei et al., 2011). The translocation of Cmu1 into the cytosol of maize cells was demonstrated by immuno-electron microscopy (immuno-EM) and a bioassay exploiting transgenic maize line expressing the biotin ligase BirA (Djamei et al., 2011; Lo Presti et al., 2017). In maize tissues infected by *cmu1* deletion mutants, increased SA levels accumulated (Djamei et al., 2011). It was proposed that Cmu1 contributes to virulence by depleting chorismate to suppress the production of SA, which benefits fungal growth *in planta* (Djamei et al., 2011).

To overcome the negative effect of plant apoplastic proteases, *U. maydis* secretes the apoplastic effector Pit2 which inhibits maize cysteine proteases (Doehlemann et al., 2011; Mueller et al., 2013). The inhibitory effect of Pit2 on cysteine proteases depends on a novel motif consisting of 14 amino acids (Mueller et al., 2013). *pit2* deletion mutants can penetrate maize tissue and proliferate in the epidermal layer, however, subsequent fungal spreading and proliferation are blocked (Doehlemann et al., 2011).

Plant secondary metabolism is also targeted by the translocated effector Tin2 of *U. maydis*. Tin2 interacts with the maize kinase ZmTTK1, which positively controls the expression of anthocyanin biosynthesis genes (Tanaka et al., 2014). Tin2 prevents ZmTTK1 from proteasomal degradation and guides the phenylpropanoid pathway into the branch to synthesize anthocyanin, presumably to inhibit the lignification of plant cells (Tanaka et al., 2014).

A typical symptom of *U. maydis* infection is tumor formation on all aerial part of maize plants. A novel organ-specific effector See1 was identified, which contributes to tumor formation on leaves (Redkar et al., 2015). See1 was detected in the plant nucleus, and directly interacted with a maize

protein SGT1, which is involved in cell cycle progression (Redkar et al., 2015). By interfering with the phosphorylation of SGT1, See1 is considered to disrupt the cell cycle control of maize leaf cells, resulting in the reactivation of DNA synthesis and cell division in infected leaves (Redkar et al., 2015).

1.3 Chorismate mutases

Chorismate is the end product of shikimate pathway, which serves as the precursor for the biosynthesis of a wide range of aromatic compounds including the aromatic amino acids tryptophan, tyrosine and phenylalanine, folate, indole-3-acetic acid (IAA), SA, anthocyanin and lignin (Dempsey et al., 2011). Chorismate mutase (CM) catalyzes the pericyclic Claisen-rearrangement of chorismate to prephenate, the first committed step leading to biosynthesis of phenylalanine and tyrosine (Dempsey et al., 2011). CMs are of great importance in various biological processes and widespread, i.e. they are found in bacteria, archaea, fungi, protists, plants and nematodes. For instance, CMs are indispensable for fungi and plants in the biosynthesis of essential amino acids tyrosine and phenylalanine (Kradolfer et al., 1977; Eberhard et al., 1996b).

CMs are classified into two groups based on structural topologies: the AroH family and AroQ family (**Fig. 3**) (Okvist et al., 2006). AroH family is represented by the monofunctional BsCM from *Bacillus subtilis*. AroH-type CMs comprise less than 150 amino acids and are only present in bacteria. They display a trimeric α/β barrel topology (Chook et al., 1993). AroQ family CMs are all helical and homodimeric. They are further divided into three subgroups: AroQ $_{\alpha}$, AroQ $_{\beta}$ and AroQ $_{\gamma}$ (Okvist et al., 2006). AroQ $_{\alpha}$ subfamily CMs are part of bifunctional proteins in bacteria and usually fused with prephenate dehydratases (P-protein for the biosynthesis of phenylalanine), prephenate dehydrogenases (T-protein for the biosynthesis of tyrosine) or 3-deoxy-D-arabinoheptulosonate-7-phosphate synthases (DAH7PS) (Helmstaedt et al., 2001; Okvist et al., 2006). The two active sites of dimeric AroQ $_{\alpha}$ subfamily CMs are formed with contribution from each monomer consisting of three helices (Lee et al., 1995). CMs from AroQ $_{\beta}$ subfamily are monofunctional eukaryotic enzymes with an intact catalytic domain and an additional regulatory domain in each monomer, including most CMs from fungi and plants. AroQ $_{\gamma}$ CMs are secreted by bacteria, fungi and nematodes, which are normally smaller than AroQ $_{\beta}$ subfamily CMs (more than 250 amino acids) (Okvist et al., 2006).

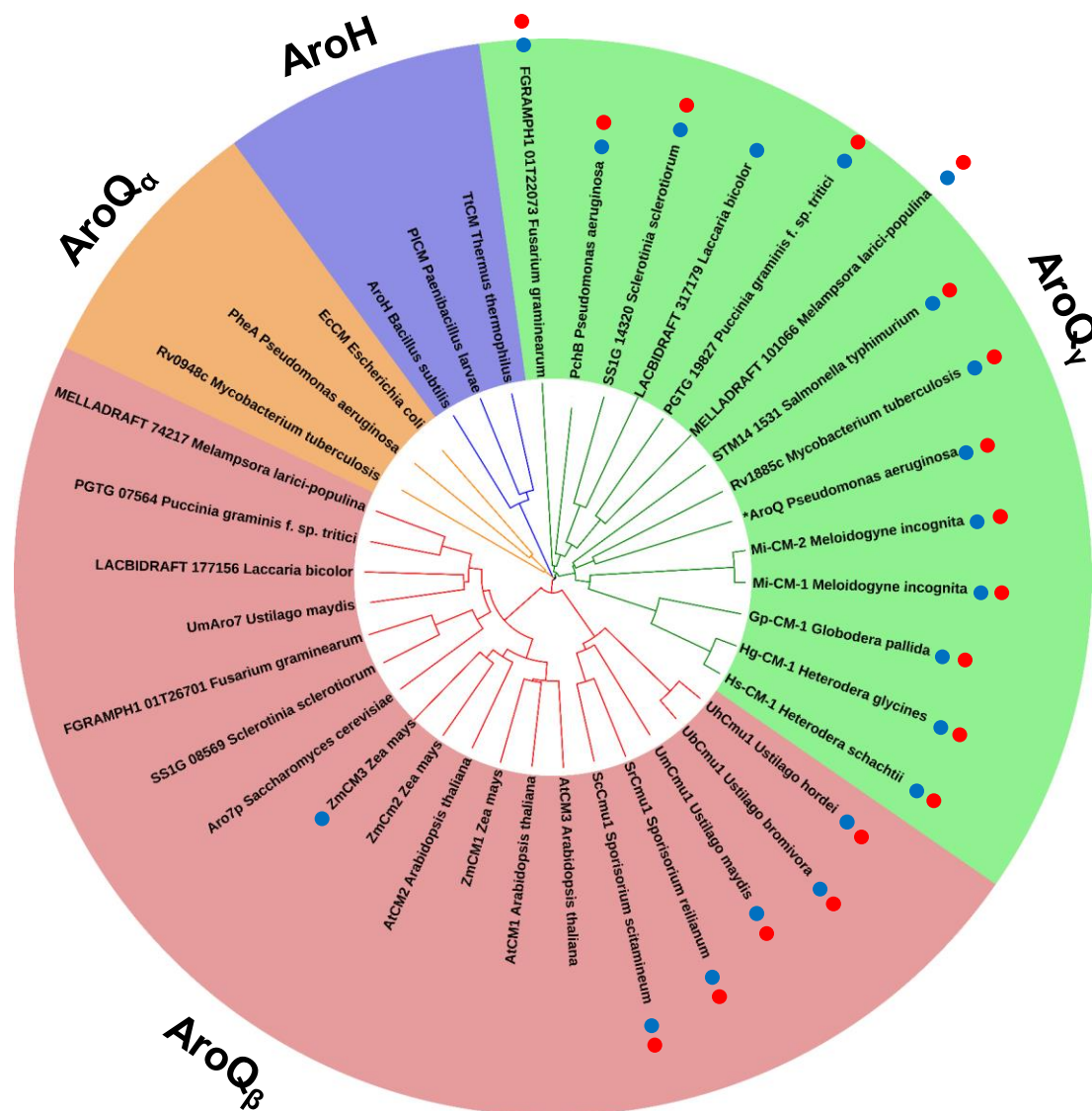


Fig. 3: Classification of CMs with 38 CMs from 24 species. AroH family CMs are marked by medium slate blue; AroQ α subfamily CMs are marked by sandy brown; AroQ β subfamily CMs are marked by salmon; AroQ γ subfamily CMs are marked by light green. Secreted CMs are highlighted with blue dots. Secreted CMs from plant or mammalian pathogens are highlighted with red dots. The list of the CMs included in the phylogeny is presented in Table 8 (Appendix). The alignment was generated with CLUSTAL Omega (Sievers et al., 2011) and the figure was produced with iTOL (Letunic and Bork, 2016).

Allosteric regulation is a characteristic feature for many CMs. For example, the CM activity of EcCM from *Escherichia coli* belonging to the AroQ α subfamily is inhibited by its end products tyrosine and phenylalanine (Dopheide et al., 1972; Christopherson, 1985). The CM Aro7p from *Saccharomyces cerevisiae* belongs to AroQ β subfamily and is regulated by tyrosine and tryptophan. While the end product tyrosine inhibits the CM activity of Aro7p, a product from another branch for chorismate tryptophan activates its activity (Xue et al., 1994; Schnappauf et al., 1998). The

binding of tyrosine and tryptophan, respectively, leads to two states of Aro7p, the T-state (inhibited) and R-state (activated) (Xue et al., 1994; Strater et al., 1996). For AtCM1 from *Arabidopsis thaliana*, another member of the AroQ β subfamily, it was discovered that phenylalanine was also able to inhibit the CM activity of AtCM1 (Westfall et al., 2014). This illustrates that allosteric regulation of CMs is highly diverse. In addition, there are only a few CMs whose activities are not regulated by aromatic amino acids, such as BsCM of *B. subtilis* and cytosolic AtCM2 of *A. thaliana* (Helmstaedt et al., 2001; Westfall et al., 2014).

With respect to the biological function of CMs, they are expected to localize intracellularly and contribute to the growth of organisms by producing metabolites such as phenylalanine or tyrosine. However, two genes for CMs are existing in some organisms, with one predicted to encode a cytosolic protein and the other one encoding a secreted protein (Calhoun et al., 2001; Prakash et al., 2005; Djamei et al., 2011). Intriguingly, many of those secreted CMs exist in plant or mammalian pathogens, and emerging evidence correlates these secreted CMs with pathogenicity (Calhoun et al., 2001; Bekal et al., 2003; Doyle and Lambert, 2003; Qamra et al., 2006; Djamei et al., 2011). For instance, the expression of secreted CMs in plant pathogenic nematodes was induced in the esophageal glands, through which most effector proteins are released (Bekal et al., 2003; Jones et al., 2003). The injection of secreted CMs into plant cells by nematodes alters the balance of metabolic fluxes to favor colonization (Doyle and Lambert, 2003). However, the biological functions of most secreted CMs still remain elusive.

1.4 Overall structure of Cmu1

To get a better understanding of how Cmu1 exerts its function, the crystal structure of Cmu1 without SP (Cmu1^{ASP}) was determined at 1.9 Å resolution by the group of Dr. Gert Bange (**Fig. 4**, J. Schuhmacher and G. Bange, unpublished). Cmu1^{ASP} shows homodimeric and each monomer consists of nine helices and the overall dimension of Cmu1 dimer is 72.5 Å×125 Å×230.8 Å (J. Schuhmacher and G. Bange, unpublished). H1, H5, H8 and H9 form a four-helix-bundle consisting of the catalytic site for its CM activity, which is similar to that of yeast Aro7p (Xue et al., 1994).

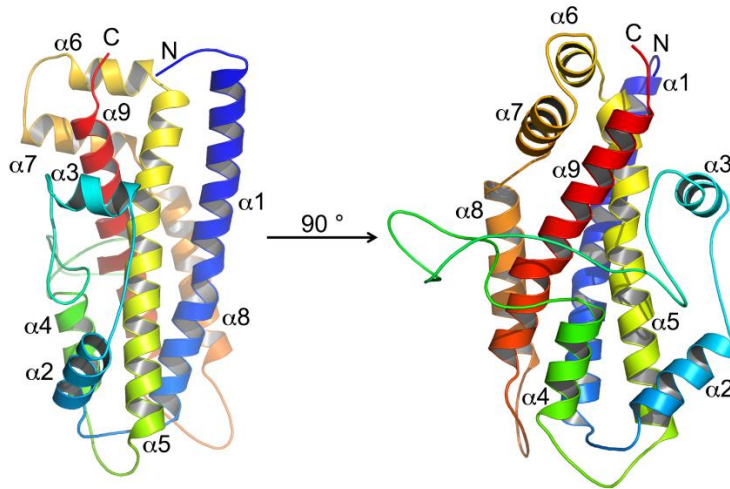


Fig. 4: Crystal structure of Cmu1. Cartoon representation of the crystal structure of Cmu1. The secondary elements are labeled with α for α -helix and numbered.

1.5 Aims of the study

Structural comparison of Cmu1 and Aro7p from yeast revealed several unique features present in Cmu1. My study was focused on a structure-function analysis of Cmu1, with the aim to answer several scientific questions: 1) What are the roles of those unique features in the biological function of Cmu1? 2) How is the CM activity of Cmu1 regulated? 3) Are there additional pathways contributing to low SA levels in *U. maydis*-infected tissue? 4) Does Cmu1 have other functions in addition to lowering SA levels? 5) Does Cmu1 interact with maize proteins to promote virulence?

2. Results

In previous work, deletion mutants of *cmu1* were generated in the solopathogenic *U. maydis* strain CL13 which is attenuated in virulence compared to the solopathogenic strain SG200 (Kämper et al., 1995; Kämper et al., 2006). The CL13 Δ *cmu1* strain showed a slight reduction in virulence with reduced tumor formation in comparison to CL13 (Djamei et al., 2011). To better visualize the phenotype of the mutant strain, the infection strategy was modified using the maize variety Gaspé Flint instead of 7-day-old seedlings of Early Golden Bantam. With this method, the virulence of CL13 strain was elevated and more tumors with larger size were produced, making it easier to discriminate the phenotype difference between CL13 and CL13 Δ *cmu1* (A. Ghosh and R. Kahmann, unpublished). Furthermore, 14-day-old seedlings of the variety Early Golden Bantam were used to replace Gaspé Flint, which retained similar phenotypic difference. In this thesis, most of the plant infection experiments with CL13 strains were performed with 14-days-old seedlings of Early Golden Bantam unless special indication.

2.1 Unique features are revealed from the crystal structure of Cmu1

Structural comparison between Cmu1 and yeast Aro7p revealed that there are several unique features that only exist in Cmu1, such as a surface exposed acidic patch, the disulfide bond, the fatty acid binding and the long loop on the surface of the structure (J. Schuhmacher and G. Bange, unpublished). In this chapter, structure-directed mutagenesis was performed to investigate the possible roles of respective features.

2.1.1 The surface exposed acidic patch is dispensable for the function of Cmu1

2.1.1.1 An acidic patch is found on the surface of Cmu1

The first half of H1 helix in the N-terminal region of Cmu1 is surprisingly rich in acidic residues, consisting of E29, E32, E34, D37, D40 and D44. The electrostatic surface potential of Cmu1 revealed that these residues form a surface-exposed acidic patch together with D196 and D200 from H5 and H6 helices, respectively (**Fig. 5**). However, the acidic patch was absent in Aro7p, suggesting that it might be important for the function of Cmu1.

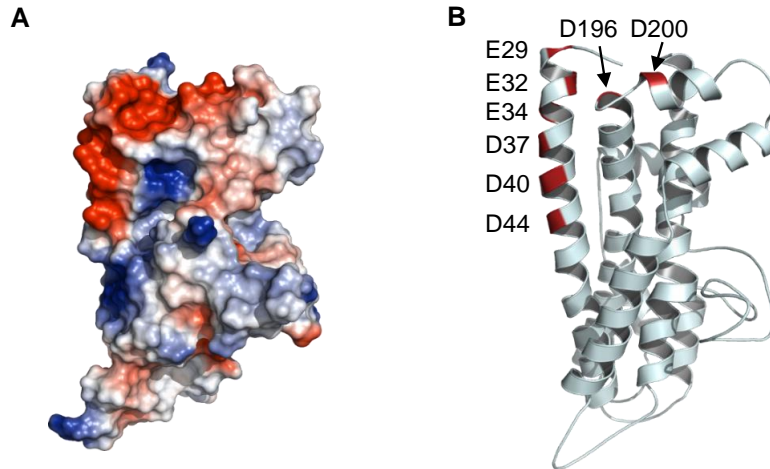


Fig. 5: An acidic patch is localized on the surface of the structure of Cmu1. **A.** Electrostatic potential (red is negative, blue is positive) highlights the position of the acidic patch in Cmu1. **B.** Eight acidic residues constituting the acidic patch are labeled and shown in dark red.

2.1.1.2 The truncation in the N-terminus of Cmu1 leads to instability of Cmu1

Previous study revealed that an N-terminal region of 19 amino acids (residues 22-40) downstream of the SP was not required for *cmu1* to complement a *S. cerevisiae aro7* mutant (A. Ghosh and R. Kahmann, unpublished). Although the mechanism underlying effector translocation of filamentous pathogens still remains unclear and controversial (Tyler et al., 2013; Wawra et al., 2013), there are a number of studies implicating the N-terminal region downstream of the SP of filamentous pathogen effectors in their translocation into plant cells (Whisson et al., 2007; Manning et al., 2008; Rafiqi et al., 2010; Schornack et al., 2010b; Petre and Kamoun, 2014). It was therefore an alternative possibility that this region might be required for translocation. In this region are E29, E32, E34, D37 and D40, which make up the acidic patch (Fig. 5).

To elucidate the role of residues 22-40 in the function of Cmu1, an HA-tagged truncated allele lacking this region was generated and introduced into the *ip* locus of CL13 Δ cmu1 in single copy (Keon et al., 1991). The complemented strain CL13 Δ cmu1-Cmu1 Δ^{22-40} -HA₃ was analyzed in plant infection experiments with 14-days-old seedlings of Gaspé Flint. Interestingly, Cmu1 Δ^{22-40} -HA₃ was only partially able to complement the phenotype of the deletion strain CL13 Δ cmu1 compared to Cmu1-HA₃ (Fig. 6A). To explain the inability of Cmu1 Δ^{22-40} -HA₃ in full complementation of CL13 Δ cmu1, the plant leaf samples were harvested from maize seedlings infected with respective strains 7 dpi. Western blot analysis was carried out with plant lysates to determine total amount of Cmu1 proteins produced during infection. Unexpectedly, compared to Cmu1 Δ^{SP} -HA₃, much less Cmu1 Δ^{41-290} -HA₃ was detected from the plant lysates (Fig. 6B), indicating that the truncation in the

N-terminus rendered Cmu1 unstable.

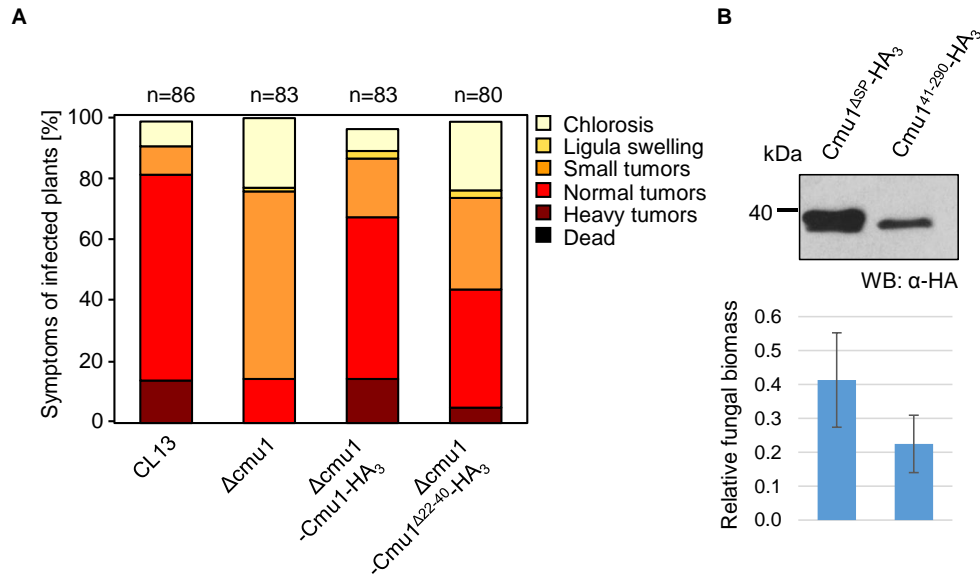


Fig. 6: The truncated Cmu1 does not fully complement the CL13 Δ Cmu1 virulence phenotype due to its instability. **A.** Infection symptoms on maize seedlings infected with CL13, the deletion strain CL13 Δ Cmu1 and complementation strains CL13 Δ Cmu1-Cmu1-HA₃ and CL13 Δ Cmu1-Cmu1 ^{Δ 22-40}-HA₃. Infection symptoms were evaluated 12 dpi. The respective symptom categories are depicted on the upper right side of the diagram. Mean values were calculated from three independent replicates. The total number (n) of plants is depicted above each column. **B.** Upper: Western blot analysis was performed with total cell lysates from leaf materials that were infected with respective complementation strains 7 dpi. Cmu1 ^{Δ SP}-HA₃ and Cmu1⁴¹⁻²⁹⁰-HA₃ were detected with the HA antibody. The molecular mass marker is depicted on the left. Lower: Relative fungal biomass of infected materials that were used in the western blot experiment was determined by qPCR. gDNA of infected plant materials 7 dpi. The relative fungal biomass was estimated by the abundance of fungal gene *ppi* that was normalized by the plant gene *gapdh*. Error bars indicate the standard deviation of three replicates.

2.1.1.3 Substitutions in the acidic patch do not affect the function of Cmu1

As Cmu1 ^{Δ 22-40} appeared to be unstable, making the assessment of its involvement in the function of Cmu1 such as translocation impossible. Therefore, a series of amino acid substitutions were introduced. To begin with, two residues D37 and D40 were chosen because they are conserved among secreted CMs from smut fungi (Fig. 7).

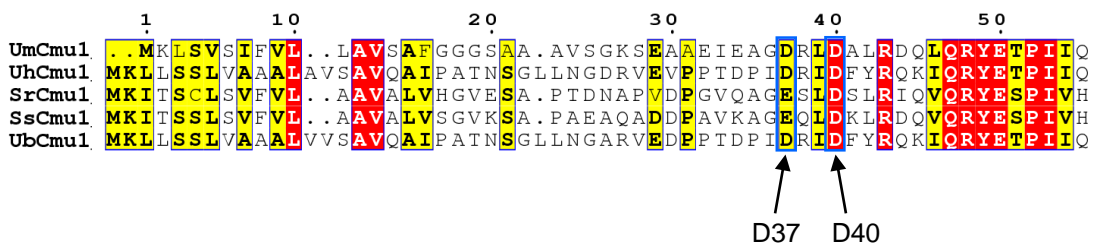
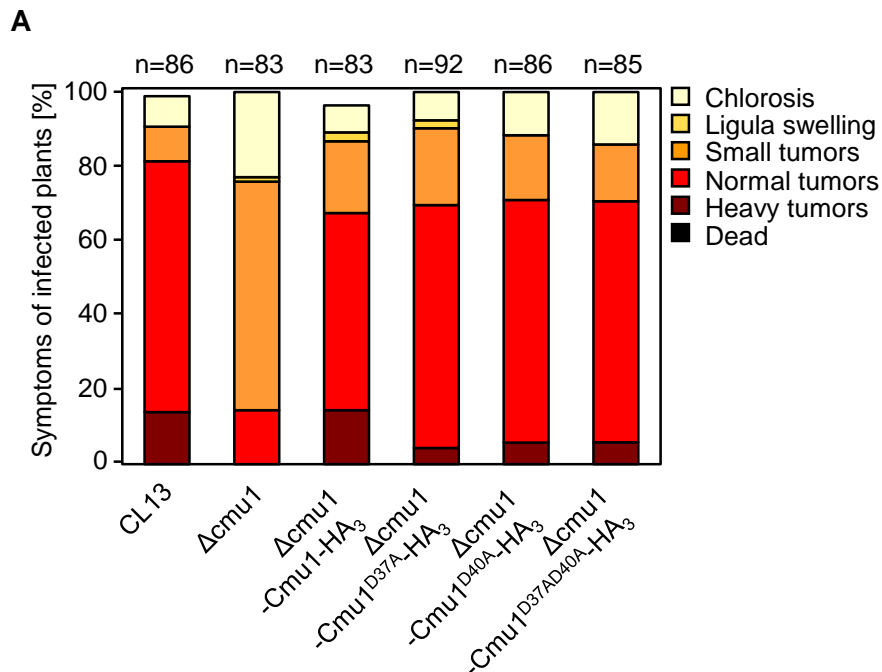


Fig. 7: D37 and D40 are conserved among secreted CMs from smut fungi. Partial amino acid sequence alignment of UmCmu1 with four orthologues SrCmu1 (CBQ69595.1) in *Sporisorium reilianum*, SsCmu1 (CDW96772.1) in *S. scitamineum*, UhCmu1 (CCF49464.1) in *U. hordei* and UbCmu1 (SAM85328.1) in *U. bromivora*. Red background indicates amino acid sequence identity, yellow background in bold letters indicates sequence similarity. Two conserved acidic amino acids are highlighted with blue boxes and labeled. The alignment was generated with CLUSTAL Omega (Sievers et al., 2011) and ESPript 3.0 (Robert and Gouet, 2014).

These two residues were substituted with alanine, and the mutant allele was introduced into CL13 Δ cmu1 with a single copy. In comparison to CL13 and CL13 Δ cmu1-Cmu1-HA₃, no significant difference in virulence could be observed for CL13 Δ cmu1-Cmu1^{D37A}-HA₃, CL13 Δ cmu1-Cmu1^{D40A}-HA₃ or CL13 Δ cmu1-Cmu1^{D37AD40A}-HA₃ (**Fig. 8A**). Subsequently, six substitutions were made in the acidic patch designated Cmu1^{6A} (E29A, E32A, E34A, D37A, D40A and D200A). In plant infection experiments, CL13 Δ cmu1 expressing Cmu1^{6A}-HA₃ showed comparable virulence to CL13 and CL13 Δ cmu1-Cmu1-HA₃ (**Fig. 8B**). Finally, all eight acidic residues in the acidic patch were substituted with alanine (Cmu1^{8A}), which was introduced into CL13 Δ cmu1. However, Cmu1^{8A}-HA₃ was still able to fully complement CL13 Δ cmu1 like Cmu1-HA₃ (**Fig. 8B**). Collectively, the acidic patch on the surface appears to be dispensable for the function of Cmu1, i.e. it is not likely to be involved in translocation of Cmu1.



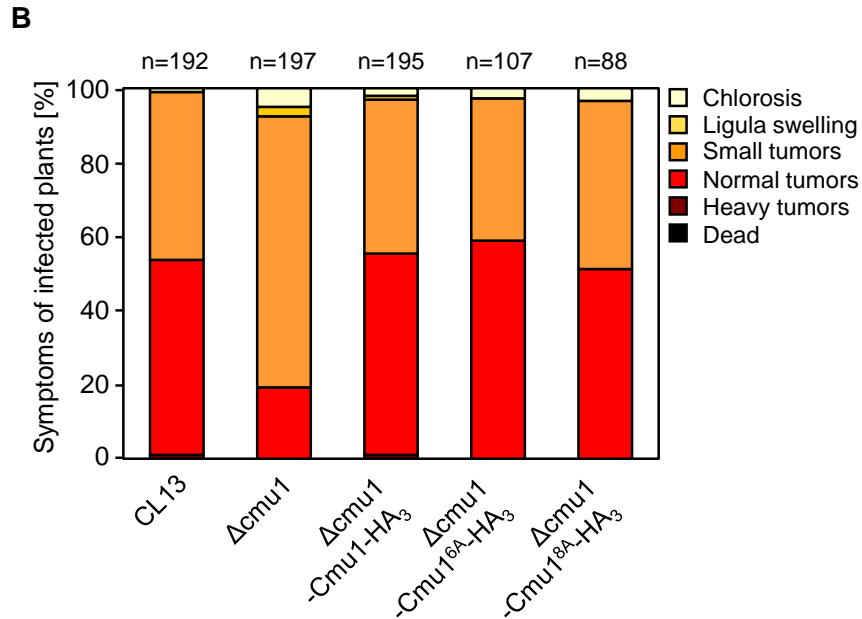


Fig. 8: Substitutions in the surface acid patch do not affect the function of Cmu1. **A.** Infection symptoms on maize seedlings infected with CL13, the deletion strain CL13 Δ cmu1 and complementation strains CL13 Δ cmu1-Cmu1-HA₃, CL13 Δ cmu1-Cmu1^{D37A}-HA₃, CL13 Δ cmu1-Cmu1^{D40A}-HA₃ and CL13 Δ cmu1-Cmu1^{D37AD40A}-HA₃. Infection symptoms were evaluated 12 dpi. The respective symptom categories are depicted on the upper right side of the diagram. The mean values were calculated from three independent replicates. The total number (n) of plants is depicted above each column. **B.** Infection symptoms on maize seedlings infected with CL13, the deletion strain CL13 Δ cmu1 and complementation strains CL13 Δ cmu1-Cmu1-HA₃, CL13 Δ cmu1-Cmu1^{6A}-HA₃ and CL13 Δ cmu1-Cmu1^{8A}-HA₃. Infection symptoms were evaluated 12 dpi. The respective symptom categories are depicted on the upper right side of the diagram. The mean values were calculated from at least three independent replicates. The total number (n) of plants is depicted above each column.

2.1.2 Disruption of disulfide bond does not impair the function of Cmu1

2.1.2.1 A disulfide bond is conserved among secreted CMs of smut fungi

Disulfide bonds are formed by two cysteine residues and common in secreted proteins to maintain their tertiary structures in the harsh extracellular environment (Sevier and Kaiser, 2002). As for effectors from filamentous plant pathogens, apoplastic and translocated effectors are likely exposed to proteases in the plant apoplast (Jashni et al., 2015). A common feature for effectors of plant pathogenic fungi is therefore a compact structure due to the presence of disulfide bonds (van den Burg et al., 2003; Kamoun, 2006; de Wit et al., 2009; Liu et al., 2009; de Guillen et al., 2015; Jashni et al., 2015; Kohler et al., 2016). While cytoplasmic CMs mostly lack disulfide bonds, secreted CMs from the *Mycobacterium tuberculosis* and the beet cyst nematode *Heterodera schachtii* contain one and four disulfide bonds, respectively (Okvist et al., 2006; Vanholme et al., 2009).

Similarly, a disulfide bond is formed by C203 and C289 in the structure of Cmu1 (**Fig. 9A**). Interestingly, multiple sequence alignment reveals that this disulfide bond is conserved among secreted CMs from smut fungi (**Fig. 9B**), suggesting that the disulfide bond might be playing a role in stabilizing Cmu1.

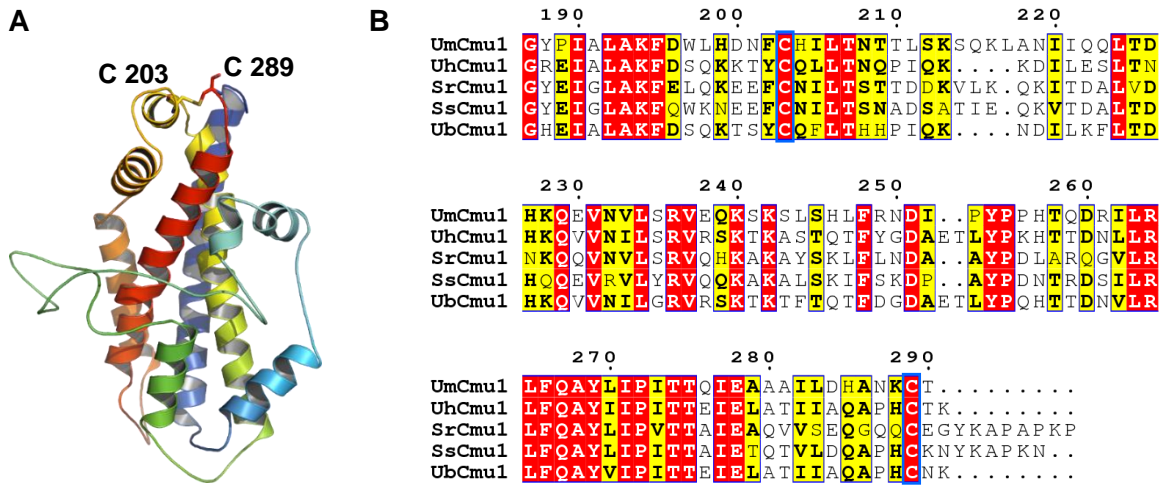


Fig. 9: The disulfide bond is conserved among smut secreted CMs. **A.** The disulfide bond formed by cysteines 203 and 289 is shown as sticks. **B.** Partial amino acid sequence alignment of UmCmu1 with four orthologues SrCmu1, SsCmu1, UhCmu1 and UbCmu1. Red background indicates amino acid sequence identity, yellow background in bold letters indicates sequence similarity. Two conserved cysteines are highlighted with blue boxes. The alignment was generated with CLUSTAL Omega (Sievers et al., 2011) and ESPript 3.0 (Robert and Gouet, 2014).

2.1.2.2 The disulfide bond is not required for the stability of Cmu1

To determine the function of the C203-C289 disulfide bond in Cmu1, cysteines C203 and C289 were both substituted with serine (Cmu1^{SS}) and CL13Δcmu1 was complemented with the mutant allele after single copy integration in the *ip* locus. CL13Δcmu1-Cmu1^{SS}-HA₃ still showed comparable virulence to CL13 or CL13Δcmu1-Cmu1-HA₃ in the plant infection experiments (**Fig. 10A**). Western blot analysis showed that the stability of Cmu1^{SS}-HA₃ was comparable to that of Cmu1-HA₃ (**Fig. 10B**).

However, it was surprising that Cmu1^{ΔSP/SS}-HA₃ migrated more slowly than Cmu1^{ΔSP}-HA₃. *In silico* prediction with NetNGlyc 1.0 showed that Cmu1 harbors two putative N-glycosylation sites (¹⁵⁹NQSS¹⁶² and ²⁰⁸NTTL²¹¹). After substitution of two cysteines with serine, another two putative N-glycosylation sites (²⁰¹NFSH²⁰⁴ and ²⁸⁷NKST²⁹⁰) are predicted, which may explain the migration difference. To substantiate the hypothesis, de-N-glycosylation of HA-tagged Cmu1 proteins immuno-precipitated from total plant lysate was performed using PNGase F (NEB). After de-

glycosylation of Cmu1^{ΔSP}-HA₃ and Cmu1^{ΔSP/SS}-HA₃, the migration difference was lost (**Fig. 10C**). This observation indicates that the disruption of the disulfide bond with serine substitutions does not affect the stability of the protein, but make the protein more accessible to glycans.

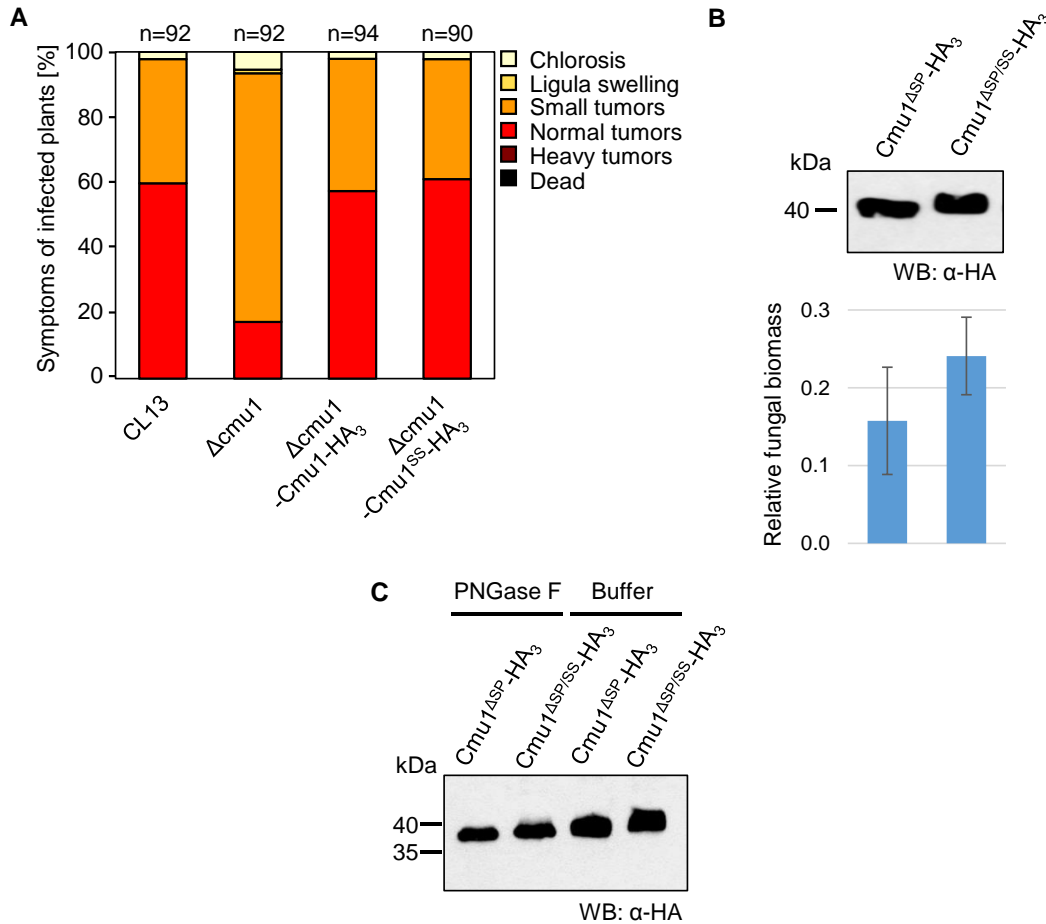


Fig. 10: The disulfide bond is dispensable for the function of Cmu1. **A.** Infection symptoms on maize seedlings infected with CL13, the deletion strain CL13Δcmu1 and complementation strains CL13Δcmu1-Cmu1-HA₃ and CL13Δcmu1-Cmu1^{SS}-HA₃. Infection symptoms were evaluated 12 dpi. The respective symptom categories are depicted on the upper right side of the diagram. The mean values were calculated from three independent replicates. The total number (n) of plants is depicted above each column. **B.** Upper: Western blot analysis was performed with total lysates from leaf materials that were infected with respective complementation strains 7 dpi. Cmu1^{ΔSP}-HA₃ and Cmu1^{ΔSP/SS}-HA₃ were detected with the HA antibody. The molecular mass marker is depicted on the left. Lower: Relative fungal biomass of infected materials that were used in the western blot experiment was determined by qPCR. gDNA of infected plant materials 7 dpi. The relative fungal biomass was estimated by the abundance of fungal gene *ppi* that was normalized by the plant gene *gapdh*. Error bars indicate the standard deviation of three replicates. **C.** Cmu1^{ΔSP}-HA₃ and Cmu1^{ΔSP/SS}-HA₃ were immuno-precipitated from total lysates of leaf materials that were infected with respective complementation strains with HA agarose beads. Cmu1^{ΔSP}-HA₃ and Cmu1^{ΔSP/SS}-HA₃ were treated with PNGase F. As negative control, PNGase F was omitted in the reactions. Cmu1^{ΔSP}-HA₃ and Cmu1^{ΔSP/SS}-HA₃ were detected with the HA antibody. The molecular mass marker is depicted on the left.

2.1.3 The abolishment of fatty acid binding has no effect on the function of Cmu1

For the structure determination of Cmu1, the protein was heterologously produced in *E. coli*. Surprisingly, a fatty acid like molecule co-crystallized with Cmu1 (**Fig. 11A**, modeled with oleic acid, J. Schuhmacher and G. Bange, unpublished). Although the structure of the small molecule was not yet solved, the electron density map modeled with unsaturated oleic acid displayed good density (J. Schuhmacher and G. Bange, unpublished). In order to explore whether or not the fatty acid binding is needed for the function of Cmu1, two substitutions V74K and L107Y were introduced to abolish the binding, yielding the mutant Cmu1^{KY} (**Fig. 11B**). The crystal structure of Cmu1^{KY} was solved, showing that the crystal no longer contained the fatty acid molecule (J. Schuhmacher and G. Bange, unpublished). To assess the functional relevance of fatty acid binding, *cmu1*^{KY} was inserted in the *ip* locus of CL13 Δ *cmu1* in single copy. The virulence of CL13 Δ *cmu1*-Cmu1^{KY}-HA₃ was determined in plant infection experiments. However, no significant difference could be seen between CL13 Δ *cmu1*-Cmu1^{KY}-HA₃ and CL13 Δ *cmu1*-Cmu1-HA₃, pointing out that fatty acid binding was not relevant for the biological function of Cmu1 (**Fig. 11C**).

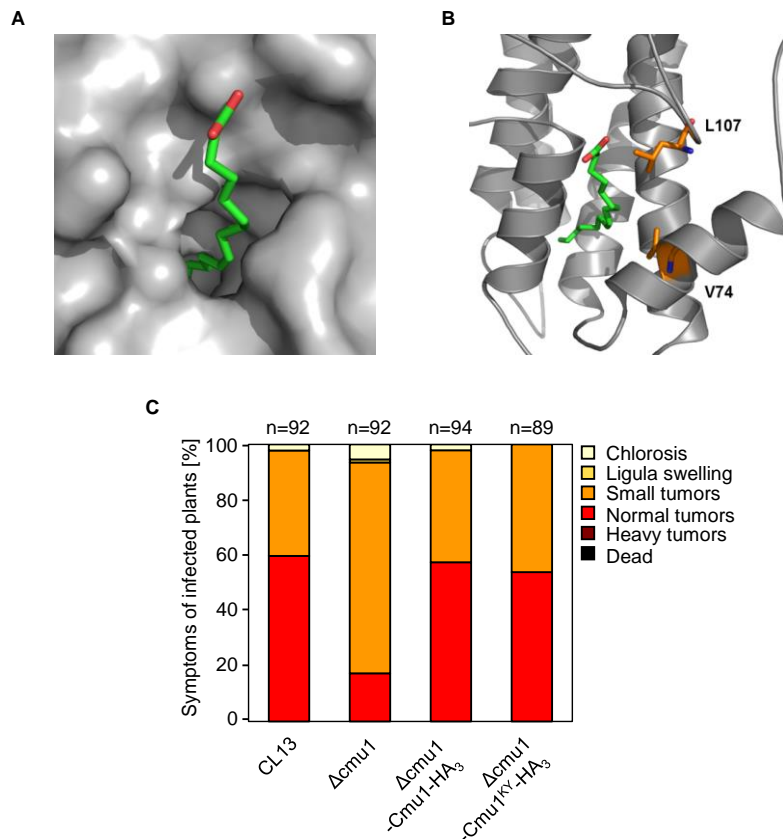


Fig. 11: A fatty acid like molecule is bound to Cmu1, but its abolishment does not impair the function of Cmu1. **A.** A fatty acid like molecule was found during the crystallization of Cmu1. The binding of the molecule in the cavity was modeled with oleic acid, which is shown in green sticks. **B.** Two residues that are predicted to be implicated in the binding are shown in orange sticks. **C.** Infection symptoms on maize seedlings infected with CL13, the deletion strain CL13 Δ Cmu1 and complementation strains CL13 Δ Cmu1-Cmu1-HA₃ and CL13 Δ Cmu1-Cmu1^{KY}-HA₃. Infection symptoms were evaluated 12 dpi. The respective symptom categories are depicted on the upper right side of the diagram. The mean values were calculated from three independent replicates. The total number (n) of plants is depicted above each column.

2.1.4 A long loop region is required for the full function of Cmu1

2.1.4.1 A long loop region is unique to Cmu1 and conserved among secreted CMs from smut fungi

Structural comparison of Cmu1 and Aro7p revealed a long loop region composed of 52 amino acids (residues 95-146) that is unique to Cmu1, while the corresponding region in Aro7p is highly distinct (**Fig. 12A**, J. Schuhmacher and G. Bange, unpublished). This region displays 56%-66% amino acid sequence identity among Cmu1 and its orthologues from smut fungi, whereas only 5%-18% amino acid sequence identity was observed when comparing the respective regions in non-secreted CMs with Cmu1 (**Fig. 12B**). Loops in proteins not only connect different domains or structures, but also play a critical role in protein-protein interactions, ligand binding, conformational dynamics, allosteric regulation and enzymatic catalysis (Espadaler et al., 2006; Papaleo et al., 2016). It is possible that the loop region might contribute to the function of Cmu1.

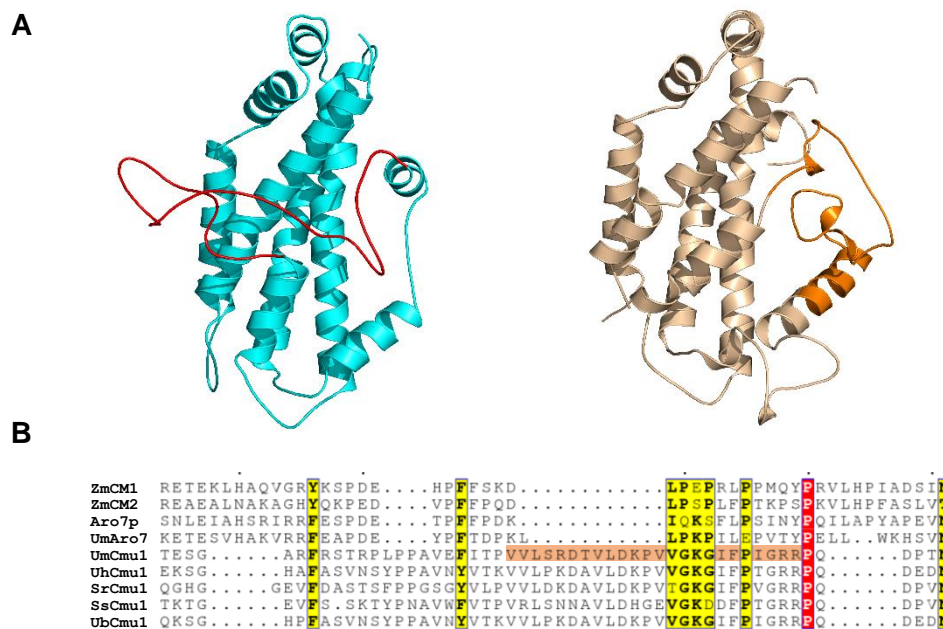


Fig. 12: The loop region of Cmu1 is conserved among smut secreted CMs. **A.** Left: The structure of Cmu1 is shown in cyan. The long loop region (residues 95-146) is highlighted in red; Right: The structure

of Aro7p is shown in tan. The region corresponding to loop of Cmu1 is highlighted in orange. **B.** Amino acid sequence alignment of the loop region (95-146) in UmCmu1 and the corresponding regions in other CMs, including non-secreted CMs including ZmCM1, ZmCM2, Aro7p and UmAro7 and secreted CMs including UhCmu1, SrCmu1, ScCmu1 and UbCmu1. Red background indicates amino acid sequence identity, yellow background in bold letters indicates sequence similarity. The residues shaded in orange (117-140) in Cmu1 was replaced with a GSGS linker. The alignment was generated with CLUSTAL Omega (Sievers et al., 2011) and ESPript 3.0 (Robert and Gouet, 2014).

2.1.4.2 Shortening of the loop region affects the function of Cmu1

To elucidate the function of the loop region, truncation in the loop region was performed. A short GSGS linker was used to replace amino acids 117-140 of Cmu1 to avoid damaging the overall structure of Cmu1 (**Fig. 12B**). The mutant allele *cmu1*^{Δ117-140} was introduced in the *ip* locus of CL13Δ*cmu1* in single copy. In the plant infection experiments, four independent strains expressing Cmu1^{Δ117-140}-HA₃ exhibited reduced virulence in comparison to CL13 or CL13Δ*cmu1*-Cmu1-HA₃ (**Fig. 13A**), demonstrating that Cmu1^{ΔSPΔ117-140}-HA₃ has partially biological activity. To rule out that the virulence defect was due to instability of Cmu1^{ΔSPΔ117-140}-HA₃, western blot analysis was carried out to determine the amount of Cmu1 proteins in respective infected plant material. The result showed that Cmu1^{ΔSP}-HA₃ and Cmu1^{ΔSPΔ117-140}-HA₃ were produced in comparable amounts during plant infection (**Fig. 13B**).

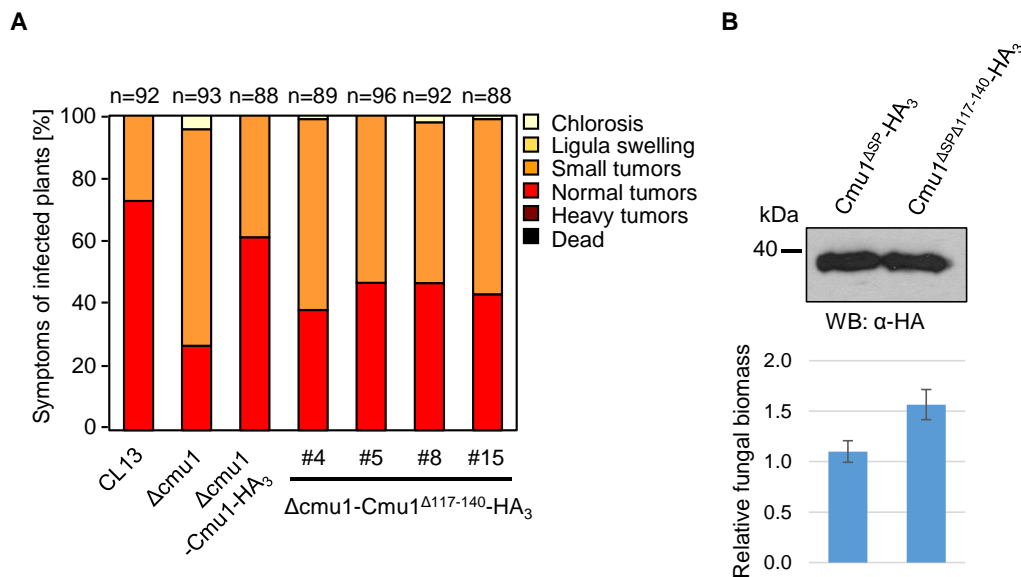


Fig. 13: The loop region of Cmu1 is required for the full virulence. **A.** Infection symptoms on maize seedlings infected with CL13, the deletion strain CL13Δ*cmu1* and complementation strains CL13Δ*cmu1*-Cmu1-HA₃ and four independent CL13Δ*cmu1*-Cmu1^{Δ117-140}-HA₃ strains. Infection symptoms were evaluated 12 dpi. The respective symptom categories are depicted on the upper right side of the diagram. The mean values were calculated from three independent replicates. The total number (n) of plants is depicted above each column. **B.** Upper: Western blot analysis was performed with total lysates from leaf

materials that were infected with respective complementation strains 7 dpi. $Cmu1^{\Delta SP}$ -HA₃ and $Cmu1^{\Delta SP\Delta 117-140}$ -HA₃ were detected with the HA antibody. The molecular mass marker is depicted on the right. Lower: Relative fungal biomass of infected materials that were used in the western blot experiment was determined by qPCR. gDNA of infected plant materials 7 dpi. The relative fungal biomass was estimated by the abundance of fungal gene *ppi* that was normalized by the plant gene *gapdh*. Error bars indicate the standard deviation of three replicates.

2.2 Biochemical characterization of Cmu1 and selected mutants

2.2.1 The allosteric site of Cmu1 possesses a novel fold

Allosteric regulation is a characteristic of some CMs such as Aro7p from yeast. The catalytic site of Aro7p binds the substrate chorismate, while the allosteric site binds allosteric regulators tryptophan and tyrosine (Helmstaedt et al., 2001). The catalytic site of Aro7p consists of four helices H2, H8, H11, and H12, which correspond to helices H1, H5, H8 and H9 of Cmu1. Five critical residues R16, R157, K168, E198 and E246 constituting the active site of Aro7p are all well conserved in Cmu1 (**Fig. 14A**). Although the structure of Cmu1 shows high similarity to Aro7p in the catalytic site, the allosteric sites in two proteins are divergent. The allosteric site of Cmu1 seems to have a novel topology compared to that of Aro7p (**Fig. 14B**), which indicates that Cmu1 might have evolved a different mechanism for regulating its CM activity.

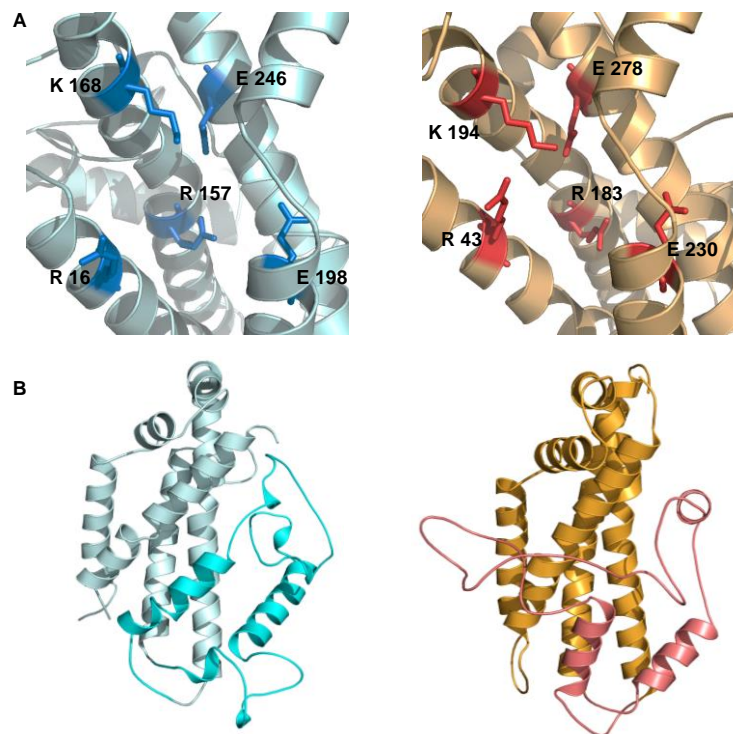


Fig. 14: Comparison of Aro7p and Cmu1 structures. A. Left: active site of Aro7p. The structure of Aro7p is shown in turquoise. Five crucial residues are highlighted by blue sticks. Right: active site of Cmu1. The

structure of Cmu1 is shown in tan. Five crucial residues are highlighted by red sticks. **B.** Left: overview of the allosteric site of Aro7p. The structure of Aro7p is shown in turquoise. The allosteric site is indicated in cyan. Right: overview of the allosteric site of Cmu1. The structure of Cmu1 is shown in tan. The allosteric site is indicated in salmon.

2.2.2 The kinetics of Cmu1 purified from *E. coli*

2.2.2.1 Purification of Cmu1^{ASP}-His₆

To overexpress recombinant Cmu1^{ASP} with a C-terminal His₆-tag, *E. coli* BL21 star (DE3) strain was transformed with pET-Cmu1^{ASP}, which carries a codon-optimized *cmu1* gene without SP (A. Djamei and R. Kahmann, unpublished). The purification of Cmu1^{ASP}-His₆ was carried out following a two-step procedure consisting of Ni-NTA affinity chromatography and subsequent size exclusion chromatography (SEC) (**Fig. 15**). The purity of Cmu1^{ASP}-His₆ was analyzed by SDS-PAGE and the concentration was determined using the absorbance at 280 nm with a NanoDrop spectrophotometer.

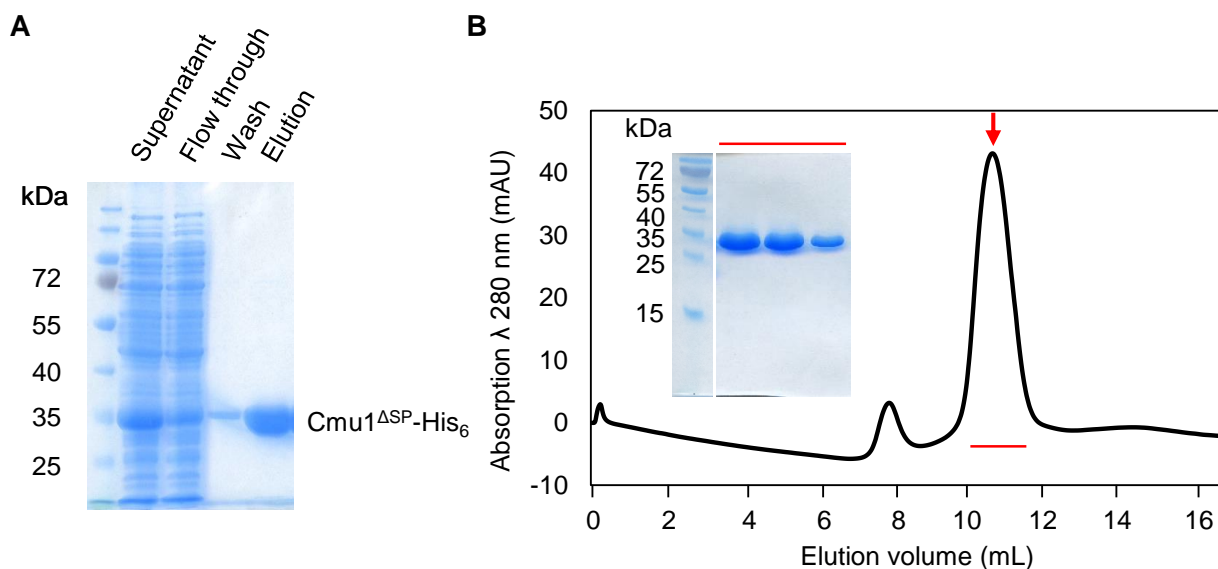


Fig. 15: Purification of Cmu1^{ASP}-His₆. **A.** BL21 star (DE3) transformed with pET-Cmu1^{ASP} was induced for 16 h in the presence of lactose. Cells were lysed and clarified. The supernatant was subjected to Ni-NTA affinity purification. Indicated fractions were separated by SDS-PAGE and stained by Instant blue solution. The molecular mass marker is depicted on the left. **B.** In size exclusion chromatography, Cmu1^{ASP}-His₆ forms the peak indicated by the red arrow. The peak fractions indicated with a red line were pooled and confirmed by SDS-PAGE (inlay), demonstrating that the Cmu1^{ASP}-His₆ is the main component in the peak fractions. The molecular mass marker is depicted on the left.

2.2.2.2 Kinetics of Cmu1^{ASP}-His₆

In Djamei et al. (2011), CM activity of Cmu1 was determined using a “stop assay” by measuring

the appearance of phenylpyruvate (converted from prephenate) at 320 nm. In this thesis, the CM activity of Cmu1 was re-visited with an “online assay” by monitoring the disappearance of chorismate at 274 nm (Kane et al., 1971; Sasso et al., 2005; Westfall et al., 2014). The kinetic parameters were determined for His-tagged Cmu1 proteins purified from *E. coli* (**Table 1**). The purified Cmu1^{ASP}-His₆ follows Michaelis-Menten Kinetics (**Fig. 16**), of which the K_m for chorismate is 0.96 ± 0.12 mM in the presence of 100 ng protein at 30°C and pH 7.5. The turnover rate (k_{cat}) of Cmu1^{ASP}-His₆ (11.2 ± 0.53 s⁻¹) was 10-fold slower than that of Aro7p (110 s⁻¹) (Helmstaedt et al., 2002), indicating that Cmu1 is less active than Aro7p.

Table 1. Kinetic parameters of Cmu1^{ASP}-His₆

	K_m (mM) *	k_{cat} (s ⁻¹) *	k_{cat}/K_m (mM ⁻¹ s ⁻¹)
Cmu1 ^{ASP} -His ₆	0.96 ± 0.12	11.2 ± 0.53	11.7

* Standard deviations (\pm) were calculated from three replicates.

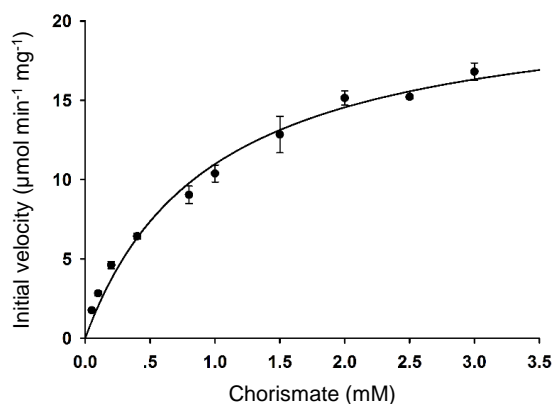


Fig. 16: Steady-state kinetic analysis of Cmu1^{ASP}-His₆. Velocity versus substrate curve is shown. The data were fit to the Michaelis-Menten-type saturation. The activity of CMs was determined by measuring the rate of chorismate disappearance at 274 nm. The amount of Cmu1^{ASP}-His₆ used in the reactions was 100 ng. Chorismate used in the reactions varied from 0 mM to 3 mM. Error bars indicate the standard deviation of three replicates.

2.2.2.3 Comparison of the CM activity of Cmu1 with selected variants

To investigate whether the bound fatty acid alters CM activity of Cmu1, Cmu1^{ASP/KY}-His₆ carrying V74K and L107Y was expressed in *E. coli* and purified following the same protocol as used for Cmu1^{ASP}-His₆. Cmu1^{ASP/KY}-His₆ showed no significant difference in kinetics compared to

Cmu1^{ASP}-His₆ (**Fig. 17A**).

Since Cmu1^{Δ117-140} was only partially biologically active, it was necessary to determine whether the CM activity of Cmu1 was affected when the loop region was partially deleted. To this end, Cmu1^{ASPΔ117-140}-His₆ with the region 117-140 replaced by a GSGS linker was purified from *E. coli*. However, Cmu1^{ASPΔ117-140}-His₆ displayed comparable CM activity to Cmu1^{ASP}-His₆ (**Fig. 17B**), which suggested that the defect of Cmu1^{Δ117-140} in complementing CL13Δcmu1 might be caused by other factors.

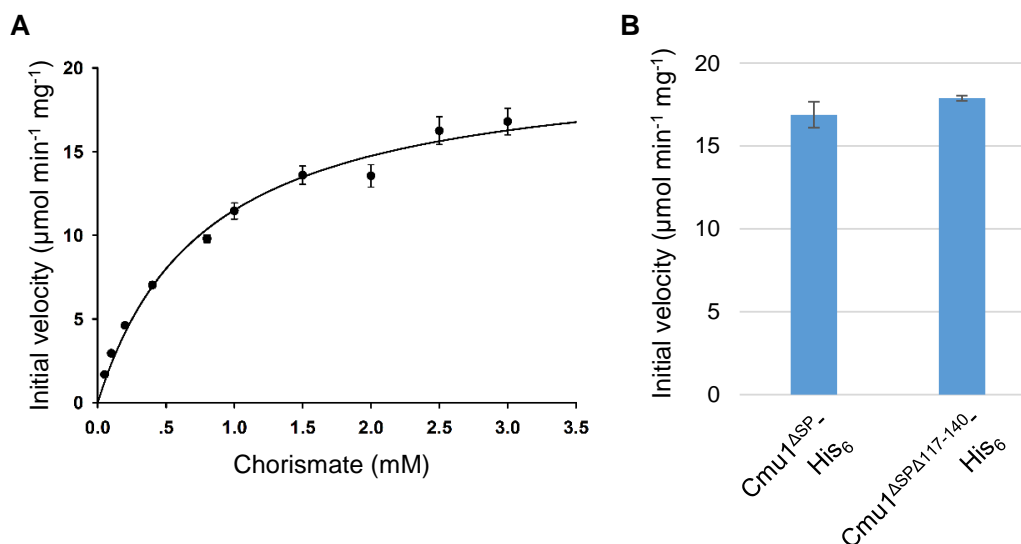


Fig. 17: Comparison of the CM activity of Cmu1^{ASP} with Cmu1^{ASP/KY} and Cmu1^{ASPΔ117-140}. **A.** Steady-state kinetic analysis of Cmu1^{ASP/KY}-His₆. Velocity versus substrate curve is shown. The data were fit to the Michaelis-Menten-type saturation. The activity of CMs was determined by measuring the rate of chorismate disappearance at 274 nm. The amount of Cmu1^{ASP/KY}-His₆ used in the reactions was 100 ng. Chorismate used in the reactions varied from 0 mM to 3 mM. Error bars indicate the standard deviation of three replicates. **B.** The activity of CMs was determined by measuring the rate of chorismate disappearance at 274 nm. The amount of Cmu1^{ASP}-His₆ or Cmu1^{ASPΔ117-140}-His₆ used in the reactions was 100 ng. Chorismate used in each reaction was 0.5 mM. Error bars indicate the standard deviation of three replicates.

2.2.3 The CM activity of Cmu1 is not activated by tryptophan

The CM activity of Aro7p from yeast is activated by the addition of tryptophan (Schnappauf et al., 1998). Cmu1 was previously reported to be not responsive to tryptophan, tyrosine and phenylalanine assayed with the “stop assay” (Djamei et al., 2011). By using the “online assay”, the effect of tryptophan on the activity of Cmu1 was re-examined (Kane et al., 1971; Sasso et al., 2005). As positive control, Aro7p-His₆ was shown to have at least 10 fold higher activity in the presence of 10 μM tryptophan (**Fig. 18A**). However, the same amount of tryptophan had no significant effect on the CM activity of Cmu1^{ASP}, and even when the concentration of tryptophan was increased to

100 μM , no significant increase in activity was observed (**Fig. 18B**).

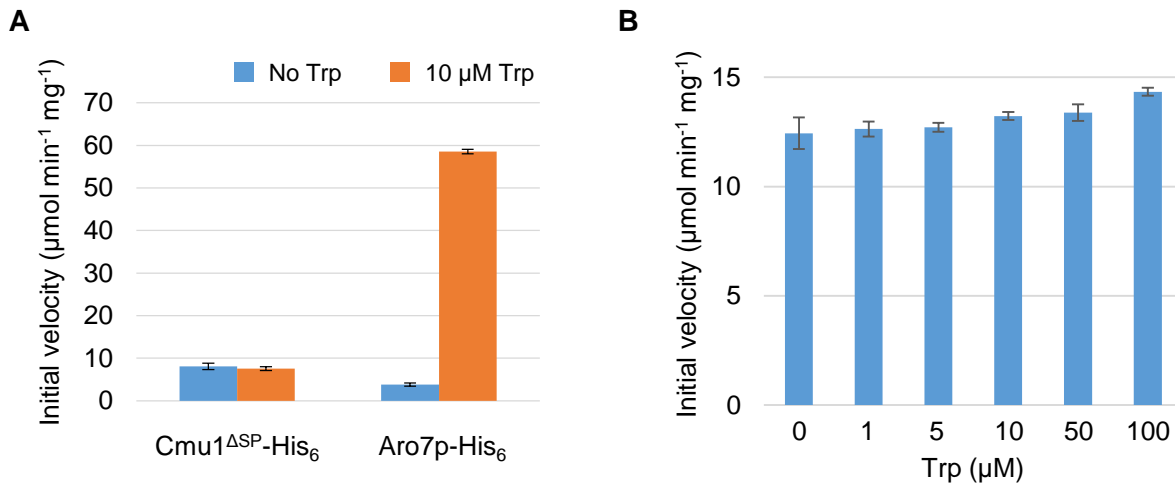


Fig. 18: Tryptophan has no effect on the CM activity of Cmu1^{ΔSP}-His₆. **A.** The CM activities of Cmu1^{ΔSP} and Aro7p were determined with or without 10 μM tryptophan (Trp). The activity of CMs was determined by measuring the rate of chorismate disappearance at 274 nm. The amount of Cmu1^{ΔSP}-His₆ or Aro7p-His₆ used in the reactions was 100 ng. Chorismate used in each reaction was 0.5 mM. Error bars indicate the standard deviation of three replicates. **B.** The activity of Cmu1^{ΔSP}-His₆ was determined by measuring the velocity of decrease in absorbance at 274 nm. The concentration of tryptophan added to the reaction varied from 0 μM to 100 μM . The amount of Cmu1^{ΔSP}-His₆ used in the reactions was 100 ng. Chorismate used in each reaction was 0.5 mM. Error bars indicate the standard deviation of three replicates.

2.3 Putative interplay between a secreted chorismate mutase, an isochorismatase and a salicylate hydroxylase in promoting virulence of *U. maydis*

The expression of *cmu1* is dramatically upregulated in the biotrophic phase of *U. maydis* (Djamei et al., 2011). However, *cmu1* deletion mutants only showed moderate reduction in virulence (Djamei et al., 2011), making it likely that other mechanisms exist to reduce SA levels in infected tissue. In addition to Cmu1, *U. maydis* was shown to produce a cytosolic salicylate hydroxylase Shy1 (Um05230), which is capable of degrading SA (Rabe et al., 2013). The expression of *shy1* is induced during colonization, implying that Shy1 has the potential to suppress SA signaling during infection (Rabe et al., 2013). Nevertheless, neither *shy1* deletion mutants nor *shy1/cmu1* double mutants exhibited pronounced virulence defect (Rabe et al., 2013). This raised the question whether additional proteins could be involved in dampening SA signaling.

Isochorismate plays a pivotal role in synthesizing SA via ICS pathway in plants (Dempsey et al., 2011). It was recently discovered that two unrelated plant pathogens *Phytophthora sojae* and

Verticillium dahliae utilize the same strategy to suppress SA accumulation (Liu et al., 2014). Isochorismatases PsIsc1 and VdIsc1, are unconventionally secreted by *P. sojae* and *V. dahliae*, respectively, translocate into plant cells and convert isochorismate to 2,3-dihydroxy-2,3-dihydrobenzoate (Liu et al., 2014). Transient expression of these two effectors in *Nicotiana benthamiana* tissue reduced SA levels and downstream plant defenses mediated by SA (Liu et al., 2014). Interestingly, an isochorismatase was also found to be encoded by *U. maydis*.

2.3.1 An isochorismatase Um12021 is encoded in *U. maydis*

Searching the PEDANT database (<http://pedant.helmholtz-muenchen.de/>) with amino acid sequence of VdIsc1 identified Um12021 in the genome of *U. maydis*. Um12021 harbors the isochorismatase domain predicted from Interpro and Pfam databases and displays 43% and 25% sequence identity to PsIsc1 and VdIsc1, respectively (Fig. 19). Catalytic activities and virulence functions of PsIsc1 and VdIsc1 depend on an Asp-Lys-Cys (D-K-C) catalytic triad (Liu et al., 2014), which is conserved in Um12021 as well (Fig. 19). This indicates that Um12021 is prone to be an isochorismatase. By SecretomeP 2.0 (<http://www.cbs.dtu.dk/services/SecretomeP/>) for the prediction of unconventional secretion, Um12021 has an NN score (neural network output scores) of 0.432, suggesting that Um12021 may also be unconventionally secreted and translocated to plant cells.

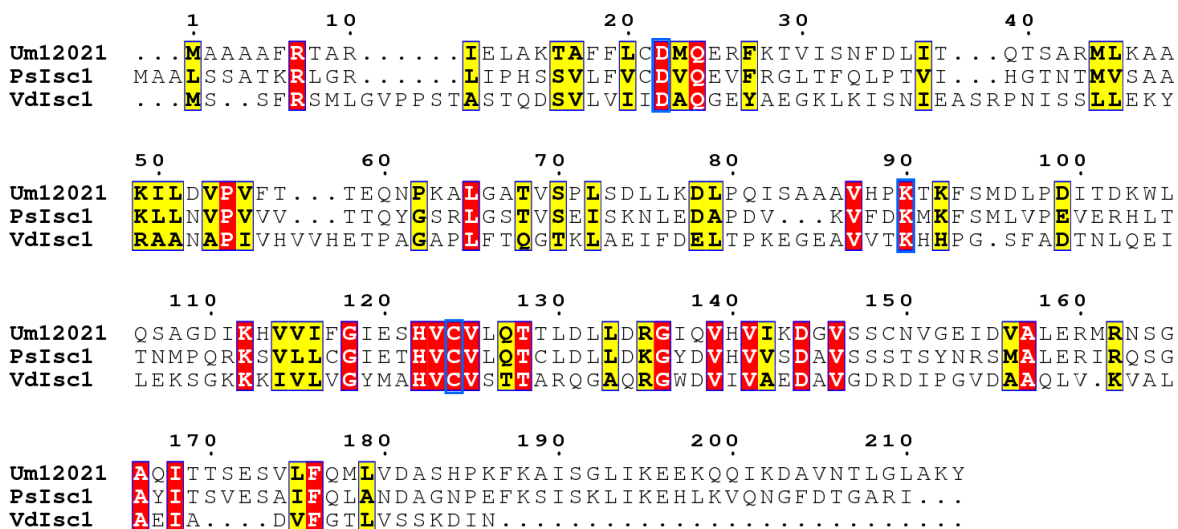


Fig. 19: Amino acid sequence alignment of Um12021 with PsIsc1 and VdIsc1. Red background indicates amino acid sequence identity, yellow background in bold letters indicates sequence similarity. Three conserved residues constituting the catalytic triad are highlighted with blue boxes. The alignment was generated with CLUSTAL Omega (Sievers et al., 2011) and ESPript 3.0 (Robert and Gouet, 2014).

2.3.2 *um12021* is not induced during the disease development of *U. maydis*

The expression pattern of *um12021* during biotrophic development of *U. maydis* was revealed by RNAseq expression profiling of FB1 × FB2 strains (D. Lanver, personal communication). The expression of *um12021* was highest in cells grown axenically, and transcripts were detected during all stages of biotrophic growth *in planta* (Fig. 20, D. Lanver, personal communication).

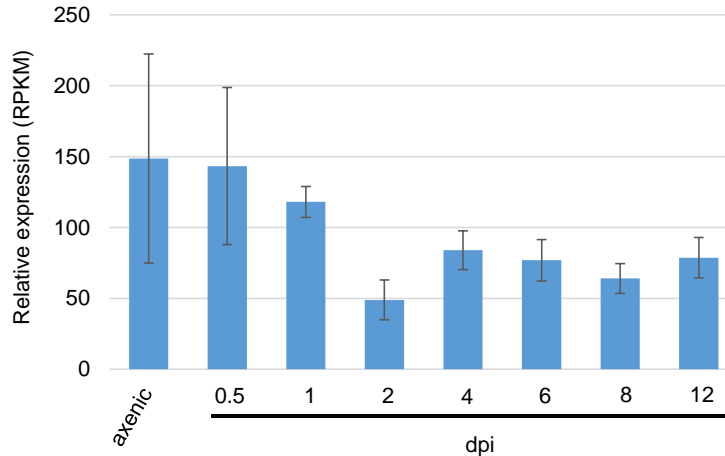


Fig. 20: Relative expression of *um12021* during biotrophic development. Relative expression of *um12021* was revealed by RNAseq analysis of FB1 and FB2 grown axenically and biotrophic stages of FB1 × FB2 (D. Lanver, personal communication). RNA samples of FB1 and FB2 were extracted from exponentially growing cells cultivated in YEPS_{light} medium and from FB1 × FB2 infected maize plants 0.5, 1, 2, 4, 6, 8 and 12 dpi. The vertical axis indicates the RNA reads per kilobase million reads (RPKM). The horizontal axis indicates the stages, i.e. axenic, 0.5, 1, 2, 4, 6, 8 and 12 dpi. Error bars indicate standard deviation of three biological replicates.

2.3.3 *Cmu1*, *Shy1* and *Um12021* might be functionally redundant

Since *Um12021* is a putative isochorismatase, it may contribute to lowering SA levels in *U. maydis* infected tissue together with *Cmu1*. To test this, *um12021* was deleted in the *U. maydis* SG200Δ*cmu1* strain. In comparison to SG200 and SG200Δ*cmu1*, there was no significant difference in virulence detected in SG200Δ*cmu1*Δ*um12021*. To further test the possibility that *Cmu1*, *Shy1* and *Um12021* cooperate in lowering SA levels, the *shy1* gene (*um05230*) was inactivated in SG200Δ*cmu1*Δ*um12021* double mutant using the CRISPR-Cas9 system (Schuster et al., 2016). Introduction of a frame-shift mutation was verified by sequencing. The triple mutant SG200Δ*cmu1*Δ*um12021**um05230*^{en} was assessed for virulence. Compared with SG200, SG200Δ*cmu1* and SG200Δ*cmu1*Δ*um12021*, SG200Δ*cmu1*Δ*um12021**um05230*^{en} was more reduced in virulence, causing fewer heavy tumors and more small tumors (Fig. 21A). To ascertain

that the defect is connected to SA levels, an HA-tagged *Cmu1* allele was introduced into the triple mutant. The triple mutant complemented with *cmu1* showed comparable virulence to SG200 (**Fig. 21B**). It is thus suggested that *Cmu1*, *Shy1* and *Um12021* might have redundant function.

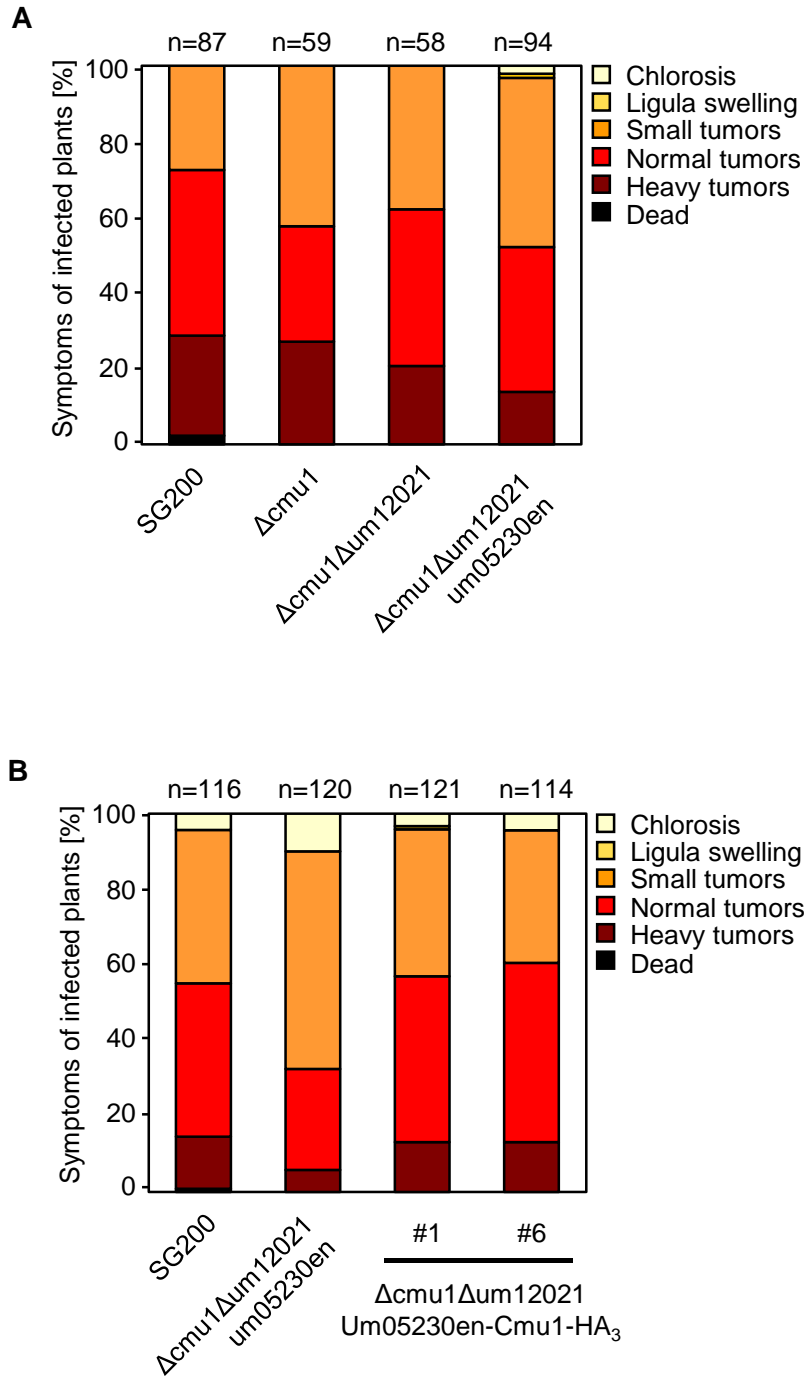


Fig. 21: *Cmu1*, *Shy1* and *Um12021* might be functionally redundant. A. Infection symptoms on maize seedlings infected with SG200, the deletion mutant SG200 $\Delta cmu1$, the double deletion mutant

SG200 Δ cmu1 Δ um12021 and the triple mutant SG200 Δ cmu1 Δ um12021um05230en. Infection symptoms were evaluated 12 dpi. The respective symptom categories are depicted on the upper right side of the diagram. The mean values were calculated from at least two independent replicates. The total number (n) of plants is depicted above each column. **B.** Infection symptoms on maize seedlings infected with SG200, the triple mutant SG200 Δ cmu1 Δ um12021um05230en and complementation strain SG200 Δ cmu1 Δ um12021um05230en-Cmu1-HA₃. Infection symptoms were evaluated 12 dpi. The respective symptom categories are depicted on the upper right side of the diagram. The mean values were calculated from at least three independent replicates. The total number (n) of plants is depicted above each column.

2.4 Investigation of the localization of Cmu1 in maize mesophyll cells

Previously, Cmu1 was shown to reside in the cytosol of maize epidermal cells after bombardment, and a hypothesis for the function of Cmu1 was proposed based on its cytosolic localization (Djamei et al., 2011). Interestingly, a secreted CM from plant pathogen *Sclerotinia sclerotiorum* was recently found to contain a chloroplast transit peptide (cTP), which mediated the entry of the secreted CM into chloroplasts where SA is synthesized (M. Dickman, personal communication). Although searching the Cmu1 sequence with the ChloroP 1.1 Server (<http://www.cbs.dtu.dk/services/ChloroP/>) did not reveal any canonical cTP, some microbes utilize non-canonical mechanism to deliver effectors into chloroplasts (Jelenska et al., 2007; Rodriguez-Herva et al., 2012). Since the localization of Cmu1 after bombardment had been previously studied in epidermal cells which mostly lack chloroplasts (Djamei et al., 2011), the localization of Cmu1 was studied in mesophyll cells which contain chloroplasts.

2.4.1 Cmu1 localizes in the cytosol of mesophyll cell

The localization of Cmu1 was examined by transiently expressing Cmu1^{ASP} with C-terminal fusion of a “superfolder” GFP (sfGFP) in uninfected mesophyll cells after biolistic bombardment (Pedelacq et al., 2006). Two days after bombardment, the localization of fluorescent proteins was visualized by confocal microscopy. Cmu1^{ASP}-sfGFP was only detected in the cytosol of mesophyll cells (**Fig. 22A**). The negative control sfGFP alone showed a similar localization in the cytosol (**Fig. 22B**), while the fluorescence of the positive control ZmCM1, the chloroplast localized CM of maize, co-localized with chloroplasts (**Fig. 22C**). To exclude the possibility that the import of Cmu1 into chloroplast might require some unknown factors from *U. maydis* or plant factors that are only expressed upon infection, maize leaves infected by SG200 (3 dpi) were transformed with plasmid p35S-Cmu1^{ASP}-sfGFP. However, confocal microscopy confirmed the localization of Cmu1^{ASP}-sfGFP in the cytosol, i.e. it did not change in the infected leaves (**Fig. 23**).

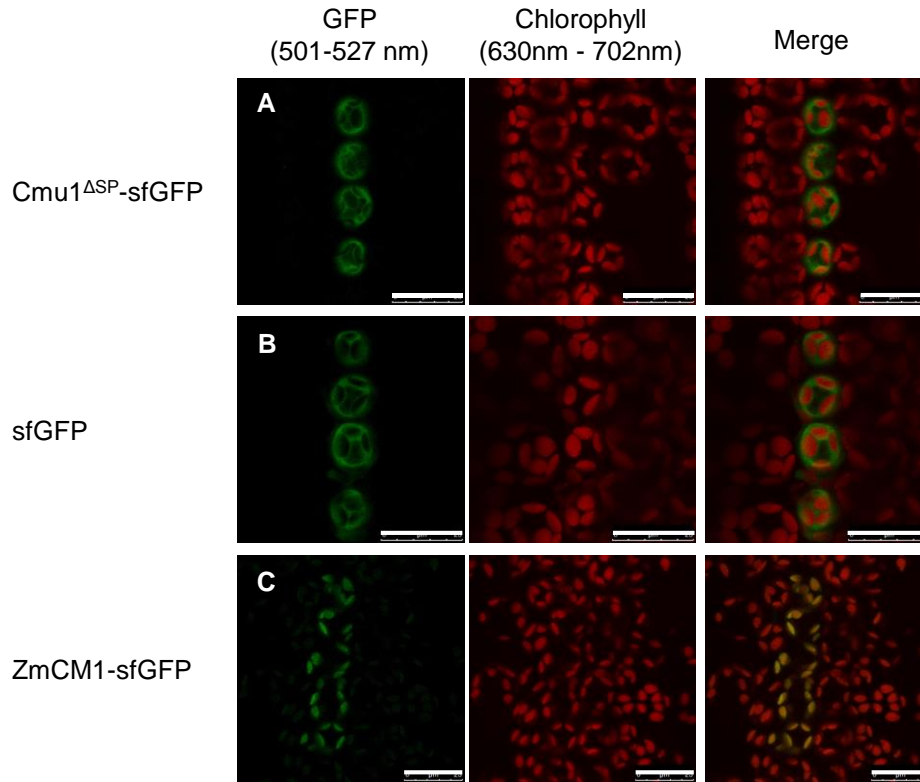


Fig. 22: Cellular localization of Cmu1 in the mesophyll cells after bombardment. **A.** Confocal microscopy of Cmu1^{ΔSP}-sfGFP transiently expressed in maize mesophyll cells after biolistic transformation with plasmid p35S-Cmu1^{ΔSP}-sfGFP. Scale bars are 25 μm. **B.** Confocal microscopy of sfGFP transiently expressed in maize mesophyll cells after biolistic transformation with plasmid p35S-sfGFP. Scale bars are 25 μm. **C.** Confocal microscopy of ZmCM1-sfGFP transiently expressed in maize mesophyll cells after biolistic transformation with plasmid p35S-ZmCM1-sfGFP. Scale bars are 25 μm.

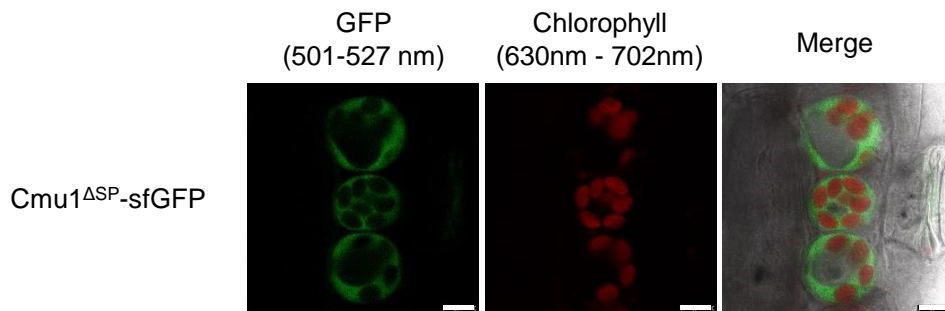


Fig. 23: Cellular localization of Cmu1 in infected mesophyll cells after bombardment. Confocal microscopy of Cmu1^{ΔSP}-sfGFP transiently expressed in infected maize mesophyll cells after biolistic transformation with plasmid p35S-Cmu1^{ΔSP}-sfGFP. Scale bars are 10 μm.

2.4.2 Fusion of Cmu1 to a cTP does not complement CL13Δcmu1

The secreted CM SsCM from *S. sclerotiorum* containing a cTP could functionally replace Cmu1 and complement the virulence phenotype of CL13Δcmu1 (F. Hartwig, personal communication).

To address whether Cmu1 fused with the cTP of SsCM is able to fulfill its biological function, the cTP of SsCM was inserted into Cmu1 downstream of the SP and the corresponding plasmid p123-P_{Cmu1}-SP-cTP-Cmu1^{ΔSP}-HA₃ was inserted in single copy in the *ip* locus of CL13Δcmu1. In comparison to Cmu1-HA₃, infection experiments conducted with three independent strains revealed that SP-cTP-Cmu1^{ΔSP}-HA₃ could only partially complement the virulence of CL13Δcmu1 (Fig. 24). However, it is still needed to test the stability of the fusion protein as well as whether SP-cTP-Cmu1^{ΔSP} is able to enter chloroplast after bombardment.

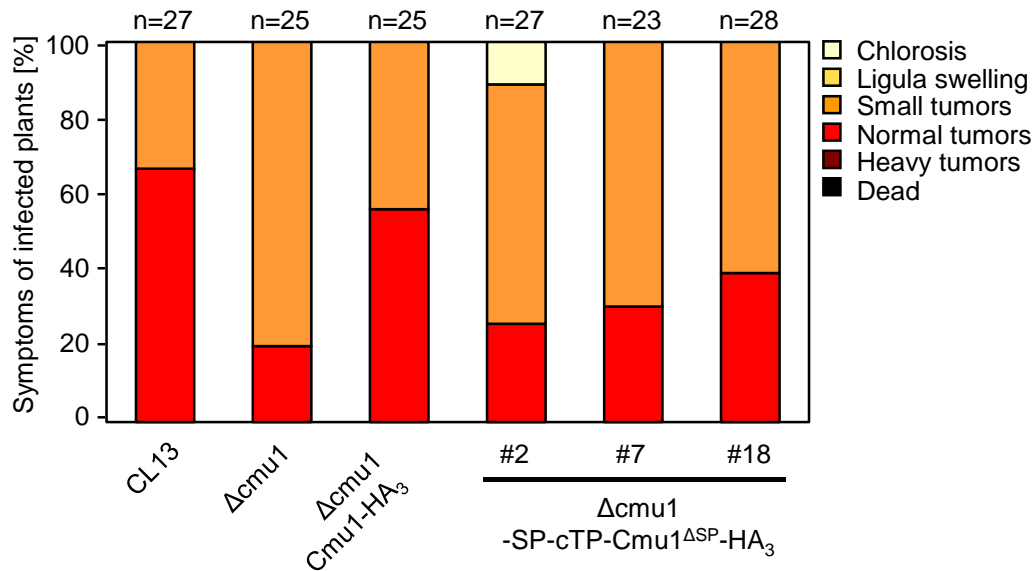


Fig. 24: Fusion of Cmu1 with a chloroplast transit peptide does not fully complement CL13Δcmu1. Infection symptoms on maize seedlings infected with CL13, the deletion strain CL13Δcmu1 and complementation strains CL13Δcmu1-Cmu1-HA₃ and CL13Δcmu1-SP-cTP-Cmu1^{ΔSP}-HA₃. Infection symptoms were evaluated 12 dpi. The respective symptom categories are depicted on the upper right side of the diagram. The total number (n) of plants is depicted above each column.

2.5 Interaction partners of Cmu1

2.5.1 A secreted maize CM does not interact with Cmu1 in Y2H assay

Djamei et al. (2011) identified two maize CMs that interacted with Cmu1 in yeast two-hybrid (Y2H) assays. Whether this interaction also occurs when Cmu1 is delivered by *U. maydis* has not been investigated. Recently, a third CM ZmCM3 (AC198937.4_FG003) was identified in maize by BlastP analysis. ZmCM3 is predicted to be a secreted protein with a SP (residues 1-28), which is different from its paralogs ZmCM1 localized in the chloroplast and ZmCM2 localized in the cytosol. To test if ZmCM3 can interact with Cmu1, pGADT7-ZmCM3²⁹⁻²⁸⁴ expressing ZmCM3

lacking the SP and pGBKT7-Cmu1^{ΔSP} expressing Cmu1 lacking the SP were co-transformed into *S. cerevisiae* AH109 strain. However, interaction of Cmu1 with positive controls ZmCM1 or ZmCM2 could be observed on high stringency plates but not with ZmCM3²⁹⁻²⁸⁴ (**Fig. 25A**). The production of respective fusion proteins was verified by western blot (**Fig. 25B**).

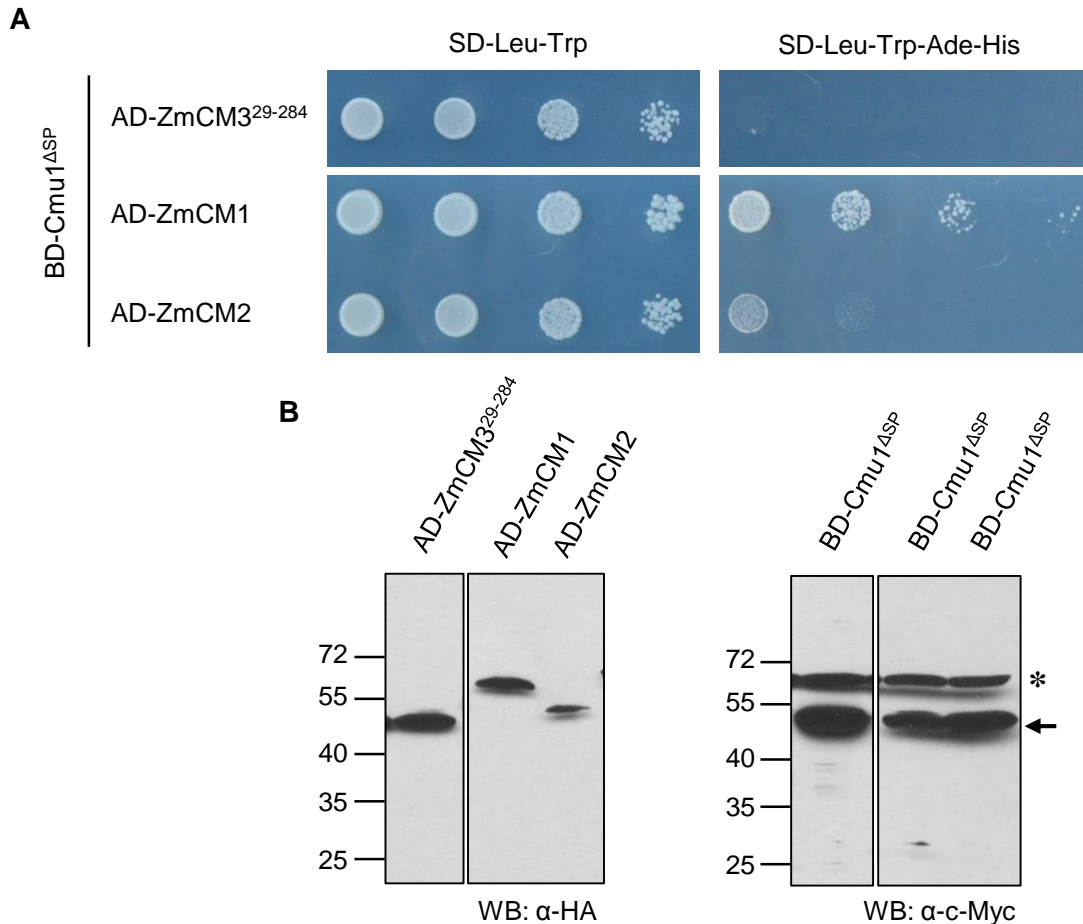


Fig. 25: ZmCM3 does not interact with Cmu1 in Y2H assay. **A.** Interaction between ZmCM3 and Cmu1 was tested in yeast two hybrid assay. *S. cerevisiae* AH109 cells expressing GAL4AD-ZmCM3²⁹⁻²⁸⁴ and GAL4BD-Cmu1^{ΔSP} were spotted on SD-Leu-Trp (low stringency) and SD-Leu-Trp-Ade-His (high stringency) plates, respectively. An HA tag was fused to the C-terminus of AD domain, while a c-Myc tag was fused to the C-terminus of BD domain. Plasmids expressing GAL4AD-ZmCM1 and GAL4AD-ZmCM2 served as positive controls. **B.** Expression of respective proteins in yeast strains used in (A) was analyzed by western blot analysis of yeast lysates. BD fusion proteins were detected using c-Myc antibody, while AD fusion proteins were detected using the HA antibody. The molecular mass marker is depicted on the left. The sizes of fusion proteins are: AD-ZmCM1: 53.5 kDa; AD-ZmCM2: 46.1 kDa; AD-ZmCM3²⁹⁻²⁸⁴: 47.3 kDa; BD-Cmu1^{ΔSP} (arrow): 50.5 kDa. The asterisk labels non-specific bands.

2.5.2 Co-IP-MS analysis identified a maize protein Cmi1 which specifically interacts with Cmu1

To analyze whether the interaction partners of Cmu1 detected by Y2H can also be found *in vivo* and to identify additional interaction partners of Cmu1, maize seedlings were infected with SG200 Δ cmu1-Cmu1-HA₃ under the control of native promoter. As negative control, mCherry-HA fused to the SP of Cmu1 at the N-terminus was expressed in SG200 under the *cmu1* promoter. Total proteins were extracted from infected leaf samples. The lysate was incubated with magnetic HA beads to immuno-precipitate bait proteins and possibly bound interaction partners. Samples were analyzed by liquid chromatography-tandem mass spectrometry (LC-MS/MS) in collaboration with Dr. Timo Glatter (Max Planck Institute for Terrestrial Microbiology). The LC-MS/MS analysis found no hits for any maize CMs. Unexpectedly, peptides of a maize protein GRMZM2G073114, which was renamed as **Cmu1 interactor 1 (Cmi1)**, were enriched on Cmu1-HA₃ bound beads, while no peptide of Cmi1 was detected on mCherry-HA bound beads (**Table 2**). A small amount of peptides of Cmu1 were also detected in negative control, which was regarded as unspecific binding since Cmu1 is highly abundant in the infected tissue. Two biological replicates yielded comparable results, making it likely that Cmi1 is a true interaction partner of Cmu1 during infection.

Table 2: Co-IP-MS analysis identifies Cmi1 as the interaction partner of Cmu1.

Protein \ Peptides	mCherry-HA			Cmu1-HA ₃		
	I	II	III	I	II	III
mCherry	17	25	27	0	0	0
Cmu1	1	3	1	56	62	65
Cmi1	0	0	0	6	7	6

a) Total spectrum counts of unique peptides for respective proteins in the first biological replicate are shown for the three technical replicates concluded (I, II, III). mCherry-HA was used as negative control.

2.5.3 Cmi1 is likely a pathogenesis related protein

Cmi1 is predicted to be a secreted protein, with residues 1-32 as SP predicted by SignalP. Another feature of Cmi1 is that it contains ten cysteines with a pattern of “C-X₁₂-C-X₇-CC-X₁₀-C-X₂₈-C-X₂₄-C-X₂₁-C-X₅-C-X₉-C”, suggesting that this secreted protein might form 5 disulfide bonds after secretion. Cmi1 is annotated as uncharacterized protein in UniProt, but contains IPR009009

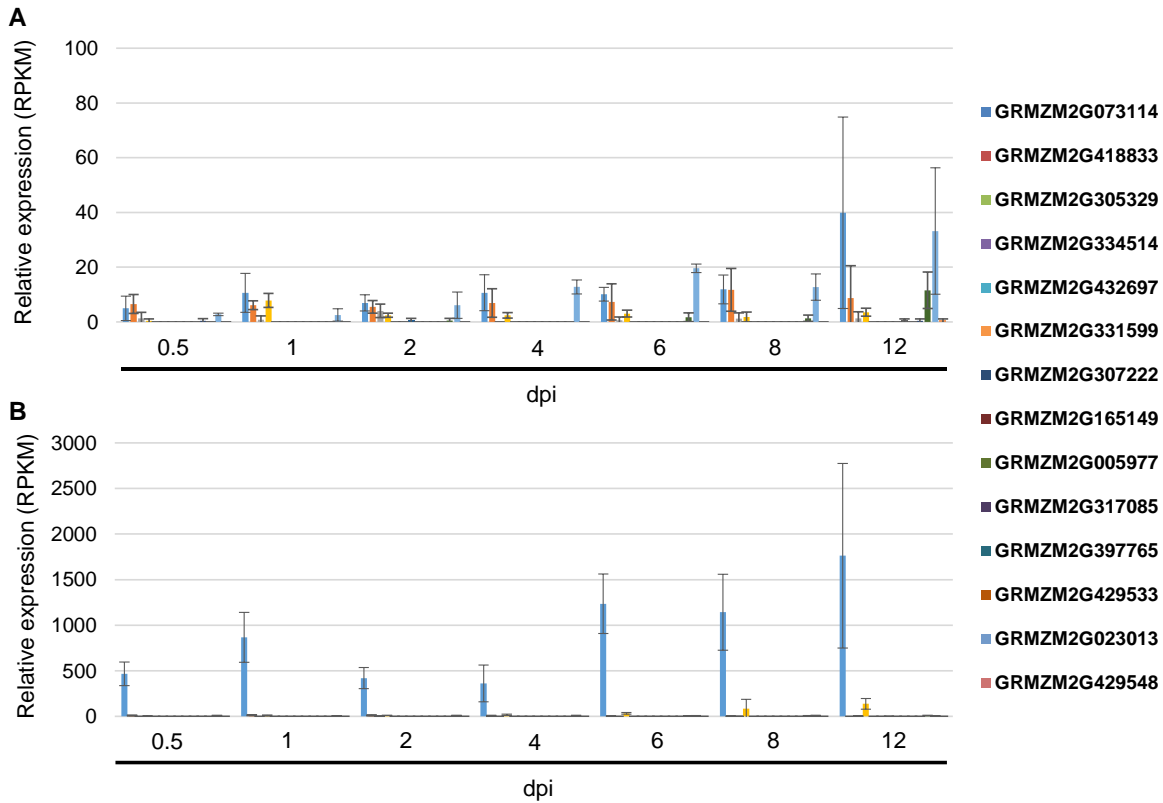


Fig. 27: Relative expression patterns of *cmi1* and 13 paralogs during biotrophic development. **A.** Relative expression patterns of *Cmi1* and 13 paralogs (listed on the right) were revealed by RNAseq analysis of RNA samples from mock infected maize plants at 0.5, 1, 2, 4, 6, 8 and 12 dpi (D. Lanver, personal communication). The vertical axis indicates the RNA reads per kilobase million reads (RPKM). The horizontal axis indicates the stages, i.e. 0.5, 1, 2, 4, 6, 8 and 12 dpi. Error bars indicate standard deviation of three biological replicates. **B.** Relative expression patterns of *Cmi1* and 13 paralogs were revealed by RNAseq analysis of RNA samples from FB1 × FB2 infected maize plants at 0.5, 1, 2, 4, 6, 8 and 12 dpi (D. Lanver, personal communication). The vertical axis indicates the RNA reads per kilobase million reads (RPKM). The horizontal axis indicates the stages, i.e. 0.5, 1, 2, 4, 6, 8 and 12 dpi. Error bars indicate standard deviation of three biological replicates. Color codes of columns for different genes are indicated on the right.

2.5.4 Verification of the interaction between *Cmi1* and *Cmu1*

To verify the interaction between *Cmi1* and *Cmu1*, Y2H assay was carried out. To this end, the *cmu1* gene and *cmi1* gene lacking the SP coding sequence were both inserted into pGADT7 and pGBKT7, respectively. However, yeast strains expressing AD-*Cmu1*^{ASP}/BD-*Cmi1*³³⁻¹⁹⁸ or BD-*Cmu1*^{ASP}/AD-*Cmi1*³³⁻¹⁹⁸ were unable to grow on SD-Leu-Trp-His (medium stringency) or SD-Leu-Trp-Ade-His (high stringency) plates (**Fig. 28A**), indicating that *Cmu1* and *Cmi1* do not interact in Y2H. The expression of respective fusion proteins was analyzed by western blot and proteins with the expected sizes were produced (**Fig. 28B**). The failure of Y2H to verify the interaction of *Cmu1*

and Cmi1 could be due to the incorrect folding of Cmi1 because Cmi1 has five possible disulfide bonds.

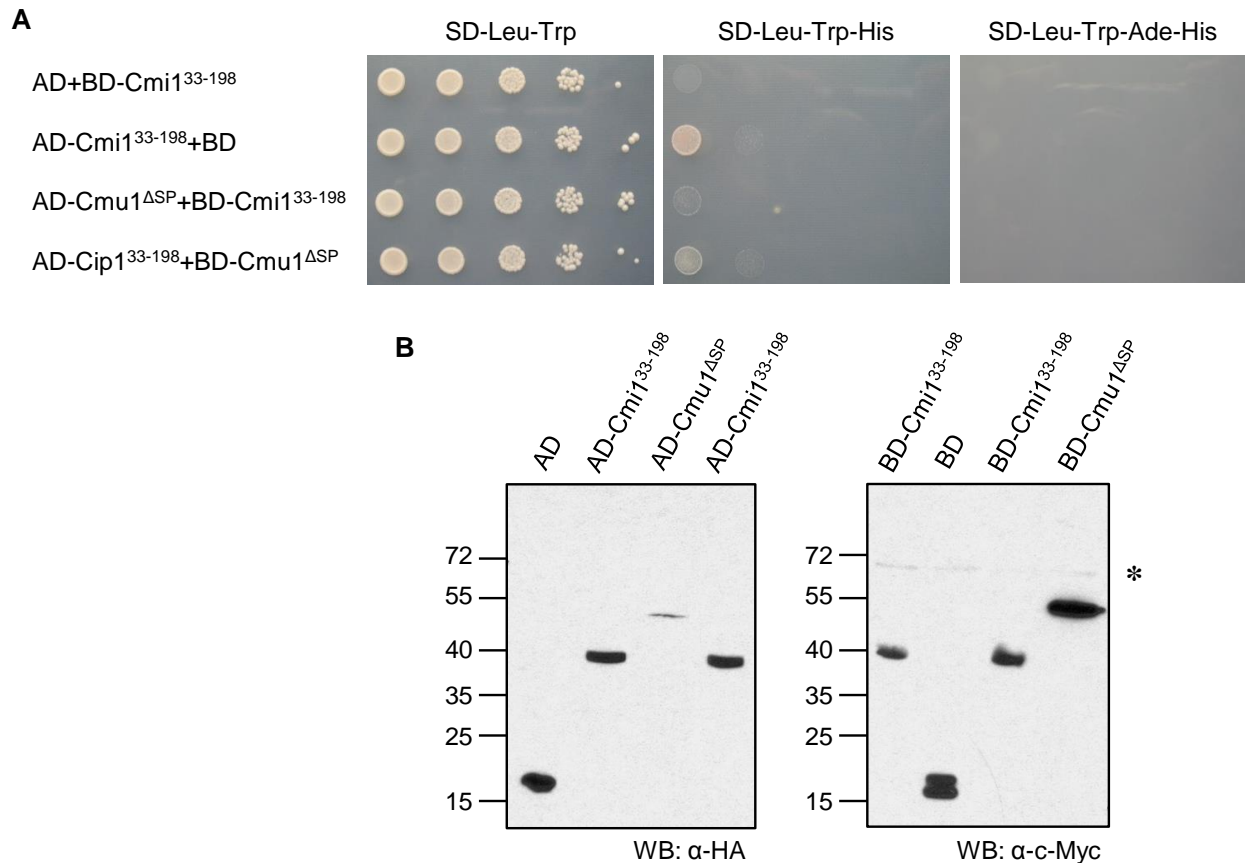


Fig. 28: Cmi1 shows no interaction with Cmu1 in Y2H assay. **A.** Interaction between Cmi1 and Cmu1 was tested in yeast two hybrid assay. *S. cerevisiae* AH109 cells expressing GAL4AD-Cmi1³³⁻¹⁹⁸/GAL4BD-Cmu1^{ΔSP} or GAL4BD-Cmi1³³⁻¹⁹⁸/GAL4AD-Cmu1^{ΔSP} were spotted on SD-Leu-Trp (low stringency), SD-Leu-Trp-His (medium stringency) and SD-Leu-Trp-Ade-His (high stringency) plates, respectively. An HA tag was fused to the C-terminus of AD domain, while a c-Myc tag was fused to the C-terminus of BD domain. Plasmids expressing GAL4AD and GAL4BD served as negative controls. **B.** Expression of respective proteins in yeast strains used in (A) was analyzed by western blot analysis of yeast lysates. BD fusion proteins were detected using c-Myc antibody and AD fusion proteins were detected using the HA antibody. The molecular mass marker is depicted on the left. The sizes of fusion proteins are: AD: 18.6 kDa; AD-Cmi1³³⁻¹⁹⁸: 35.3 kDa; AD-Cmu1^{ΔSP}: 48.4 kDa; BD: 20.7 kDa; BD-Cmi1³³⁻¹⁹⁸: 37.7 kDa; BD-Cmu1^{ΔSP}: 50.5 kDa. The asterisk labels non-specific bands.

Next, the interaction between Cmi1 and Cmu1 was investigated by *in vitro* pull-down assay. Cmi1 was transiently expressed in *Nicotiana benthamiana* via agroinfiltration. pEZRK vector expressing Cmi1-His₆ was transformed into *Agrobacterium tumefaciens* GV3101 strain and the resulting transformant was used to infiltrate young *N. benthamiana* leaves. As negative control, GV3101 carrying empty vector (EV) pEZRK was used. Cmu1-HA₃ was overexpressed and secreted by a *U. maydis* strain (AB33-P_{otef}-Cmu1-HA₃) under the control of a strong constitutive promoter P_{otef}

(Spellig et al., 1996) and the resulting supernatant was concentrated with Amicon centrifugal filter unit. Plant lysates of infiltrated tobacco leaves expressing Cmi1-His₆ were incubated with the concentrated supernatant containing Cmu1^{ΔSP}-HA₃. After pull-down performed with Ni-NTA agarose, Cmu1^{ΔSP}-HA₃ could be enriched by Cmi1-His₆ bound Ni-NTA beads. Only minimal binding was detected in the EV negative control, which was regarded as unspecific binding (**Fig. 29**).

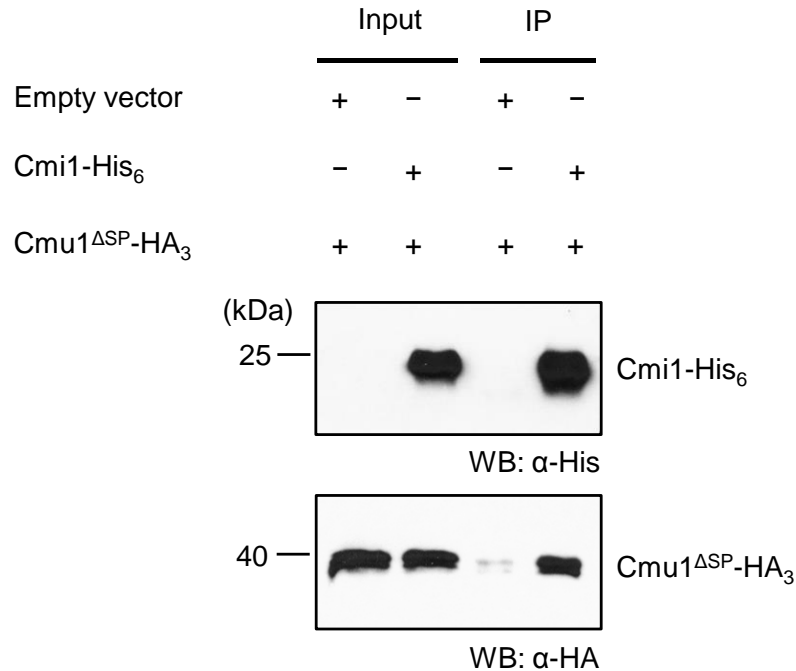


Fig. 29: *In vitro* pull-down assay confirmed the interaction of Cmi1 with Cmu1. Concentrated supernatant of AB33-P_{otef}-Cmu1-HA₃ was incubated with Ni-NTA agarose and plant lysates of tobacco leaves infiltrated with GV3101 transformed with pEZRK or pEZRK-Cmi1-His₆. Cmi1-His₆ was detected with the His antibody, and Cmu1^{ΔSP}-HA₃ was detected with the HA antibody. The molecular mass marker is depicted on the left.

2.5.5 Purification of Cmi1³³⁻¹⁹⁸-His₆

After failures due to insolubility of the proteins, pET-Cmi1³³⁻¹⁹⁸ was introduced into the *E. coli* strain SHuffle® T7 (NEB), which is suitable for expression of cysteine-rich proteins (Lobstein et al., 2012). In this strain solubility of Cmi1-His₆ was dramatically increased when induced at 16°C (**Fig. 30A**). Subsequently, Cmi1³³⁻¹⁹⁸-His₆ was purified with the two-step procedure which was also used for Cmu1 purification (**Fig. 30B**). The purity of Cmi1 was analyzed by SDS-PAGE and the concentration was determined using the absorbance at 280 nm with a NanoDrop spectrophotometer.

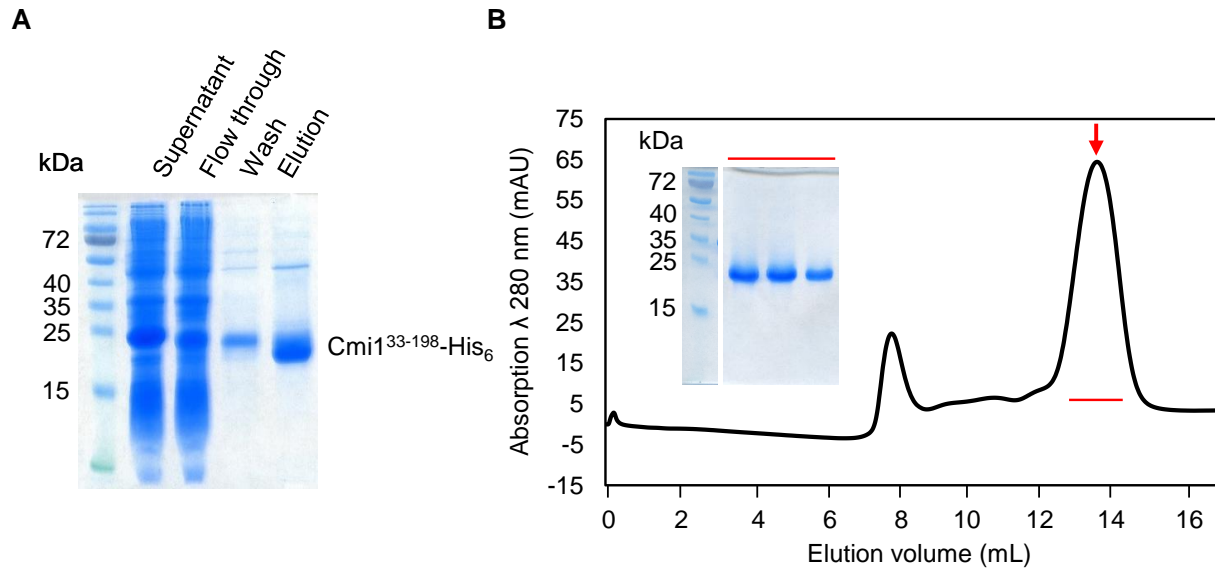


Fig. 30: Purification of Cmi1³³⁻¹⁹⁸-His₆. **A.** Shuffle T7 strain transformed with pET-Cmi1³³⁻¹⁹⁸ was induced with 0.5 mM IPTG at 16°C for 16 h. Cells were lysed and clarified. The supernatant was subjected to Ni-NTA affinity purification. Indicated fractions were separated by SDS-PAGE and stained by Instant blue solution. The molecular mass marker is depicted on the left. **B.** The size exclusion chromatogram shows Cmi1³³⁻¹⁹⁸-His₆ forms the peak indicated by the red arrow. The peak fractions indicated with a red line were pooled and confirmed by SDS-PAGE (inlay), demonstrating that the Cmi1³³⁻¹⁹⁸-His₆ is the main component in the peak fractions. The molecular mass marker is depicted on the left.

2.5.6 Cmi1 inhibits the CM activity of Cmu1

The enzymatic activity of many CMs is allosterically regulated by aromatic amino acids (Helmstaedt et al., 2001; Westfall et al., 2014). It was also shown that interaction of CMs with other proteins could alter the CM activity (Sasso et al., 2009; Webby et al., 2010). To determine whether the CM activity of Cmu1 is altered upon the addition of Cmi1, the “online assay” was performed with Cmu1^{ΔSP} in the presence of Cmi1³³⁻¹⁹⁸-His₆. Unexpectedly, the addition of Cmi1 inhibited the activity of Cmu1 in a dose-dependent manner, while 80 nM BSA did not influence the activity of Cmu1. This inhibitory activity is specific as the CM activity of Aro7p was not altered in the presence of 80 nM Cmi1 (**Fig. 31**).

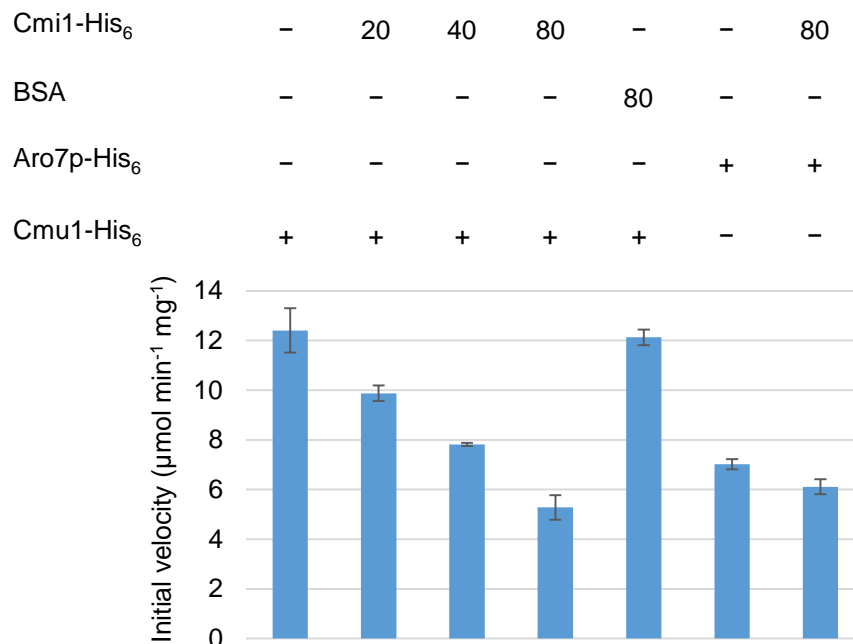


Fig. 31: Inhibition of Cmi1 on the CM activity of Cmu1. The activity of CMs was determined by measuring the rate of chorismate disappearance at 274 nm. Numbers indicate the final concentration (in nM) of Cmi1³³⁻¹⁹⁸-His₆ or BSA in the reactions. The amount of Cmu1^{ΔSP}-His₆ or Aro7p-His₆ used in the reactions was 100 ng. Chorismate used in each reaction was 0.5 mM. Error bars indicate the standard deviation of three replicates.

2.5.7 Identification of the interaction interface between Cmu1 and Cmi1 via HDX/MS

Hydrogen-deuterium exchange mass spectrometry (HDX) technique has been emerging a powerful tool to investigate protein dynamics or map the protein-protein interaction interface (Englander, 2006; Wales and Engen, 2006; Konermann et al., 2011). The exchange rate of the amide hydrogen with deuterium is slowed down when they are hydrogen bonded (Wales and Engen, 2006). In order to map the interaction interface between Cmu1 and Cmi1, HDX was applied in cooperation with Dr. Wieland Steinchen in the group of Dr. Gert Bange (LOEWE-Zentrum für Synthetische Mikrobiologie). The complex of Cmu1^{ΔSP}-His₆ and Cmi1³³⁻¹⁹⁸-His₆ was prepared via Ni-NTA affinity purification and SEC. Cmu1^{ΔSP}-His₆ and Cmi1³³⁻¹⁹⁸-His₆ were separately purified by Ni-NTA affinity purification, well mixed and subjected to SEC. Cmu1^{ΔSP}-His₆ alone formed a protein peak with the elution volume of 10.67 mL, whereas Cmu1^{ΔSP}-His₆/Cmi1³³⁻¹⁹⁸-His₆ complex gave rise to a shifted peak with the elution volume of 10.04 mL, which again confirmed the interaction of Cmu1 with Cmi1 (**Fig. 32**). The peak fractions of the complex were pooled and used for HDX analysis together with purified Cmu1^{ΔSP}-His₆ and Cmi1³³⁻¹⁹⁸-His₆. HDX analysis revealed that the

interaction interface between Cmu1 and Cmi1 involved amino acid regions 33-55, 114-147 and 220-233 in Cmu1 (**Fig. 33**, W. Steinchen, personal communication).

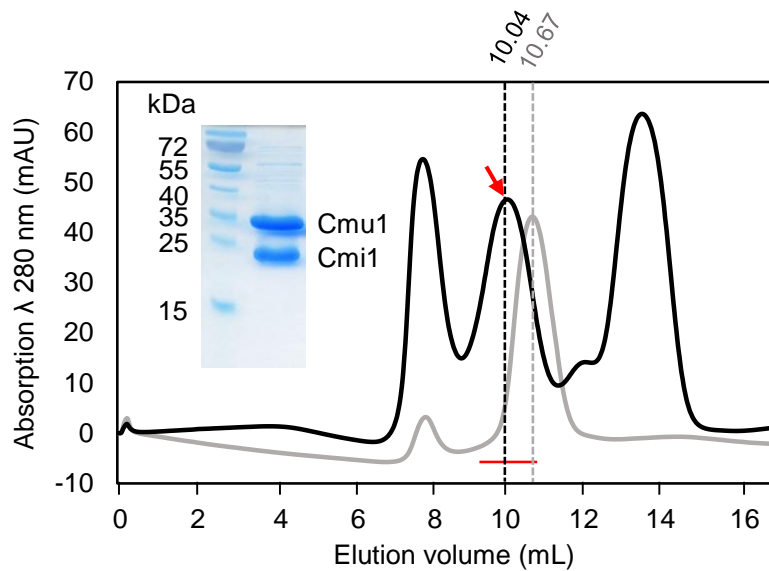


Fig. 32: Purification of Cmu1^{ΔSP}-His₆/Cmi1³³⁻¹⁹⁸-His₆ complex. The size exclusion chromatogram shows Cmu1^{ΔSP}-His₆/Cmi1³³⁻¹⁹⁸-His₆ complex forms the peak indicated by the red arrow. The size exclusion chromatogram of is shown in grey. The complex (10.04 mL) gives rise to a shift in elution volume in comparison to Cmu1^{ΔSP}-His₆ alone (10.67 mL). The peak fractions indicated with a red line were pooled and confirmed by SDS-PAGE (inlay), demonstrating that the Cmu1^{ΔSP}-His₆/Cmi1³³⁻¹⁹⁸-His₆ complex is the main component in the peak fractions. The molecular mass marker is depicted on the left.

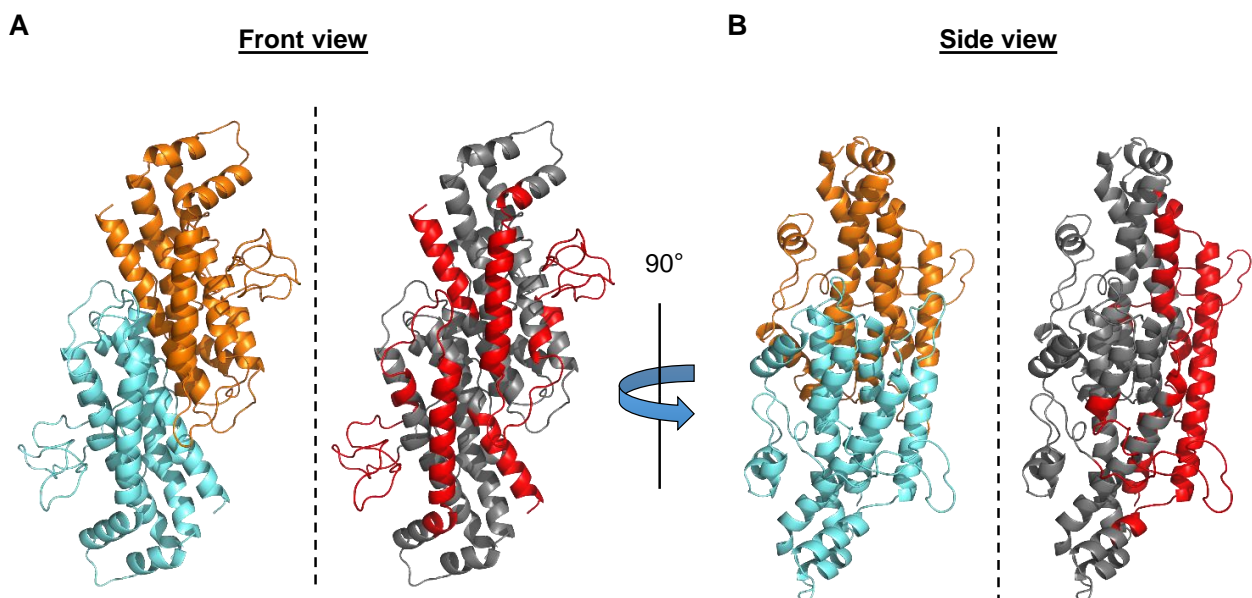


Fig. 33: Interaction interface of Cmu1 in complex with Cmi1 revealed from HDX analysis. Front view (A) and side view (B) of the interaction interface of Cmu1^{ASP}-His₆ in complex with Cmi1³³⁻¹⁹⁸-His₆. Left: Crystal structure of dimeric Cmu1^{ASP}-His₆ with the two monomers colored in orange and cyan, respectively. Right: All regions in which differences in HDX were observed are colored in red. Regions without any difference in HDX are shown in grey.

2.5.8 The loop region of Cmu1 is necessary for the interaction with Cmi1

HDX analysis revealed the interaction interface between Cmu1 and Cmi1. Surprisingly, part of the loop region in Cmu1 was located in the interaction interface, which was previously shown to be needed for the function of Cmu1. The Cmu1^{Δ117-140}-HA₃ with partial deletion of the loop region was tested for its ability to interact with Cmi1-His₆ by *in vitro* pull-down experiment. Interestingly, Cmu1^{Δ117-140} lost its ability to interact with Cmi1 (Fig. 34A). In accordance with this, unlike the wildtype Cmu1^{ASP}, the CM activity of Cmu1^{ASPΔ117-140}-His₆ upon the addition of Cmi1 was not significantly reduced (Fig. 34B).

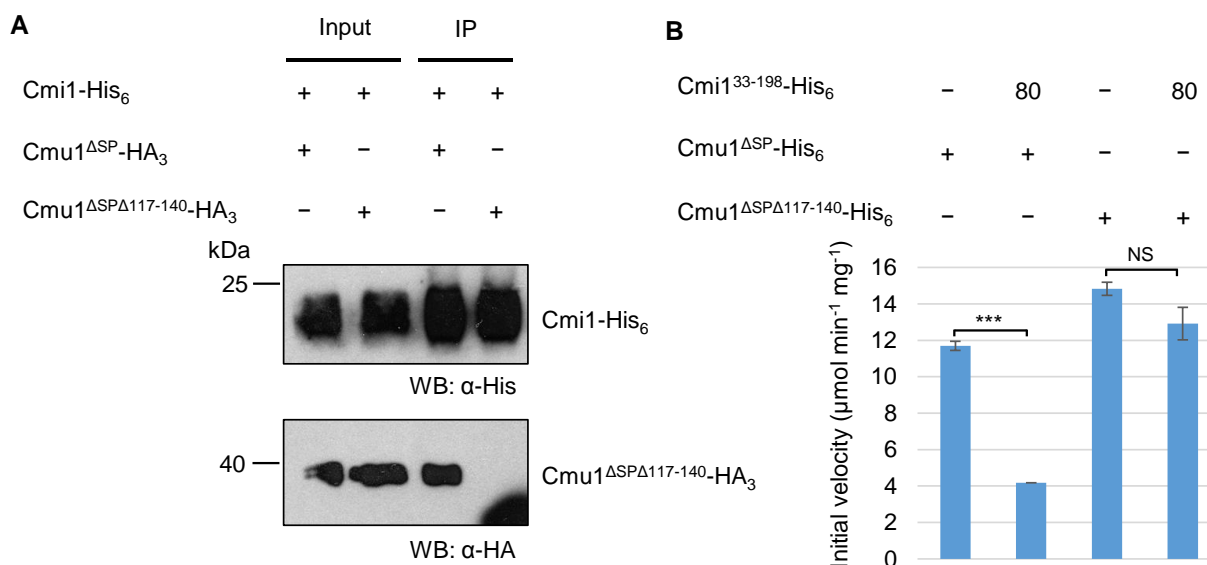


Fig. 33: *In vitro* pull-down experiment shows that Cmu1^{Δ117-140} fails to interact with Cmi1. A. Supernatants of AB33-P_{oter}-Cmu1-HA₃ and AB33-P_{oter}-Cmu1^{Δ117-140}-HA₃ were incubated with Ni-NTA agarose and plant lysates of tobacco leaves infiltrated with GV3101 transformed with pEZRK-Cmi1-His₆, respectively. Cmi1-His₆ was detected with the His antibody, while Cmu1^{ASP}-HA₃ or Cmu1^{ASPΔ117-140}-HA₃ was detected with the HA antibody. The molecular mass marker is depicted on the left. B. The activity of CMs was determined by measuring the rate of chorismate disappearance at 274 nm. Numbers indicate the final concentration (in nM) of Cmi1³³⁻¹⁹⁸-His₆ in the reactions. The amount of Cmu1^{ASP}-His₆ or Cmu1^{ASPΔ117-140}-His₆ used in the reactions was 100 ng. Chorismate used in each reaction was 0.5 mM. Error bars indicate the standard deviation of three replicates. Statistical analysis was performed with Student's t-test: P>0.05 (NS), P≤0.05 (*), P≤0.01 (**), P≤0.001 (***)

3. Discussion

In this thesis, comparisons of the secreted CM Cmu1 of *U. maydis* and the non-secreted CM Aro7p of *S. cerevisiae* revealed several interesting features that are unique to Cmu1. The novel fold of the putative allosteric site of Cmu1 suggested the potential of Cmu1 to employ a different mechanism for the regulation of its CM activity. In addition, a loop region in Cmu1 was found to be required for full virulence. A secreted PR-4 like protein Cmi1 from maize was identified to be an interaction partner of Cmu1, indicating that Cmu1 might have a secondary function in the apoplast in addition to its interference with SA biosynthesis after uptake into plant cells. Furthermore, HDX/MS experiments revealed that the interaction interface between Cmu1 and Cmi1 involves the unique loop region of Cmu1.

3.1 Secreted chorismate mutases - universal enzymes but divergent strategies

Secreted CMs can be found in bacteria, fungi and nematodes, most of which are plant or animal pathogens, suggesting a possible role in virulence. In support for this, it was shown that several genes encoding secreted CMs are induced during host infection, e.g. the expression of *cmu1* is strongly induced during the biotrophic interaction of *U. maydis* with maize (Djamei et al., 2011). Similarly, the secreted CM Hg-cm-1 from the phytopathogenic nematode *Heterodera glycines* was specifically expressed in esophageal glands, a tissue in which many virulence factors of nematodes are upregulated (Bekal et al., 2003). The promoter for the periplasmic CM in *Salmonella enterica* serovar Typhimurium was induced after infection of mice (Bumann, 2002). Secondly, it was found that several secreted CM encoding genes reside in regions that are related to pathogenicity. For example, *Rv1885c* is one of the seven genes in an operon of *M. tuberculosis*. The two flanking genes, *Rv1884c* and *Rv1886c*, which encode resuscitation-promoting factor RpfC and mycolyltransferase FbpB, respectively, might be involved in pathogenesis (Wiker and Harboe, 1992; Mukamolova et al., 2002a; Mukamolova et al., 2002b; Sasso et al., 2005; Forrellad et al., 2013). In *Rhodococcus equi*, the causative agent for pneumonia diseases in animals, the coding gene for a secreted CM is located on a pathogenicity island (Takai et al., 2000). Therefore, secreted CMs might be a universal strategy contributing to virulence of various pathogens (Calhoun et al., 2001; Bekal et al., 2003; Doyle and Lambert, 2003; Sasso et al., 2005; Djamei et al., 2011).

However, the mechanisms underlying the functions of different secreted CMs are likely to be divergent. Cmu1 from *U. maydis* enters the plant cytosol and contributes to virulence by lowering the SA levels in the infected tissue to suppress plant defenses, whereas Hg-cm-1 of *H. glycines* is considered to be injected into plant cells to interfere with auxin homeostasis (Doyle and Lambert, 2003). Although the functions of secreted CMs in animal pathogenic bacteria remain elusive, their function is likely to be different because these CMs are secreted to the periplasmic space and their hosts lack the SA or auxin hormonal pathways. Knockout mutants for respective secreted CMs in pathogenic bacteria are needed to unravel their functions.

3.2 The N-terminal region of Cmu1

The N-terminus of effectors of filamentous pathogens may be implicated in their translocation into plant cells (Whisson et al., 2007; Manning et al., 2008; Rafiqi et al., 2010; Schornack et al., 2010b; Petre and Kamoun, 2014). It is interesting that the E29, E32, E34, D37, D40 and D44 in the N-terminus of Cmu1 with D196 and D200 constitute a surface exposed acidic patch revealed from the crystal structure (J. Schuhmacher and G. Bange, unpublished). However, disruption of the acidic patch with alanine substitutions of eight acidic residues had no influence on the function of Cmu1. The full complementation of Cmu1^{8A} mutant protein in comparison to the wildtype protein implies that the translocation of the effector is not affected in the absence of the acidic patch. Although it is still a mystery that how effectors from filamentous microorganisms are translocated into plant cells (Petre and Kamoun, 2014; Lo Presti and Kahmann, 2017), extracellular vesicles (EVs) have been implicated in transporting virulence factors of pathogens in various kingdoms into their hosts recently (Kuehn and Kesty, 2005; An et al., 2006; Rodrigues et al., 2008; Bomberger et al., 2009; Szempruch et al., 2016; Katsir and Bahar, 2017; Raab-Traub and Dittmer, 2017). The potential role of such EVs in effector translocation remains to be investigated.

3.3 The unique disulfide bond in Cmu1 proteins from smut fungi may not contribute to stability

The disulfide bond of Cmu1 was thought to stabilize the overall fold of the protein since it is highly conserved among secreted CMs from smut fungi. Disulfide bonds are typically found in secreted CMs (Okvist et al., 2006; Qamra et al., 2006; Vanholme et al., 2009), suggesting that they might be important for secreted CMs. However, disulfide bonds not only stabilize proteins, but also have other functions. For example, three conserved disulfide bonds of scorpion toxin charybdotoxin are

needed for keeping protein structure as well as the toxin activity (Drakopoulou et al., 1998). The removal of two disulfide bonds affected the folding and the activity of the toxin, whereas the effect of the third one was minor (Drakopoulou et al., 1998). In *P. aeruginosa*, the PST-01 protease has two disulfide bonds, of which one is crucial for protease activity and the other for stability, respectively (Ogino et al., 2001). Two disulfide bonds in the apoplastic effector Pep1 of *U. maydis* were implicated in the secretion of the effector (Doehle et al., 2009). Unexpectedly, the disruption of the disulfide bond in Cmu1 did not affect its ability to complement *cmu1* deletion mutants. The disulfide bond in Cmu1 formed by C203 and C289 connects H6 and H9 helices. It is likely that the removal of the disulfide bond may not affect the spatial arrangement of H9 related to H6. Since the active site of Cmu1 includes the residue E278 on H9, the catalytic site of Cmu1 should be affected if H9 and H6 are not associated. Cmu1 mutant protein lacking the disulfide bond was purified from *E. coli* and tested for CM activity. However the mutant Cmu1 protein was not affected in its CM activity compared to wildtype protein (data not shown), suggesting a structurally unaltered active site in the mutant protein lacking the disulfide bond. When Cmu1 is secreted to the apoplast, there may be other factors contributing to the stability of Cmu1. For example, Cmu1 is predicted to undergo both N-glycosylation and O-glycosylation, which could help to stabilize its structure. The substitutions of cysteines with serine have resulted in two additional putative N-glycosylation sites, which may also enhance the stability of Cmu1.

3.4 The regulation of the CM activity of Cmu1

Chorismate lies in the branching point of shikimate pathway and serves as the precursor for a variety of secondary metabolites in plants (Helmstaedt et al., 2001; Dempsey et al., 2011). CMs catalyze the conversion of chorismate to prephenate, which is the committed step in the phenylpropanoid pathway (Xue et al., 1994; Strater et al., 1996; Helmstaedt et al., 2001). The regulation of chorismate metabolism is tightly controlled in plants (Westfall et al., 2014). Allosteric regulation is an important feature for many CMs from bacteria, fungi and plants. However, the mechanism regulating CM activity greatly varies among different CMs (Dopheide et al., 1972; Kradofer et al., 1977; Christopherson, 1985; Brown and Dawes, 1990; Schmidheini et al., 1990; Eberhard et al., 1996b; Schnappauf et al., 1998; Helmstaedt et al., 2001; Webby et al., 2010; Westfall et al., 2014). The comparison of the crystal structures of Cmu1 and Aro7p revealed that the allosteric sites in two proteins are divergent (J. Schuhmacher and G. Bange, unpublished), suggesting a possibly different mechanism for the regulation of CM activity of Cmu1. The CM

activity of Aro7p from *S. cerevisiae* is regulated by tryptophan and tyrosine, and the binding site of allosteric regulators in Aro7p involves residues R75, R76, G141, S142 and T145 (Xue and Lipscomb, 1995; Helmstaedt et al., 2001). In AtCM1 from *A. thaliana* a more precise binding site for the binding of phenylalanine or tyrosine reveals a slightly different set of residues involved, which are R79, H145, V148, G149, and R150 from chain A with N-211, G213, S214, and V217 from chain B (Westfall et al., 2014). When comparing allosteric and non-allosteric CMs (**Fig. 34**), it is interesting that G141 from Aro7p (G213 in AtCM1), which is located in the longest helix H8, plays a vital role in direct contact with regulators (Xue and Lipscomb, 1995; Westfall et al., 2014). The substitution of glycine in this position of Aro7p or AtCM1 completely abolishes the allosteric control (Xue and Lipscomb, 1995; Westfall et al., 2014). However, the corresponding position is replaced by proline in AtCM2 and a gap in Cmu1, respectively (**Fig. 34**). Another important residue is H145 in AtCM1 (H71 in Aro7p) (**Fig. 34**). Substitution of H145 with glutamate resulted in a 20-fold decrease in tyrosine binding and around a 3-fold decrease in tryptophan and phenylalanine binding (Westfall et al., 2014). This position also harbors different residues in AtCM2 and Cmu1, which are glutamine and threonine, respectively (**Fig. 35**). Taken together, the findings above might explain why Cmu1 is insensitive to the regulation by the three aromatic amino acids. It would be interesting to determine whether the response of Cmu1 to aromatic amino acids would change if respective positions were substituted with residues which are found in the allosterically regulated CMs.

The biochemical characterization of Cmu1 produced in *E. coli* showed that the activity of Cmu1 was about 10-fold lower than that of Aro7p. Given that Cmu1 is supposed to undergo post-translational modifications such as glycosylation during secretion, it would be helpful to understand the functionality of Cmu1 when the protein for CM assay is produced from *U. maydis* in axenic culture. However, it was not successful to obtain sufficient amounts of protein from the supernatant of axenic culture of a *U. maydis* strain overexpressing Cmu1-His₆ under the control of P_{otef} (data not shown). In future it should be attempted to isolate Cmu1-HA₃ from maize leaves infected by SG200Δcmu1-P_{cmu1}-Cmu1-HA₃ under the native promoter since P_{cmu1} is one of the strongest promoters during plant colonization (D. Lanver, personal communication).

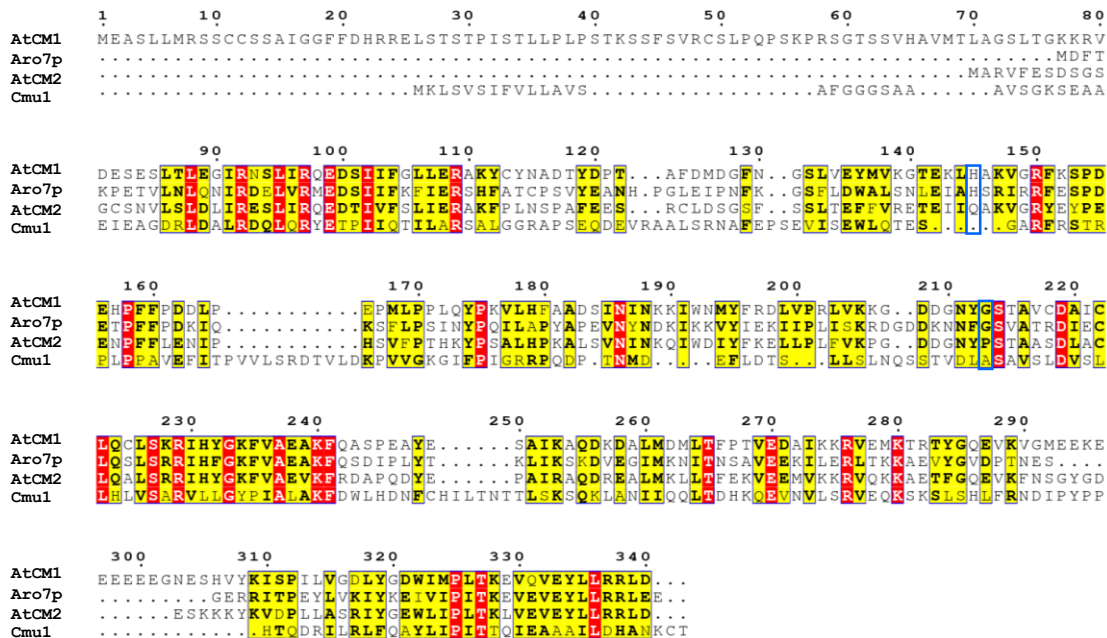


Fig. 35: Amino acid sequence alignment of Cmu1 with its homologs. Alignment of Cmu1 and AtCM1, AtCM2 and Aro7p is shown. Red background indicates amino acid sequence identity, yellow background in bold letters indicates sequence similarity. H145 and G213 in AtCM1 for binding allosteric regulators and corresponding residues in other proteins are highlighted with blue boxes. The alignment was generated with CLUSTAL Omega (Sievers et al., 2011) and ESPript 3.0 (Robert and Gouet, 2014).

Cmu1 heterologously expressed in *E. coli* binds a fatty acid molecule during crystallization, indicating that it has the potential to associate with some small molecules. In the natural context, the unknown molecule could be either fungal derived or plant derived. Therefore, infected maize leaves were extracted with 90% methanol and the resulting organic extract was tested for the effect on the CM activity of Cmu1. However, no significant difference was observed in the presence of organic extract (data not shown). It cannot be ruled out that the concentration of the unknown molecule was not high enough to regulate the CM activity or that molecule in the extract could not replace the fatty-acid like molecule present in the proteins produced in *E. coli*: It is also possible that the activity of Cmu1 is regulated by proteinaceous molecules.

Some effectors of pathogens get activated by plant proteins. For instance, it was shown that the protease activity of bacterial effector AvrRpt2 in *Pseudomonas syringae* is activated by a plant cyclophilin (Coaker et al., 2005). Likewise, the Nudix hydrolase effector Avr3b of *P. sojae* has hijacked soybean cyclophilin GmCYP1 to activate its hydrolase activity aiding to promote virulence (Kong et al., 2015). Interestingly, it was reported that the intracellular CM of *M. tuberculosis* (Rv0948c) formed a complex with another enzyme DAH7PS in the shikimate

pathway, leading to a more than 100-fold increase of its CM activity of Rv0948c (Sasso et al., 2009; Webby et al., 2010). To determine whether the CM activity of Cmu1 is regulated by any proteinaceous molecule, infected maize leaves can be extracted with aqueous buffer and the CM activity of Cmu1 will be tested in the presence of the resulting extract.

3.5 SA signaling targeted by *U. maydis*

SA signaling plays an important role in mediating plant defenses against (hemi)-biotrophic pathogens (Glazebrook, 2005; Vlot et al., 2009; Berens et al., 2017). In turn, plant pathogens utilize a variety of strategies to interfere with SA pathways (Kazan and Lyons, 2014; Tanaka et al., 2015). Cmu1 of *U. maydis* is the first characterized effector from plant pathogenic fungi that inhibits SA biosynthesis via depleting substrate chorismate in the plastids (Djamei et al., 2011). *P. sojae* and *V. dahliae* produce isochorismatases PsIsc1 and VdIsc1, respectively, to scavenge isochorismate, a crucial intermediate for SA synthesis (Liu et al., 2014). In addition, SA can be degraded by salicylate hydroxylases (Yamamoto et al., 1965). Despite the fact that there is no direct evidence that salicylate hydroxylases are involved in pathogen virulence, introduction of salicylate hydroxylase coding genes into plants could confer susceptibility to various pathogens. For instance, tobacco plants expressing the salicylate hydroxylase NahG from *P. putida* are blocked in SA accumulation and exhibit reduced resistance against tobacco mosaic virus (Gaffney et al., 1993). Moreover, transgenic *nahG* *A. thaliana* plants abolish non-host resistance to *P. syringae* pv. *phaseolicola* (van Wees and Glazebrook, 2003).

In the *U. maydis*-maize pathosystem it was shown that treatment of SA can compromise the virulence of the pathogen (Djamei et al., 2011). To downregulate SA signaling during infection, *U. maydis* may use the salicylate hydroxylase Shy1 in addition to Cmu1. Shy1 is a cytoplasmic *U. maydis* protein, which was shown to be induced upon colonization and enzymatically active (Rabe et al., 2013). However, the deletion mutants of *shy1* did not show a reduction of virulence (Rabe et al., 2013). In this thesis, the isochorismatase Um12021, a homolog of PsIsc1 and VdIsc1 (Liu et al., 2014), was uncovered from the *U. maydis*. This suggested a putative interplay of three different enzymes of *U. maydis* targeting the SA pathway. Interestingly, triple deletion mutants lacking *cmu1*, *um12021* and *shy1* had a stronger virulence phenotype than any single or double mutants. The ability of *cmu1* to complement the virulence defect suggested an interplay between these three enzymes. However, to substantiate this finding, it will be necessary to complement the triple mutant with the other two genes to see if similar results can be observed. In addition, a quantification of

SA levels in the infected tissues will be needed to support the presumed cooperative function of all three enzymes targeting SA pathway during infection.

3.6 The loop region is essential for the biological activity of Cmu1

Loops are usually disordered regions in protein structures (Papaleo et al., 2016). They are not only responsible for connecting different secondary structural elements, but also play roles in enzymatic activity, allosteric regulation and protein-protein interactions (Espadaler et al., 2006; Papaleo et al., 2016). Loops in the effector AvrLm4–7 from *L. maculans* contribute to Rlm4 or Rlm7 binding and are also found to be likely involved in the translocation of AvrLm4–7 (Blondeau et al., 2015). A conserved HPD loop in the J domain of the *P. syringae* effector HopI1 is essential for interaction with Hsp70, which plays an important role in the virulence function of HopI1 (Jelenska et al., 2007; Jelenska et al., 2010). The loop region of Cmu1 comprising 52 residues is found on the surface of the structure (J. Schuhmacher and G. Bange, unpublished), which is conserved in smut secreted CMs. When part of the loop (117-140) was replaced with GSGS linker, the biological activity of the mutant protein was reduced and only partial complementation of CL13Δcmu1 virulence phenotype was observed. To explain the lack of full complementation, it was considered that the replacement in the loop region might affect protein stability, CM activity, translocation or protein-protein interactions. It has been shown that Cmu1 carrying the replacement in the loop region exhibited comparable CM activity to wildtype Cmu1. Furthermore, Cmu1 mutant protein showed comparable amount to the wildtype protein, demonstrating that the stability is not affected when the loop is partially deleted. However, it remains unclear whether the mutant protein was affected in translocation, which needs to be further investigated by performing immuno-EM and an uptake assay exploiting transgenic maize plants expressing the biotin ligase BirA. Interestingly, *in vitro* pull-down experiment showed that the interaction of Cmu1 with the maize protein Cmi1 was almost abolished due to the replacement in the loop region, which will be discussed in the following chapter.

3.7 Interaction partners of Cmu1

3.7.1 Maize CMs

CMs play a critical role in biosynthesis of phenylalanine and tyrosine, which are necessary for protein synthesis in plants and other organisms (Tzin and Galili, 2010). Plants harbor at least two

CMs with one in the plastid and the other in the cytosol (Eberhard et al., 1996a; Eberhard et al., 1996b; Colquhoun et al., 2010; Djamei et al., 2011; Westfall et al., 2014). Plastidic CMs can be allosterically regulated by tryptophan, tyrosine and phenylalanine, whereas cytosolic CMs are not responsive to these three amino acids (Goers and Jensen, 1984; Eberhard et al., 1996b; Westfall et al., 2014). It was shown that a third CM is present in some plant species (Mobley et al., 1999; Westfall et al., 2014). The third CM found in *A. thaliana* also contain a putative plastid transit peptide and is allosterically regulated (Mobley et al., 1999; Westfall et al., 2014).

Because of the existence of cytosolic CMs, it has been proposed that chorismate is transported from plastids to the cytosol (Eberhard et al., 1996b). Moreover, expression of the bacterial chorismate pyruvatelyase that utilizes chorismate in the cytosol of tobacco resulted in the formation of 4-hydroxybenzoate, reinforcing the hypothesis that chorismate might also reside in the plant cytosol (Sommer and Heide, 1998). In the plant cytosol, there may also exist a partial shikimate pathway (Reinbothe et al., 1994; Eberhard et al., 1996b; Maeda and Dudareva, 2012). The entry of Cmu1 of *U. maydis* is hypothesized to increase the CM activity in plant cytosol, which may disrupt the homeostasis of chorismate in the cytosol and drive the flux of chorismate from the plastid to the cytosol (Djamei et al., 2011).

In maize, five CMs are found in the genome. ZmCM1 has three paralogs: GRMZM2G028369, GRMZM2G116087 and GRMZM2G124365 that are predicted to localize in the plastid and ZmCM2 is thought to reside in the cytosol. However, the third CM, ZmCM3, is predicted to be a secreted protein. It displays higher identity to cytosolic ZmCM2 (49.5%) than that to plastidic ZmCM1 (37.7%), indicating that ZmCM3 is likely a non-allosteric regulated CM.

The expression profiling shows one ZmCM1 paralog GRMZM2G116087 is significantly induced upon infection of *U. maydis* (D. Lanver, personal communication), suggesting that GRMZM2G116087 is pathogenesis-related. The function of this enzyme needs to be studied to elucidate such a possible connection to pathogenesis. It is possible that Cmu1 after uptake can increase the CM activity in plant cytosol and that this fulfills its virulence function. However, it cannot be excluded that Cmu1 might interact with plant CMs to reprogram the SA pathway. In a previous study, Cmu1 was shown to interact with ZmCM1 and ZmCM2 in Y2H assay (Djamei et al., 2011). In experiments conducted in this thesis, Co-IP/MS did not detect an interaction of Cmu1 with any of the maize CMs. This is likely to reflect that such interactions are an artifact of the Y2H assays where Cmu1 was co-expressed with the maize CMs. However, whether it is necessary for

Cmu1 to interact with plant CMs to suppress SA biosynthesis needs to be further investigated. It will also be interesting to test the virulence phenotype of CL13 Δ cmu1 strains on transgenic plants in which individual CMs are downregulated.

3.7.2 The interaction of Cmu1 with Cmi1 is likely to occur in the apoplast

By conducting Co-IP/MS, the maize protein Cmi1 was found to interact with Cmu1. The interaction of Cmu1 and Cmi1 was confirmed by *in vitro* pull-down, while an interaction in Y2H could not be demonstrated. This might be caused by the incorrect folding of Cmi1 protein in yeast since it has five putative disulfide bonds. Cmi1 is predicted to be a secreted protein, pointing out that Cmu1 might possess a secondary function in the apoplast. Through HDX/MS, a loop region of Cmu1 was mapped to be part of the interaction interface.

3.7.2.1 Cmi1 might be a PR-4 protein

Beside the SP of Cmi1, there is an RlpA-like double-psi beta-barrel (DPBB) domain predicted in the C-terminus. Proteins having DPBB domains constitute a large family of pathogenesis-related protein 4 (PR-4) proteins. Members of this family are required for plants to cope with abiotic or biotic stresses, including the wound-induced proteins Win-1 and Win-2 from potato, plant defense related Barwin protein from barley and pathogenesis-related 4 (PR-4) proteins from tobacco and pepper (Stanford et al., 1989; Friedrich et al., 1991; Svensson et al., 1992; Guevara-Morato et al., 2010). Overexpression of a PR-4 protein (VpPR4-1) from the wild Chinese grape *Vitis pseudoreticulata* in another species *V. vinifera* enhanced powdery mildew resistance (Dai et al., 2016), suggesting a positive role of PR-4 protein protecting against fungal pathogens

PR-4 genes are usually induced upon abiotic and biotic stresses. In *V. vinifera*, mRNA for synthesizing grape ripening-induced-protein 22 (Grip 22) was significantly accumulated during the ripening of grape berries (Davies and Robinson, 2000). Comparative transcript profiling also uncovered that PR-4 related gene encoding the kiwellin homolog TC197025 from potato was highly upregulated in plants challenged by *P. infestans* compared to uninfected plants (Draffehn et al., 2013). Another kiwellin-like protein (Pepper05849) from pepper (*Capsicum annuum*) is one of the most upregulated genes when *C. annuum* is infected by *Pepper golden mosaic virus* (PepGMV) (Gongora-Castillo et al., 2012). Although 13 paralogs of Cmi1 are present in maize, only *cmi1* shows drastic induction upon infection of *U. maydis* (D. Lanver, personal communication). This

strongly indicates that Cmi1 might be a PR-4 protein of maize that is involved in defenses against *U. maydis*.

3.7.2.2 Putative functions of Cmi1

PR-4 proteins are widespread in the plant kingdom. Many PR-4 proteins have been reported to possess antifungal activity, which contributes to plant defenses against pathogens. For instance, a PR-4 protein isolated from barley grain and stressed leaves exhibited antifungal activity toward *Trichoderma harzianum* in microtiter plate assays (Hejgaard et al., 1992). CBP20 from *N. tabacum* showed inhibitory effect on the growth of *T. viride* and *Fusarium solani* (Ponstein et al., 1994). Wheatwin1, a PR-4 protein from wheat, was found to inhibit the spore germination and hyphal growth of *F. culmorum* (Caporale et al., 2004). In the course of this study, no antifungal activity of Cmi1 could be demonstrated yet. However, for this assay Cmi1 protein produced in *E. coli* was used. Given that Cmi1 is predicted to be a secreted protein, it is unclear whether this protein is properly folded when produced in *E. coli*. It is also possible that it may lack posttranslational modifications which could be needed for its activity.

It should be noted that chitinases also have the DPBB topology, implying that PR-4 proteins could have chitin binding activities. However, amino acid sequence alignment of Cmi1 and its homologs revealed that Cmi1 does not harbor the chitin binding domain (**Fig. 36**). Therefore it is unlikely that Cmi1 binds chitin.

A number of PR-4 proteins have been shown to have nuclease activity. Wheatwin1 is able to digest RNA from wheat coleoptiles (Caporale et al., 2004), while a PR-4 protein induced in *C. chinense* plants displays both RNase and DNase activity (Guevara-Morato et al., 2010). The antifungal activity of wheatwin1 was correlated to its RNase activity because the catalytically inactive wheatwin1 mutant was not able to inhibit spore germination or hyphae growth of *F. culmorum* (Bertini et al., 2009). The ribonuclease activity of PR-4 proteins requires two conserved histidine residues (Bertini et al., 2009). These two histidine residues are absent in Cmi1 (**Fig. 36**), making it unlikely that Cmi1 has ribonuclease activity.

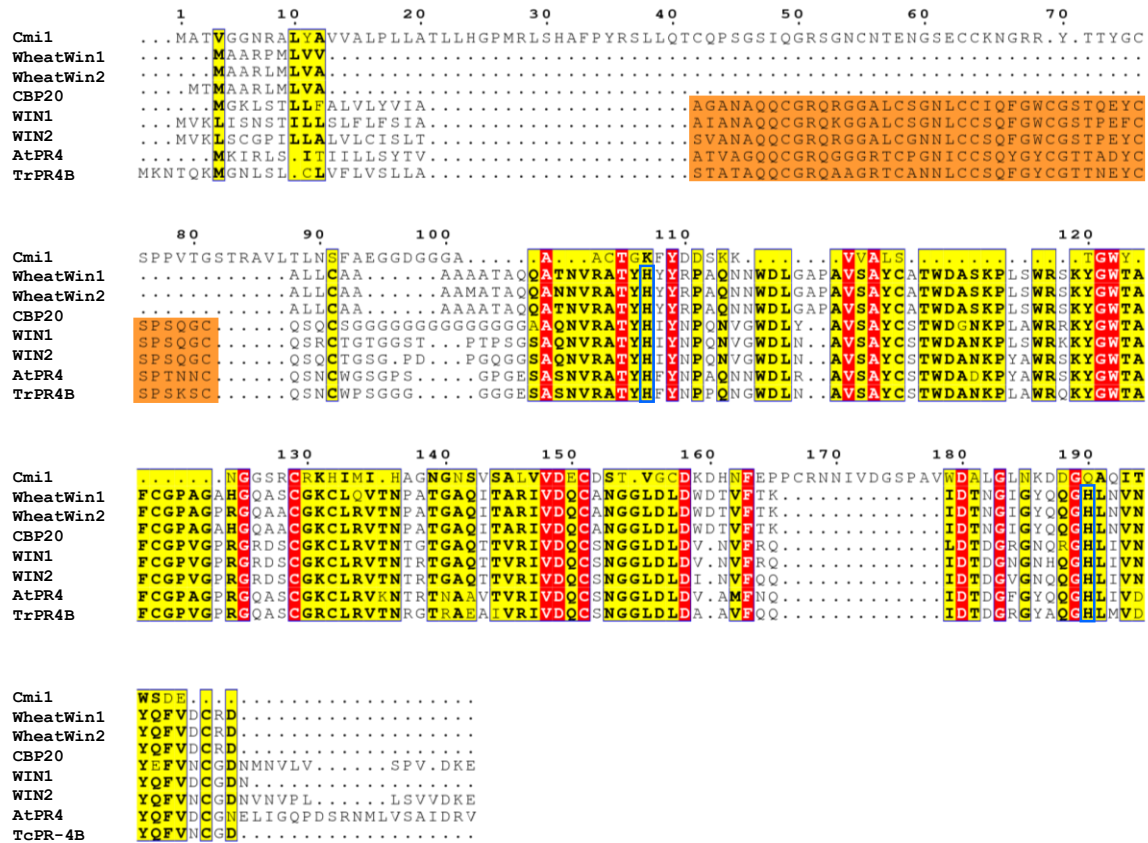


Fig. 36: Amino acid sequence alignment of Cmi1 with its homologs. Cmi1 homologs used here are WheatWin1 (*Triticum aestivum*, CAA06856.1), WheatWin2 (*T. aestivum*, CAA06857.1), CBP20 (*N. tabacum*, AAB29959.2), WIN1 (*S. tuberosum*, XP_006347743.1), WIN2 (*S. tuberosum*, NP_001275628.1), AtPR4 (*A. thaliana*, AEE74125.1) and TcPR-4B (*Theobroma cacao*, EOY25834.1). Red background indicates amino acid sequence identity, yellow background in bold letters indicates sequence similarity. The chitin binding domains are shaded in orange. Two conserved histidine residues for ribonuclease activity are highlighted with blue boxes. The alignment was generated with CLUSTAL Omega (Sievers et al., 2011) and ESPript 3.0 (Robert and Gouet, 2014).

It was recently uncovered that PR-4 proteins are able to induce cell death. *Agrobacterium*-mediated transient expression of CaPR4b from pepper (*C. annuum*) induced hypersensitive cell death in *N. benthamiana* leaves, and the secretion of CaPR4b to the apoplastic space was required for the cell death induction (Hwang et al., 2014). Another PR-4 protein CaPR4c from pepper was also able to induce cell death when transiently expressed with the SP in pepper leaves, which was accompanied by the production of H₂O₂ and decreased expression of defense related genes (Kim and Hwang, 2015). Moreover, CaPR4c localizes to plasma membrane of plant cells after transient expression (Kim and Hwang, 2015). The detailed mode of action for cell death inducing of CaPR4b and CaPR4c is yet to be discovered.

3.7.2.3 The biological relevance of the interaction of Cmu1 with Cmi1

Since Cmi1 is putatively secreted by plant cells, the interaction between Cmu1 and Cmi1 is likely to happen in the apoplast. It was also shown that the CM activity of Cmu1 was inhibited by Cmi1. If Cmu1 interacts with Cmi1 in the apoplast, this suggests that maize may have evolved to inactivate Cmu1 and prevent its uptake. Nevertheless, given the high expression of Cmu1, there may still be sufficient protein which might enter into plant cells to exert its function in interference with the SA pathway. Therefore, Cmi1 might be the weapon of maize to disarm the effector Cmu1 to compromise virulence of *U. maydis*. To substantiate this possibility, the *cmi1* gene needs to be silenced and tested for the susceptibility to CL13 Δ cmu1 mutants.

Given the fact that *U. maydis* successfully colonizes maize, this indicates that Cmu1 might be able to surpass Cmi1. Furthermore, Cmu1 ^{Δ 117-140} with a partial deletion of the loop region lost the interaction with Cmi1 and exhibited only partial complementation, suggesting that the interaction between Cmu1 and Cmi1 is biologically relevant. Supposing that Cmi1 has antifungal activity as its homologs, it can be speculated that Cmu1 may inhibit the inhibitory effect of Cmi1 on *U. maydis* (**Fig. 37**). When Cmu1 loses its ability to interact with Cmi1, Cmi1 could inhibit the growth of *U. maydis*, thereby reducing its virulence *in planta*. Secondly, homologs of Cmi1 were shown to possess cell death inducing ability (Hwang et al., 2014; Kim and Hwang, 2015), suggesting the potential of Cmi1 to induce cell death. If Cmi1 has similar function, it is possible that Cmu1 would inhibit cell death that is caused by Cmi1 to favor the biotrophic growth of *U. maydis* on maize (**Fig. 37**). On the contrary, emerging evidences show that some effectors of plant pathogens also trigger cell death when expressed *in planta* (Schornack et al., 2010a; Liu et al., 2011; Yu et al., 2012; Ma et al., 2015; Zhang et al., 2015). Considering the high abundance of Cmu1 during *U. maydis* infection, the possibility that Cmu1 induces cell death, which may be suppressed by Cmi1, should also be taken into account (**Fig. 37**). In both cases, the loss of interaction between Cmu1 and Cmi1 could result in cell death, which will compromise the virulence (**Fig. 37**). To test these hypotheses, Cmi1 or Cmu1 will be introduced into maize leaves individually or together via infiltration or biolistic transformation to investigate their abilities to induce cell death and whether the resulting cell death is inhibited when two partners are both present.

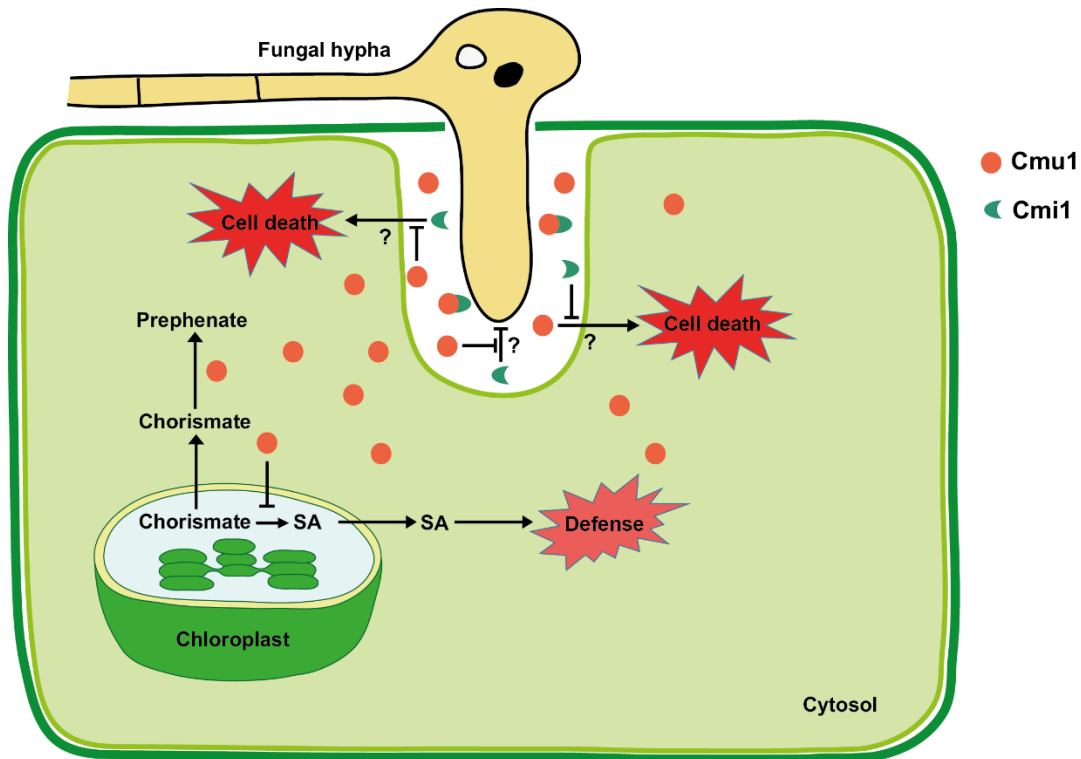


Fig. 37: Hypothetic model of the functions of Cmu1. Cmu1 is firstly secreted to the apoplast, where it interacts with maize protein Cmi1. It is possible that Cmi1 has antifungal activity and inhibits *U. maydis*, which is blocked by Cmu1. It is also possible that Cmu1 or Cmi1 alone could induce cell death, which could be inhibited by the other partner. After being translocated into the plant cell, Cmu1 in the cytosol depletes chorismate in the chloroplast, thus suppressing SA mediated defenses. Dark green and olive green lines represent the plant cell wall and plasma membrane. The apoplast is schematically enlarged.

4. Materials and Methods

4.1 Materials

4.1.1 Chemicals

All chemicals used in the study were obtained from Difco (Augsburg, Germany), AppliChem (Darmstadt, Germany), GE Healthcare (Munich, Germany), Invitrogen (Darmstadt, Germany), Merck (Darmstadt, Germany), Roche (Mannheim, Germany), Roth (Karlsruhe, Germany), IBA (Göttingen, Germany) and Sigma-Aldrich (Deisenhofen, Germany).

4.1.2 Buffers

Standard buffers and solutions were prepared according to Ausubel *et al.* (1987) and Sambrook *et al.* (1989). Special buffers and solutions were listed along with the corresponding methods. All buffers and solutions were autoclaved at 121°C for 5 min. Heat sensitive solutions were filter-sterilized (Stericup, pore size 0.2 µm, Merck, Darmstadt, Germany).

4.1.3 Enzymes and antibodies

All the restriction enzymes were purchased from New England Biolabs (NEB, Frankfurt, Germany). DNA polymerases like Phusion® Hot Start High-Fidelity DNA polymerase was bought from Thermo Scientific (Bonn, Germany) and the BioMix™ Red containing the Taq polymerase was bought from Bioline (Luckenwalde, Germany). Ligation of DNA fragments was performed with T4 DNA ligase (NEB, Frankfurt, Germany) or self-made Gibson Assembly® Master Mix. Enzymatic degradation of fungal cell walls was carried out by using Novozyme 234 (Novo Nordisk, Copenhagen, Denmark). Antibodies used in the studies were described along with the methods sections.

4.1.4 Kits

Purification of DNA fragments from agarose gels was carried out with Wizard® SV Gel and PCR Clean-Up System from Promega (Mannheim, Germany). Plasmids were isolated by using the QIAprep® Spin Miniprep Kit or QIAGEN Plasmid Midi Kit from Qiagen (Hilden, Germany). The substitutions of amino acids in plasmids were performed using the QuikChange Lightning Multi Site-Directed Mutagenesis Kit (Agilent, Waldbronn, Germany). For digoxigenin (DIG) labeling of

PCR products, PCR DIG Probe Synthesis Kit (Roche, Mannheim, Germany) was used. Amersham ECL™ Prime Western Blotting System (GE Healthcare, Munich, Germany) or SuperSignal West Femto Maximum Sensitivity Substrate (Thermo Scientific, Bonn, Germany) were used for chemiluminescence detection.

Size standards for agarose gel electrophoresis were 1 kb and 2-log ladder (NEB, Frankfurt, Germany) and for SDS-polyacrylamide gel electrophoresis was PageRuler™ Prestained Protein Ladder, 10 to 180 kDa (Thermo Scientific, Bonn, Germany). Additional materials were listed in individual method sections.

4.2 Media and cultivation methods for microbes

The recipes of all media for cultivation of various microbes were listed below. The media were autoclaved at 121°C for 5 min, unless otherwise indicated.

4.2.1 Media and cultivation of *E. coli* and *A. tumefaciens* strains

E. coli strains or *A. tumefaciens* strains were cultivated in dYT or LB liquid medium and grown on YT solid medium (Ausubel et al., 1987; Sambrook et al., 1989). For selection of transformants, appropriate antibiotics were added in the media to certain final concentrations (Ampicillin (Amp), 100 µg/mL; Kanamycin (Kan), 50 µg/mL; Spectinomycin (Spec), 50 µg/mL; Rifampicin (Rif), 50 µg/mL; Chloramphenicol (Chl), 34 µg/mL; Gentamicin (Gent), 25 µg/mL). Liquid cultures were incubated at 37°C or 28°C under continuous shaking at 200 rpm. Solid media were incubated under aerobic condition at 37°C or 28°C. For long-term storage, overnight cultures were mixed with dYT glycerol medium at a ratio of 1:1 and stored at -80°C.

dYT medium

1.6% (w/v) Tryptone (Bacto)
1.0% (w/v) Yeast-Extract (Bacto)
0.5% (w/v) NaCl (Roth)
Dissolved in ddH₂O and autoclave.

LB medium

1.0% (w/v) Tryptone (Bacto)
0.5% (w/v) Yeast-Extract (Bacto)
1.0% (w/v) NaCl (Roth)
2.0% (w/v) Agar (Bacto, for plates only)
Dissolved in ddH₂O and autoclave.

YT agar medium

0.8% (w/v) Tryptone (Bacto)
0.5% (w/v) Yeast-Extract (Bacto)
0.5% (w/v) NaCl (Roth)

2.0% (w/v) Agar (Bacto)
Dissolved in ddH₂O and autoclave.

dYT glycerol medium 1.6% (w/v) Tryptone (Bacto)
1.0% (w/v) Yeast-Extract (Bacto)
0.5% (w/v) NaCl (Roth)
80.0% (v/v) 87% Glycerol (f. c. 69.6%)
Dissolved in ddH₂O and autoclave.

4.2.2 Media and cultivation of *S. cerevisiae* strains

S. cerevisiae strains were cultivated in YPD or SD liquid medium and grown on YPD or SD solid medium. YPD medium was used as complete medium to maintain strains. For selection of transformants, SD media supplemented with appropriate nutrients (L-Adenine hemisulfate salt (Ade), 20 mg/L; L-Histidine HCl monohydrate (His), 20 mg/L; L-Leucine (Leu), 100 mg/L and L-Tryptophan (Trp), 20 mg/L) were utilized. Liquid cultures were incubated at 28°C under continuous shaking at 200 rpm. Solid media were incubated under aerobic condition at 28°C. For long-term storage, overnight cultures were mixed with NSY glycerol medium at a ratio of 1:1 and stored at -80°C.

YPD medium 2.0% (w/v) Peptone (Bacto)
1.0% (w/v) Yeast-Extract (Bacto)
2.0% (w/v) Agar (Bacto, for plates only)
Dissolve in ddH₂O and autoclave.
2.0% (w/v) Glucose (Roth) added after autoclaving.

SD-Leu-Trp-Ade-His medium 0.67% (w/v) Yeast nitrogen base without amino acids
0.06% (w/v) Dropout Supplement (-Ade, -His, -Leu, -Trp)
Dissolve in ddH₂O and autoclave.
2.0% (w/v) Agar (Bacto, for plates only)
Dissolve in ddH₂O and autoclave.
2.0% (w/v) Glucose (Roth) added after autoclaving.

NSY glycerol medium 0.8% (w/v) Nutrient broth (Difco)
0.1% (w/v) Yeast-Extract (Bacto)
0.5% (w/v) Sucrose (Roth)
80.0% (v/v) 87% Glycerol (f. c. 69.6%)
Dissolve in ddH₂O and autoclave.

4.2.3 Media and cultivation of *U. maydis* strains

U. maydis strains were cultivated in YEPS_{light} or CM liquid medium and grown on PD or

Regenerationagar_{light} medium. To select transformants, carboxin (Cbx), hygromycin B (Hyg) and geneticin G418 (Neo) were supplemented in PD solid medium or Regenerationagar_{light} medium to final concentrations at 2 µg/mL (Cbx), 200 µg/mL (Hyg) and 400 µg/mL (Neo), respectively. Liquid cultures were incubated at 28°C under continuous shaking at 200 rpm. Solid media were incubated under aerobic condition at 28°C. For long-term storage, overnight cultures were mixed with NSY glycerol medium at a ratio of 1:1 and stored at -80°C.

YEPS_{light} liquid medium	1.0% (w/v) Yeast-Extract (Bacto) 0.4% (w/v) Peptone (Bacto) 0.4% (w/v) Sucrose (Roth) Dissolve in ddH ₂ O and autoclave.
CM liquid medium	0.25% (w/v) Casamino acids (Difco) 0.1% (w/v) Yeast-Extract (Bacto) 1.0% (v/v) Vitamin solution (Holliday, 1974) 6.25% (v/v) Salt solution (Holliday, 1974) 0.05% (w/v) DNA from herring sperm degenerated (Sigma) 0.15% (w/v) NH ₄ NO ₃ (Roth) 1.0% (v/v) 1 M Tris/HCl pH 8.0 (f. c.10 mM) Dissolve in ddH ₂ O, adjust pH to 7.0 with 5 M NaOH and autoclave. 2.0% (w/v) Glucose (Roth) added after autoclaving.
Vitamin solution (Holliday, 1974)	0.1‰ (w/v) Thiamine hydrochloride (Sigma) 0.05‰ (w/v) Riboflavin (Sigma) 0.05‰ (w/v) Pyridoxine hydrochloride (Sigma) 0.2‰ (w/v) D-Pantothenic acid hemicalcium salt (Sigma) 0.05‰ (w/v) 4-Aminobenzoic acid (Sigma) 0.2‰ (w/v) Nicotinic acid (Sigma) 0.2‰ (w/v) Choline chloride (Sigma) 1.0‰ (w/v) myo-Inositol (Sigma) Dissolve in ddH ₂ O, prepare 40 mL aliquots in 50 mL tubes and freeze at -20°C.
Salt solution (Holliday, 1974)	16.0‰ (w/v) KH ₂ PO ₄ 4.0‰ (w/v) Na ₂ SO ₄ 8.0‰ (w/v) KCl 2.0‰ (w/v) MgSO ₄ ·7H ₂ O 1.32‰ (w/v) CaCl ₂ ·2H ₂ O 8.0‰ (v/v) Trace elements (Holliday, 1974)

	Dissolve in ddH ₂ O and sterile filtrate.
Trace elements (Holliday, 1974)	0.06‰ (w/v) H ₃ BO ₃ 0.14‰ (w/v) MnCl ₂ ·4H ₂ O 0.4‰ (w/v) ZnCl ₂ 0.4‰ (w/v) Na ₂ MoO ₄ ·2H ₂ O 0.1‰ (w/v) FeCl ₃ ·6H ₂ O 0.03‰ (w/v) CuSO ₄ Dissolve in ddH ₂ O.
PD agar medium	2.4% (w/v) Potato Dextrose Broth (Difco) 2.0% (w/v) Agar (Bacto) Dissolve in ddH ₂ O and autoclave.
Regenerationagar_{light} medium (Schulz et al., 1990)	1.0% (w/v) Yeast-Extract (Bacto) 0.4% (w/v) Peptone (Bacto) 0.4% (w/v) Sucrose (Roth) 18.22% (w/v) Sorbitol (Sigma, f. c. 1 M) 1.5% (w/v) Agar (Bacto) Dissolve in ddH ₂ O and autoclave.

4.2.4 Determination of cell density

The cell density of liquid cultures was determined photometrically using an Ultrospec 3000 pro UV/Visible Spectrophotometer (Biochrom, Cambridge, UK) at 600 nm (OD₆₀₀). To determine the optical density, cell cultures were diluted 1:10 in the respective medium. The OD₆₀₀ of sterile medium was used as a reference value.

4.3 Strains, oligonucleotides and plasmids

4.3.1 *E. coli* strains

E. coli Top10 and DH5 α strains were used for plasmid amplification in cloning procedures. *E. coli* BL21 (DE3) star and SHuffle® T7 strains were used for heterologous overexpression of proteins.

TOP10 (Invitrogen, Karlsruhe, Germany): (F⁻ *mcrA* Δ (*mrr-hsdRMS-mcrBC*) Φ 80*lacZ* Δ M15 Δ *lacX74 recA1 araD139* Δ (*araleu*)7697 *galU galK rpsL (StrR) endA1 nupG*)

DH5 α (Thermo Scientific, Bonn, Germany): (F⁻ Φ 80*lacZ* Δ M15 Δ (*lacZYA-argF*) U169 *recA1 endA1 hsdR17(r_k⁻, m_k⁺) phoA supE44 thi-1 gyrA96 relA1 λ ⁻)*

BL21 (DE3) star (Thermo Scientific, Bonn, Germany): (F⁻ *ompT hsdS_B (r_B⁻, m_B⁻) gal dcmrne131* (DE3))

SHuffle® T7 (NEB, Frankfurt, Germany): (F' *lac, pro, lacI^q /* Δ (*ara-leu*)7697 *araD139 fhuA2*)

lacZ::T7 gene1 Δ(phoA)PvuII phoR ahpC galE (or U) galK λatt::pNEB3-r1-cDsbC (Spec^R, lacI^q) ΔtrxB rpsL150(Str^R) Δgor Δ(malF)3*

4.3.2 *A. tumefaciens* strains

A. tumefaciens GV3101 strain was used for transient expression of protein in *Nicotiana benthamina*.

4.3.3 *S. cerevisiae* strains

S. cerevisiae AH109 was used as host strain for yeast two-hybrid assays.

AH109 (Clontech, Saint-Germain-en-Laye, France): (*MATa*, *trp1-901*, *leu2-3, 112*, *ura3-52*, *his3-200*, *gal4Δ*, *gal80Δ*, *LYS2::GAL1_{UAS}-GAL1_{TATA}-HIS3*, *GAL2_{UAS}-GAL2_{TATA}-ADE2*, *URA3::MEL1_{UAS}-MEL1_{TATA}-lacZ*)

4.3.4 *U. maydis* strains

U. maydis strains described in previous studies are listed in Table 3. *U. maydis* strains generated in this study are listed in Table 4.

Table 3. *U. maydis* strains described in previous studies

Serial number	Name	Genotype	Resistance ¹	Reference
AD303	CL13	<i>a1: bE1 bW2</i>	-	Bölker et al., 1995
AD1606	AB33	<i>a2: P_{nar}: bW2 bE1</i>	Phleo	Brachmann et al., 2001
UVT94	SG200	<i>a1: mfa2 bW2 bE1</i>	Phleo	Kämper et al., 2006
AD417	CL13Δ <i>cmu1</i>	<i>a1: bE1 bW2 Δum05731</i>	Hyg	Djamei et al., 2011
AD1478	CL13Δ <i>cmu1</i> - <i>Cmu1-HA₃</i>	<i>a1: bE1 bW2 Δum05731 ip^R[P_{um05731}-um05731]ip^S</i>	Hyg, Cbx	Djamei et al., 2011
AD1618	SG200Δ <i>cmu1</i>	<i>a1: mfa2 bW2 bE1 Δum05731</i>	Phleo, Hyg	Djamei et al., 2011
FH33	SG200Δ <i>cmu1</i> - <i>Cmu1-HA₃</i>	<i>a1: mfa2 bW2 bE1 Δum05731 ip^R[P_{um05731}-um05731]ip^S</i>	Phleo, Hyg, Cbx	F. Hartwig, unpublished

¹ phleomycin (Phleo), hygromycin (Hyg), carboxin (Cbx)

Table 4. *U. maydis* strains generated in this study

Serial number	Name	Genotype	Resistance ¹
AD1490	CL13Δcmu1-Cmu1 ^{Δ22-40} -HA ₃	<i>a1: bE1 bW2 Δum05731 ip^R[P_{um05731-um05731}^{Δ22-40}]ip^S</i>	Hyg, Cbx
AD1510	CL13Δcmu1-Cmu1 ^{D37A} -HA ₃	<i>a1: bE1 bW2 Δum05731 ip^R[P_{um05731-um05731}^{D37A}]ip^S</i>	Hyg, Cbx
AD1511	CL13Δcmu1-Cmu1 ^{D40A} -HA ₃	<i>a1: bE1 bW2 Δum05731 ip^R[P_{um05731-um05731}^{D40A}]ip^S</i>	Hyg, Cbx
AD1488	CL13Δcmu1-Cmu1 ^{D37AD40A} -HA ₃	<i>a1: bE1 bW2 Δum05731 ip^R[P_{um05731-um05731}^{D37AD40A}]ip^S</i>	Hyg, Cbx
AD1657	CL13Δcmu1-Cmu1 ^{6A} -HA ₃	<i>a1: bE1 bW2 Δum05731 ip^R[P_{um05731-um05731}^{6A}]ip^S</i>	Hyg, Cbx
AD1684	CL13Δcmu1-Cmu1 ^{8A} -HA ₃	<i>a1: bE1 bW2 Δum05731 ip^R[P_{um05731-um05731}^{8A}]ip^S</i>	Hyg, Cbx
AD1661	CL13Δcmu1-Cmu1 ^{SS} -HA ₃	<i>a1: bE1 bW2 Δum05731 ip^R[P_{um05731-um05731}^{SS}]ip^S</i>	Hyg, Cbx
AD1669	CL13Δcmu1-Cmu1 ^{KY} -HA ₃	<i>a1: bE1 bW2 Δum05731 ip^R[P_{um05731-um05731}^{KY}]ip^S</i>	Hyg, Cbx
AD1720	CL13Δcmu1-Cmu1 ^{Δ117-140} -HA ₃ #4	<i>a1: bE1 bW2 Δum05731 ip^R[P_{um05731-um05731}^{Δ117-140}]ip^S</i>	Hyg, Cbx
AD1721	CL13Δcmu1-Cmu1 ^{Δ117-140} -HA ₃ #5	<i>a1: bE1 bW2 Δum05731 ip^R[P_{um05731-um05731}^{Δ117-140}]ip^S</i>	Hyg, Cbx
AD1737	CL13Δcmu1-Cmu1 ^{Δ117-140} -HA ₃ #8	<i>a1: bE1 bW2 Δum05731 ip^R[P_{um05731-um05731}^{Δ117-140}]ip^S</i>	Hyg, Cbx
AD1738	CL13Δcmu1-Cmu1 ^{Δ117-140} -HA ₃ #15	<i>a1: bE1 bW2 Δum05731 ip^R[P_{um05731-um05731}^{Δ117-140}]ip^S</i>	Hyg, Cbx
AD1686	CL13Δcmu1-SP-cTP-Cmu1 ^{ASP} -HA ₃ #2	<i>a1: bE1 bW2 Δum05731 ip^R[P_{um05731-SP-cTP-um05731}^{ASP}]ip^S</i>	Hyg, Cbx
AD1687	CL13Δcmu1-SP-cTP-Cmu1 ^{ASP} -HA ₃ #7	<i>a1: bE1 bW2 Δum05731 ip^R[P_{um05731-SP-cTP-um05731}^{ASP}]ip^S</i>	Hyg, Cbx
AD1688	CL13Δcmu1-SP-cTP-Cmu1 ^{ASP} -HA ₃ #18	<i>a1: bE1 bW2 Δum05731 ip^R[P_{um05731-SP-cTP-um05731}^{ASP}]ip^S</i>	Hyg, Cbx
AD1666	SG200Δcmu1Δum12021	<i>a1: mfa2 bW2 bE1 Δum05731Δum012021</i>	Phleo, Hyg, Neo
AD1700	SG200Δcmu1Δum12021 um05230en	<i>a1: mfa2 bW2 bE1 Δum05731Δum012021um05230Δ365</i>	Phleo, Hyg, Neo
AD1734	SG200Δcmu1Δum12021 um05230en-Cmu1-HA ₃ #1	<i>a1: mfa2 bW2 bE1 Δum05731Δum012021um05230Δ365 ip^R[P_{um05731-um05731}]ip^S</i>	Phleo, Hyg, Neo, Cbx

AD1735	SG200 Δ cmu1 Δ um12021 um05230en-Cmu1-HA ₃ #6	<i>a1: mfa2 bW2 bE1</i> <i>Δum05731Δum012021um05230Δ365</i> <i>ip^R[P_{um05731}-um05731]ip^S</i>	Phleo, Hyg, Neo, Cbx
AD1599	AB33-Cmu1-HA ₃	<i>a2: P_{nar}: bW2 bE1</i> <i>ip^R[P_{otef}-um05731]ip^S</i>	Phleo, Cbx
AD1731	AB33-Cmu1 ^{Δ117-140} -HA ₃	<i>a2: P_{nar}: bW2 bE1</i> <i>ip^R[P_{otef}-um05731^{Δ117-140}]ip^S</i>	Phleo, Cbx

¹phleomycin (Phleo), hygromycin (Hyg), carboxin (Cbx), neomycin (Neo)

4.3.5 Oligonucleotides

All oligonucleotides used in this study were purchased from Eurofins Genomics (Munich, Germany). The names, the nucleotide sequences, potential restriction sites integrated by the oligonucleotide and the respective applications are listed in Table 5.

Table 5: Oligonucleotides used in this study

Name	Sequence ¹	Restriction site	Application ²
AD993	AGACGAGTTGGAGCGAAACG	/	Sequencing <i>cmu1</i> sequence (F)
AD214	CATCGCAAGACCGGCAACAGGATTC	/	Sequencing <i>cmu1</i> sequence (R)
ppi-F	ACATCGTCAAGGCTATCG	/	qPCR primer that amplifies <i>ppi</i> (F)
ppi-R	AAAGAACACCGGACTTGG	/	qPCR primer that amplifies <i>ppi</i> (R)
gapdh-F	CTTCGGCATTGTTGAGGGTTTG	/	qPCR primer that amplifies <i>gapdh</i> (F)
gapdh-R	TCCTTGGCTGAGGGTCCGTC	/	qPCR primer that amplifies <i>gapdh</i> (R)
XW005	TCTGAACAGGACGAAAAACGTGCTG CTCTGTCTC	/	Mutagenic primer that substitutes V74K in pAD1752
XW007	CGTTCTACCCGTCCGTATCCGCCGGC TGTTGAATTC	/	Mutagenic primer that substitutes L107Y in pAD1752
XW012	TGCACGACAACCTTCTCTCACATCCTG ACCAAC	/	Mutagenic primer that substitutes C203S in pAD1752
XW013	ACCACGCTAACAAATCTACCCTCGA GCACCACC	/	Mutagenic primer that substitutes C289S in pAD1752

XW030	GACCACGCCAACAAAGTCGACCGGCG GCCGCGAG	/	Mutagenic primer that substitutes C289S in pAD2205
XW034	GAG <u>CCCCGGG</u> GATGAAGTTGAGCGTGT C	<i>XmaI</i>	Cloning <i>cmuI</i> sequence to p123 (F)
XW039	CGGTCGACGCGACCGTACCCGCCTG CTGTTCGAG	/	Mutagenic primer that substitutes L107Y in pAD2239
XW041	GTTCTCGCCCTTCGACATGCCGCCG GTGCACTTGTGGCGTGG	/	Amplification of <i>cmuI^{ASP}</i> overlapping with <i>sfGFP</i> (R)
XW043	AAGTGCACCGGCGGCATGTGAAGG GCGAGGAAC	/	Amplification of <i>sfGFP</i> overlapping with <i>cmuI^{ASP}</i> (F)
XW044	GGTGATTTTTGCGGACTCTAGATTAC TTGTAGAGTTCGTCCATGC	/	Amplification of <i>sfGFP</i> overlapping with p35S vector (R)
XW046	AGAGAATTCATGTGAAGGGCGAGG AAC	<i>EcoRI</i>	Amplification of <i>sfGFP</i> (F)
XW047	AAGTCTAGATTACTTGTAGAGTTCGT CCATGC	<i>XbaI</i>	Amplification of <i>sfGFP</i> (R)
XW048	CGATAAGCTTGATATCGAATTCACCA TGGCGGCTGTATCTGGCAAGTC	/	Amplification of <i>cmuI^{ASP}</i> overlapping with p35S vector (F)
XW049	GTATCTGGCAAGTCGGCGGCGGCAG CCATCGCTGCGGGCGCTCGACTG	/	Mutagenic primer that substitutes E29AE32A E34A in pAD2286
XW050	TTCGACTGGCTCCACGCCAACTTCTG CCACATC	/	Mutagenic primer that substitutes D200A in pAD2322
XW051	AGAGAATTCGGGCTCAGCCTGGACA C	<i>EcoRI</i>	Cloning <i>ZmCM3²⁹⁻²⁸⁴</i> to pGADT7 or pGBKT7 (F)
XW052	TCTGGATCCTCAGTCGAGGCGATGG AGAAG	<i>BamHI</i>	Cloning <i>ZmCM3²⁹⁻²⁸⁴</i> to pGADT7 or pGBKT7 (R)
XW079	CTCGAGTTTTTCAGCAAGATAATATT TTGATCGACCATCTGTAACG	/	Amplification of the left border of <i>um12021</i> overlapping with pJET (F)
XW080	TTGTCACGCCATGGTGGCCATCTAGG CCGGTTGATTCAAGCGACAC	/	Amplification of the left border of <i>um12021</i> overlapping with <i>neo</i> cassette (R)

XW081	GCCGCATTAATAGGCCTGAGTGGCC TCCGCTTCATTTCGCTGTC	/	Amplification of the right border of <i>um12021</i> overlapping with <i>neo</i> cassette (F)
XW082	AGGAGATCTTCTAGAAAGATAATAT TATAATACACGATGACTTAAGC	/	Amplification of the right border of <i>um12021</i> overlapping with pJET (R)
XW086	GAGCTCGGTACGGGTACATC	/	Amplification of the <i>neo</i> cassette overlapping the left border of <i>um12021</i> (F)
XW087	GACGCGTGTACGCATGTAAC	/	Amplification of the <i>neo</i> cassette overlapping the right border of <i>um12021</i> (R)
XW102	CTGGCTGCACTTCGTGCCCAACTGCA GAGGTACGAG	/	Mutagenic primer that substitutes D44A in pAD2318
XW103	GCGCTCGCTAAATTCGCTGGCTCCA CGCCAAC	/	Mutagenic primer that substitutes D196A in pAD2318
XW108	CGATAAGCTTGATATCGAATTCACCA TGGCCTTCAAGCTGATC	/	Amplification of <i>ZmCMI</i> overlapping with p35S vector (F)
XW109	CTTCGACATGCCGCCATCCAGCCTCT TAAGCAAATAC	/	Amplification of <i>ZmCMI</i> overlapping with <i>sfGFP</i> (R)
XW110	GGCTGGATGGCGGCATGTCTGAAGGG CGAGGAA	/	Amplification of <i>sfGFP</i> overlapping with <i>ZmCMI</i> (F)
XW111	GGTGATTTTTGCGGACTCTAGATTAC TTGTAGAGTTCGTCCATG	/	Amplification of <i>sfGFP</i> overlapping with p35S vector (R)
XW112	TCGAACTGCAAGAGCTCTAGGTTAC GATGAAGTTGAGCGTGTCCATC	/	Amplification of <i>SP-cTP</i> overlapping with p123 (F)
XW113	ACAGCCGCGCACGTGGTGCCATTTG G	/	Amplification of <i>SP-cTP</i> overlapping with <i>cmu1</i> ²²⁻²⁹⁰ (R)
XW114	CCACGTGCGCGGCTGTATCTGGCAA G	/	Amplification of <i>cmu1</i> ²²⁻²⁹⁰ overlapping with <i>SP-cTP</i> (F)
XW115	GGCAACAGGATTCAATCTTAAGAAA CTTTATTGCCAAATGTTTGAAC	/	Amplification of <i>cmu1</i> ²²⁻²⁹⁰ overlapping with p123 (R)

XW122	ACCTTTGCACCTTGCATCAC	/	Amplification of partial <i>um05230</i> to find CRISPR mutations (F)
XW127	TCGAACACGGCTATGAATCC	/	Amplification of partial <i>um05230</i> to find CRISPR mutations (R)
XW131	GTTTTCGAACTGCAAGAGCTCTAGGT TACGATGAAGTTGAGCG	/	Amplification of <i>cmuI</i> ¹⁻¹¹⁶ overlapping with p123 (F)
XW132	GGCGAGCCCAGCCGGGCGTGATGA ACTCGAC	/	Amplification of <i>cmuI</i> ¹⁻¹¹⁶ overlapping with <i>cmuI</i> ¹⁴¹⁻²⁹⁰ (R)
XW133	CATCACGCCCCGGCTCGGGCTCGCCG CAGGATCCGACCAAC	/	Amplification of <i>cmuI</i> ¹⁴¹⁻²⁹⁰ overlapping with <i>cmuI</i> ¹⁻¹¹⁶ (F)
XW134	ACCGGCAACAGGATTCAATCTTAAG AAACTTTATTGCCAAATGTTTGAAC	/	Amplification of <i>cmuI</i> ¹⁴¹⁻²⁹⁰ overlapping with p123 (R)
XW135	ATGGCTACCGTCGGGGGCAATCGTG CTCTC	/	Amplification of <i>cmiI</i> ¹ (F)
XW136	TCACTCGTCGGACCAGGTGATCTGTG CC	/	Amplification of <i>cmiI</i> ¹ (R)
XW137	AAACATATGTTCCCATACCGTTCCCT ACTCC	<i>NdeI</i>	Cloning <i>cmiI</i> ³³⁻¹⁹⁸ to pGADT7 or pGBKT7 (F)
XW138	TTTGGATCCTCACTCGTCGGACCAGG TGATC	<i>BamHI</i>	Cloning <i>cmiI</i> ³³⁻¹⁹⁸ to pGADT7 or pGBKT7 (R)
XW139	CGCGGTACCATGGCTACCGTCGGGG GCAATC	<i>KpnI</i>	Cloning <i>cmiI</i> to pEZRK (F)
XW140	CGCTCTAGATCAGTGGTGGTGGTGGT GGTGCTCGTCGGACCAGGTGATCTG	<i>XbaI</i>	Cloning <i>cmiI</i> to pEZRK (R)
XW142	AAACATATGTTCCCATACCGTTCCCT ACTC	<i>NdeI</i>	Cloning <i>cmiI</i> ³³⁻¹⁹⁸ to pET28a (F)
XW143	TTTCTCGAGCTCGTCGGACCAGGTGA TCTG	<i>XhoI</i>	Cloning <i>cmiI</i> ³³⁻¹⁹⁸ to pET28a (R)
XW150	CTTTAAGAAGGAGATATCATATGGC TGCTGTTTCTGGTAAATC	/	Amplification of <i>cmuI</i> ²²⁻¹¹⁶ overlapping with pET28a (F)
XW151	CGGAGAGCCAGAGCCCCGGGGTGATG AATTCAAC	/	Amplification of <i>cmuI</i> ²²⁻¹¹⁶ overlapping with <i>cmuI</i> ¹⁴¹⁻²⁹⁰ (R)
XW152	TCACCCCGGGCTCTGGCTCTCCGCAG GACCCGACCAAC	/	Amplification of <i>cmuI</i> ¹⁴¹⁻²⁹⁰ overlapping with <i>cmuI</i> ²²⁻¹¹⁶ (F)

inserted into pET28a using *NdeI/XhoI*. The expression of *cmi1* was controlled by T7-lacO promoter. The plasmid confers Kan resistance.

pXW037 (pET-Cmu1^{ΔSPΔ117-140}, this study):

This plasmid derived from pET28a was used to overexpress C-terminal His₆-tagged Cmu1^{ΔSPΔ117-140} in *E. coli*. *cmu1*²²⁻¹¹⁶ and *cmu1*¹⁴¹⁻²⁹⁰ were separately amplified from pAD1752 with primers XW150/XW151 and XW152/XW153, respectively. The yielding fragments were assembled with *NdeI/XhoI* digested pET28a by Gibson assembly. The expression of *cmu1* was controlled by T7-lacO promoter. The plasmid confers Kan resistance.

4.3.6.2 Plasmids for transient expression of proteins via bombardment or *A. tumefaciens*-mediated transformation

pAD2316 (p35S-Cmu1^{ΔSP}-sfGFP, this study):

This plasmid derived from p35S vector was used to transiently express Cmu1^{ΔSP} fused with sfGFP in maize cells via bombardment. *cmu1*^{ΔSP} was amplified from pAD672 with primers XW041/XW048. *sfGFP* was amplified from p123_pCmu_tin2_sfGFP_HA_3xNLS (S. Tanaka, unpublished) with primers XW043/XW044. The yielding fragments were assembled with *EcoRI/XhoI* digested p35S-mCherry by Gibson assembly. The expression of *cmu1* was driven by 35S promoter.

pAD2317 (p35S-sfGFP, this study):

This plasmid derived from p35S vector was used to transiently express sfGFP in maize cells via bombardment. *sfGFP* was amplified from p123_pCmu_tin2_sfGFP_HA_3xNLS (S. Tanaka, unpublished) with primers XW046/XW047. The yielding fragment was inserted into *EcoRI/XhoI* digested p35S-mCherry. The expression of *sfGFP* was driven by 35S promoter.

pAD2326 (p35S-ZmCMI-sfGFP, this study):

This plasmid derived from p35S vector was used to transiently express ZmCMI fused with sfGFP in maize cells via bombardment. *ZmCMI* was amplified from pAD704 with primers XW108/XW109. *sfGFP* was amplified from p123_pCmu_tin2_sfGFP_HA_3xNLS (S. Tanaka, unpublished) with primers XW110/XW111. The yielding fragment was inserted into *EcoRI/XhoI* digested p35S-mCherry. The expression of *ZmCMI-sfGFP* was driven by 35S promoter.

pAD2331 (pEZRK-Cmi1-His₆, this study):

This plasmid derived from pEZRK vector was used to transiently express His₆ tagged Cmi1 in *N. bethamiana* via agroinfiltration. *cmi1* was amplified from pJET-Cmi1 with primers

XW139/XW140. The yielding fragment was inserted into *KpnI/XbaI* digested pEZRK. The expression of *cmi1* was driven by 35S promoter.

4.3.6.3 Plasmids for the transformation of *S. cerevisiae* AH109 and subsequent yeast two-hybrid analysis

pGADT7 (Clontech):

This plasmid expresses HA-tagged GAL4AD domain and *LEU2* selection marker.

pGBKT7 (Clontech):

This plasmid expresses c-Myc-tagged GAL4bD domain and *TRP1* selection marker.

pAD670 (pGADT7-Cmu1²²⁻²⁹⁰, Djamei et al., 2011):

This plasmid derived from pGADT7 was used to express GAL4AD-Cmu1²²⁻²⁹⁰ in *S. cerevisiae* AH109. *Cmu1*²²⁻²⁹⁰ was inserted in the multiple cloning site of pGADT7.

pAD671 (pGBKT7-Cmu1²²⁻²⁹⁰, Djamei et al., 2011):

This plasmid derived from pGBKT7 was used to express GAL4BD-Cmu1²²⁻²⁹⁰ in *S. cerevisiae* AH109. *Cmu1*²²⁻²⁹⁰ was inserted in the multiple cloning site of pGBKT7.

pAD704 (pGADT7-ZmCM1, Djamei et al., 2011):

This plasmid derived from pGADT7 was used to express GAL4AD-ZmCM1 in *S. cerevisiae* AH109. *ZmCM1* was inserted in pGADT7.

pAD703 (pGADT7-ZmCM2, Djamei et al., 2011):

This plasmid derived from pGADT7 was used to express GAL4AD-ZmCM2 in *S. cerevisiae* AH109. *ZmCM2* was inserted in pGADT7.

pAD2323 (pGBKT7-ZmCM3²⁹⁻²⁸⁴, this study):

This plasmid derived from pGBKT7 was used to express GAL4BD-ZmCM3²⁹⁻²⁸⁴ in *S. cerevisiae* AH109. *ZmCM3*²⁹⁻²⁸⁴ was amplified from cDNA of maize leaves infected by SG200 with primers XW051/XW052. The yielding fragment was inserted into pGBKT7 using *EcoRI/BamHI*. The expression of *ZmCM3* was driven by T7 promoter.

pAD2324 (pGADT7-ZmCM3²⁹⁻²⁸⁴, this study):

This plasmid derived from pGADT7 was used to express GAL4AD-ZmCM3²⁹⁻²⁸⁴ in *S. cerevisiae* AH109. *ZmCM3*²⁹⁻²⁸⁴ was amplified from cDNA of maize leaves infected by SG200 with primers XW051/XW052. The yielding fragment was inserted into pGADT7 using *EcoRI/BamHI*. The expression of *ZmCM3* was driven by T7 promoter.

pAD2359 (pGADT7-Cmi1³³⁻¹⁹⁸, this study):

This plasmid derived from pGADT7 was used to express GAL4AD-Cmi1³³⁻¹⁹⁸ in *S. cerevisiae* AH109. Cmi1³³⁻¹⁹⁸ was amplified from pJET-Cmi1 with primers XW137/XW138. The yielding fragment was inserted into pGADT7 using *NdeI/BamHI*. The expression of *cmi1* was driven by T7 promoter.

pAD2360 (pGBKT7-Cmi1³³⁻¹⁹⁸, this study):

This plasmid derived from pGBKT7 was used to express GAL4BD-Cmi1³³⁻¹⁹⁸ in *S. cerevisiae* AH109. Cmi1³³⁻¹⁹⁸ was amplified from pJET-Cmi1 with primers XW137/XW138. The yielding fragment was inserted into pGBKT7 using *NdeI/BamHI*. The expression of *cmi1* was driven by T7 promoter.

4.3.6.4 Plasmids for generation of stable *U. maydis* mutants

p123 (Aichinger et al., 2003):

The plasmid contains a *gfp* gene under the control of P_{otef} promoter and T_{nos} terminator. It is resistant to Cbx. The plasmid was used to integrate genes into the *U. maydis ip* locus.

pAD672 (p123-P_{cmu1}-Cmu1-HA₃, Djamei et al., 2011):

This plasmid derived from p123 was used to express Cmu1-HA₃ in *U. maydis*. The expression of *cmu1* was driven by its native promoter P_{cmu1}. For stable integration, the plasmid was linearized by *BsrGI* or *PsrI* and integrated into the *ip* locus of CL13Δ*cmu1*.

pAD2205 (p123-P_{cmu1}-Cmu1^{C203S}-HA₃, A. Ghosh, unpublished):

This plasmid derived from p123 carries C203S in Cmu1-HA₃.

pAD2239 (p123-P_{cmu1}-Cmu1^{V74K}-HA₃, A. Ghosh, unpublished):

This plasmid derived from p123 carries V74K in Cmu1-HA₃.

pAD2386 (p123-P_{cmu1}-Cmu1^{D37AD40A}-HA₃, this study):

This plasmid derived from p123 was used to express Cmu1^{D37AD40A}-HA₃ in *U. maydis*. The expression of *cmu1* was driven by its native promoter P_{cmu1}. For stable integration, the plasmid was linearized by *PsrI* and integrated into the *ip* locus of CL13Δ*cmu1*.

pAD2318 (p123-P_{cmu1}-Cmu1^{6A}-HA₃, this study):

This plasmid derived from p123 was used to express Cmu1^{6A}-HA₃ in *U. maydis*. Primers XW049 and XW050 were used to mutagenize pAD2286. The expression of *cmu1* was driven by its native promoter P_{cmu1}. For stable integration, the plasmid was linearized by *BsrGI* and integrated into the *ip* locus of CL13Δ*cmu1*.

pAD2320 (p123-P_{cmu1}-Cmu1^{8A}-HA₃, this study):

This plasmid derived from p123 was used to express Cmu1^{8A}-HA₃ in *U. maydis*. Primers XW102 and XW103 were used to mutagenize pAD2318. The expression of *cmu1* was driven by its native promoter P_{cmu1}. For stable integration, the plasmid was linearized by *BsrGI* and integrated into the *ip* locus of CL13Δ*cmu1*.

pAD2314 (p123-P_{cmu1}-Cmu1^{SS}-HA₃, this study):

This plasmid derived from p123 was used to express Cmu1^{SS}-HA₃ in *U. maydis*. Primer XW030 was used to mutagenize pAD2205. The expression of *cmu1* was driven by its native promoter P_{cmu1}. For stable integration, the plasmid was linearized by *BsrGI* and integrated into the *ip* locus of CL13Δ*cmu1*.

pAD2302 (p123-P_{cmu1}-Cmu1^{KY}-HA₃, this study):

This plasmid derived from p123 was used to express Cmu1^{KY}-HA₃ in *U. maydis*. Primer XW039 was used to mutagenize pAD2239. The expression of *cmu1* was driven by its native promoter P_{cmu1}. For stable integration, the plasmid was linearized by *BsrGI* and integrated into the *ip* locus of CL13Δ*cmu1*.

pAD2352 (p123-P_{cmu1}-Cmu1^{Δ117-140}-HA₃, this study):

This plasmid derived from p123 was used to express Cmu1^{Δ117-140}-HA₃ in *U. maydis*. *cmu1*¹⁻¹¹⁶ and *cmu1*¹⁴¹⁻²⁹⁰ were separately amplified from pAD672 with primers XW131/XW132 and XW133/XW134, respectively. The expression of *cmu1* was driven by its native promoter P_{cmu1}. For stable integration, the plasmid was linearized by *BsrGI* and integrated into the *ip* locus of CL13Δ*cmu1*.

pAD2329 (p123-P_{cmu1}-SP-cTP-Cmu1²²⁻²⁹⁰-HA₃, this study):

This plasmid derived from p123 was used to express SP-cTP-Cmu1²²⁻²⁹⁰-HA₃ in *U. maydis*. SP-cTP-Cmu1²²⁻²⁹⁰-HA₃ comprises a cTP between the SP of Cmu1 and Cmu1²²⁻²⁹⁰. *SP-cTP* was amplified from pFH3 (F. Hartwig, unpublished) with primers XW112/XW113. *cmu1*²²⁻²⁹⁰ was amplified from pAD672 with primers XW114/XW115. *SP-cTP*, *cmu1*²²⁻²⁹⁰ and *SacI/AflIII* digested pAD672 were assembled with Gibson assembly. For stable integration, the plasmid was linearized by *BsrGI* and integrated into the *ip* locus of CL13Δ*cmu1*.

pXW033 (pJET-Δ*um12021*-Neo):

This plasmid derived from pJET1-Stuffer was used to knockout the isochorismatase coding gene *um12021*. The plasmid contains a *neo* resistance cassette, the left border (1 kb) and right border (1 kb) of *um12021*. The left and right borders of *um12021* were amplified from genomic DNA of SG200 strain with primers XW079/XW080 and XW081/XW082, respectively. The *neo* resistance

cassette was amplified from pUMa1057 with primers XW086/XW087. The *neo* resistance cassette, the left and right borders of *um12021* and *EcoRV* digested pJET1-Stuffer were assembled by Gibson assembly. For stable integration, the plasmid was cut using *SspI* and the resulting 4.2 kb fragment was integrated into the *U. maydis* genome.

pAD2332 (pCas9-sgRNA-um05230):

This plasmid derived from pCas9_sgRNA_0 (Schuster et al., 2016) was used to introduce frame-shift mutations in the locus of *um05230* via CRISPR-Cas9 system. The plasmid comprises of *NLS-cas9-HA-NLS* driven by P_{otef} promoter and the small guide RNA (sgRNA) of *um05230* that guides Cas9 to the *um05230* locus. A gBlock containing the target sequence of *um05230* (GATGAAAGTATCCAGCAGTT) was synthesized from IDT (Coralville, USA). The gBlock was ligated with *Acc65I*-linearized pCas9_sgRNA_0 vector via Gibson assembly. For stable integration, the circular plasmid was transformed into *U. maydis*.

pAD2303 (p123-P_{otef}-Cmu1-HA₃):

This plasmid derived from p123 was used to overexpress Cmu1-HA₃ under the control of P_{otef} promoter. *cmu1* gene was amplified from pAD672 with primers XW034/AD214. The yielding fragment was inserted into p123 using *XmaI/AflIII*. For stable integration, the plasmid was linearized by *BsrGI* and integrated into the *ip* locus of AB33.

pAD2368 (p123-P_{otef}-Cmu1^{Δ117-140}-HA₃):

This plasmid derived from p123 was used to overexpress Cmu1^{Δ117-140}-HA₃ under the control of P_{otef} promoter. *cmu1*^{Δ117-140} gene was amplified from pAD2352 with primers XW034/AD214. The yielding fragment was inserted into p123 using *XmaI/AflIII*. For stable integration, the plasmid was linearized by *BsrGI* and integrated into the *ip* locus of AB33.

4.4 Microbiological methods

4.4.1 Competent cell preparation and transformation of *E. coli*

Competent cell preparation and chemical transformation of *E. coli* were modified from Cohen *et al.* (1972). *E. coli* cells were grown in 20 mL dYT medium at 28°C or 37°C with continuous shaking at 200 rpm overnight. Cultures were diluted 1:50 in 100 mL dYT medium supplemented with MgCl₂ and MgSO₄ to a final concentration of 10 mM, respectively. Cultures were grown to a cell density OD₆₀₀ of about 0.6 at 28°C or 37°C and 200 rpm for 2-2.5 hours. The culture was transferred to a microcentrifuge tube, incubated on ice for 30 min and centrifuged at 4°C for 8 min at 3,000 rpm. The supernatant was discarded and cells were resuspended in 33 mL (1/3 of the initial

volume) of pre-chilled RF1-solution and incubated for 30 min on ice at 4°C. The suspension was centrifuged at 4°C for 8 min at 3,000 rpm and the supernatant was discarded. *E. coli* cells were resuspended in 1/20 culture volume (5 mL) of pre-chilled RF2-solution and incubated on ice for 30 min. Finally, competent cells were aliquoted in 50 µL and stored at -80°C for later use.

To transform *E. coli*, 50 µL aliquots of competent *E. coli* cells were thawed on ice for 2 min. Subsequently, up to 1-5 µL DNA solution was added, gently mixed and incubated on ice for 10 min. *E. coli* cells were then heat shocked at 42°C for 1 min and immediately cooled on ice. For the recovery of the cells, 200 µL dYT medium (without antibiotics) was added and cells were incubated on a heating block (Eppendorf, Wesseling-Berzdorf, Germany) at 1000 rpm for 30 to 60 min (for transformations using Kan) at 30°C or 37°C. The *E. coli* cells were then plated on YT-agar containing the appropriate selective antibiotics and incubated at 30°C or 37°C overnight.

RF1-solution	100 mM RbCl 50 mM MnCl ₂ ·4H ₂ O 30 mM Potassium acetate* 10 mM CaCl ₂ ·2H ₂ O 15% (w/v) Glycerol pH was adjusted to 5.8 (glacial acetic acid) and sterile-filtered (Stored at 4°C)
---------------------	---

* Use 1 M Potassium acetate solution adjusted to pH=7.5 using glacial acetic acid.

RF2-solution	10 mM MOPS* 10 mM RbCl 75 mM CaCl ₂ ·2H ₂ O 15% (w/v) Glycerol pH was adjusted to 5.8 (NaOH) and sterile-filtered (Stored at 4°C)
---------------------	--

*Use 0.5 M MOPS adjusted to pH=6.8 using NaOH

4.4.2 Protoplast preparation and transformation of *U. maydis*

Protoplast preparation and transformation of *U. maydis* strains was performed as described in Schulz *et al.* (1990). *U. maydis* cells were incubated overnight in 5 mL YEPS_{light} medium at 28°C with continuous shaking at 200 rpm. Next day, cell cultures were inoculated in fresh YEPS_{light} to a cell density of OD₆₀₀ 0.1-0.2 and grown to a cell density of OD₆₀₀ 0.8-1.0. Cells were harvested by centrifugation at 4 °C for 5 min at 3,500 rpm, washed in 25 mL SCS solution and resuspended in 2 mL SCS containing 3.5 mg/mL Novozyme. Cells were incubated for about 5 min at room temperature to digest the cell wall, which was monitored under the microscope. When 50% of *U.*

maydis cells became protoplasts, cells were washed three times with 10 mL ice cold SCS and centrifuged at 2,400 rpm for 10 min at 4 °C. This was followed by an additional wash with 20 mL ice cold STC solution and centrifugation step. Finally, protoplast pellets were carefully resuspended in 0.5 mL of ice cold STC, and 60 µL of protoplasts were aliquoted into pre-chilled 1.5 mL microcentrifuge tubes for immediate use, or stored at -80 °C for later use.

For transformation of protoplasts, 1 µL heparin (stock solution 15 mg/mL) and up to 10 µL of DNA (3-5 µg) was added to the protoplast aliquot and incubated for 15 min on ice. Afterwards, 500 µL STC/PEG were added to the protoplasts, mixed gently, and incubated for another 15 min on ice. The transformation mix was plated on Regenerationagar_{light} plates. Transformed colonies appeared after 4-6 days and were singled out on PD-agar plates containing the appropriate antibiotic. Single colonies were picked and saved on PD-plates. The Regenerationagar_{light} plates were prepared by first pouring a bottom phase with 10 mL Regenerationagar_{light} containing the appropriate concentration of antibiotic (double the concentration indicated in chapter 4.2.3). Later, 10 mL of Regenerationagar_{light} without antibiotic was poured on top and solidified.

SCS solution**Solution 1**

0.6 % (w/v) Sodium citrate 2H₂O (f. c. 20 mM)
18.2 % (w/v) Sorbitol (Sigma S-1876) (f. c. 1 M)

Solution 2

0.4 % (w/v) Citric acid H₂O (f. c. 20 mM)
18.2 % (w/v) Sorbitol (Sigma S-1876) (f. c. 1 M)

Dissolve each in ddH₂O. Add enough Solution 2 to Solution 1 to reach pH 5.8 (The ratio between Solution 1 to Solution 2 is approximately 5:1) and autoclave.

STC solution

10 mM Tris-Cl, pH 7.5
100 mM CaCl₂
1 M Sorbitol
Dissolve in ddH₂O and sterile filtered.

STC/PEG solution

60.0 % (v/v) STC solution
40.0 % (w/v) PEG3350
Mix and sterile filtered.

4.4.3 Competent cell preparation and transformation of *A. tumefaciens*

The transformation of *A. tumefaciens* was conducted by electroporation. *A. tumefaciens* GV3101

cells were cultivated overnight in 5 mL LB medium supplemented with Rif (50 µg/mL) and Gent (25 µg/mL) at 28°C with continuous shaking at 200 rpm. Next morning, 100 µL overnight culture was harvested and subsequently washed three times with ddH₂O. The pellet was resuspended in 100 µL ddH₂O, and gently mixed with 1 µL plasmid (from Miniprep). The suspension mix was transferred into a pre-chilled 1 mm electroporation cuvette (PEQLAB, Erlangen, Germany). The cuvette was then placed onto *E. coli* Pulser (Bio-Rad, Munich, Germany), and the pulser was set to 2.0 kV. After electroporation, 1 mL LB medium without antibiotic was immediately added to the cuvette. The cell suspension was then transferred to a 1.5 mL microcentrifuge tube and recovered at 28°C with continuous shaking. Finally, 15 µL of the cell suspension was plated on LB agar plate containing appropriate antibiotics.

4.4.4 Competent cell preparation and transformation of *S. cerevisiae*

The transformation of *S. cerevisiae* was slightly modified from one-step protocol (Chen et al., 1992). *S. cerevisiae* AH109 cells were cultivated overnight in 5 mL YPD medium at 28°C with continuous shaking at 200 rpm. Next day, fresh YPD medium was inoculated with overnight culture to a cell density of OD₆₀₀ 0.2. After 3-4 h shaking at 28°C, the cell culture was harvested with centrifugation at 4000 rpm for 5 min and washed once with yeast transformation solution (YTS). The supernatant was removed and the pellet was resuspended in 50 µL of YTS solution. The prepared cell suspension was gently mixed with 1 µg plasmid and incubated at 42°C for 60 min. Subsequently, 50 µL of YPD medium was added into the suspension mix and gently mixed. Finally, the suspension was spread on the SD plate with appropriate selection pressure incubated for 3-5 days at 28 °C.

Yeast transformation solution (YTS)	40% (w/v) PEG3350
	200 mM LiAC
	100 mM DTT
	15% (w/v) Glycerol
	pH was adjusted to 5.8 (glacial acetic acid) and sterile-filtered (Stored at 4°C)

4.4.5 Spotting assay for *S. cerevisiae*

The yeast two hybrid analysis was performed using the Matchmaker GAL4 Two-Hybrid System 3 (Clontech, Saint-Germain-en-Laye, France) following the manufacturer's instructions. Yeast cells were grown in 5 mL of SD-Leu-Trp medium at 28°C overnight with continuous shaking at 200

rpm. The cell density of OD₆₀₀ was adjusted to 0.2 with the same medium in the next morning and the culture was grown to reach the cell density of OD₆₀₀ 1.0. Afterwards, 2 mL of the culture was harvested with centrifugation at 4000 rpm for 5 min and the resulting pellet was washed twice with sterile ddH₂O. Lastly, the pellet was resuspended in sterile ddH₂O to an OD₆₀₀ of 1 followed by four serial dilutions (1:10, 1:100, 1:1000 and 1:10000). For each dilution, 5 µL of the suspension was spotted on low stringency plates (SD-Leu-Trp), medium stringency plates (SD-Leu-Trp-His) and high stringency plates (SD-Leu-Trp-Ade-His), respectively. The plates were incubated at 28 °C for 4-5 days.

4.5 Molecular microbiological methods

4.5.1 Isolation of nucleic acids

4.5.1.1 Isolation of plasmid DNA from *E. coli*

Preparation of plasmids from *E. coli* was performed using QIAprep[®] Spin Miniprep Kit or QIAGEN Plasmid Midi Kit according to the manufacturer's instructions.

4.5.1.2 Isolation of genomic DNA from *U. maydis*

U. maydis cultures were grown in YEPS_{light} at 28°C and 200 rpm for 16 hours. *U. maydis* cultures were then harvested with 2 mL microcentrifuge tubes with centrifugation at 13,000 rpm for 1 min. After the supernatant was discarded, 200 µL glass beads, 500 µL of *Ustilago*-lysis buffer and 500 µL of TE-phenol/chloroform were added. The cells were lysed on a Vibrax-VXR shaker (IKA) at 1,600 rpm for 15-20 min. Next, samples were centrifuged for 15 min at 13,000 rpm and 400 µL of the aqueous phase in the upper layer was transferred to a new 1.5-mL microcentrifuge tube. Afterwards, 1 mL of ethanol was added and mixed by inverting 6 times. Subsequently the mixtures were centrifuged for 5 min at 13,000 rpm. The DNA pellets were washed once with 70 % ethanol. Then, the pellets were briefly centrifuged at 13,000 rpm to remove the leftover ethanol. Finally, DNA pellets were dissolved in 50 µL TE buffer containing 50 µg/mL RNase A, and incubated on a heating block at 55 °C with gentle shaking for 15 min. Genomic DNA was stored at -20°C until use.

<i>Ustilago</i>-lysis buffer	2% (v/v) Triton X-100
	1% (w/v) SDS
	100 mM NaCl
	10 mM Tris-Cl, pH 8.0

1 mM EDTA
dissolve in ddH₂O

TE-phenol/chloroform

Mix phenol (in TE-buffer) and chloroform
in a 1:1 ratio

4.5.1.3 Isolation of genomic DNA from infected maize tissue

To isolate genomic DNA, the infected maize tissue was excised from maize plants infected by *U. maydis* strains, frozen with liquid N₂ and homogenized with mortar and pestle under constant liquid N₂ cooling. The ground leaf materials were subjected to the procedures of the protocol described in chapter 4.5.1.2, beginning directly from *Ustilago*-lysis buffer and TE-phenol/chloroform step (without glass beads). Genomic DNA was stored at -20°C until use.

4.5.1.4 Isolation of total RNA from infected maize tissue

To isolate total RNA, 1 mL TRIzol Reagent (Invitrogen, Darmstadt, Germany) was added to 200 µL ground plant tissue in a 1.5 mL microcentrifuge tube. The mixture was vortexed and incubated at room temperature for 10 min. After centrifugation at 13000 rpm for 10 min at 4°C, the supernatant was transferred to a fresh 1.5 mL microcentrifuge tube and 0.2 mL chloroform was subsequently added. The sample was shaken vigorously by hand for 15 s and incubated at room temperature for 3 min. After that the sample was centrifuged at 13000 rpm for 15 min at 4°C for phase separation. The aqueous upper phase was transferred to a fresh 1.5 mL microcentrifuge tube and mixed with 0.5 mL isopropanol to precipitate RNA. After incubation at room temperature for 10 min, the sample was centrifuged at 13000 rpm for 10 min at 4°C to pellet RNA. The supernatant was removed and the pellet was washed with 1 mL 70% ethanol. Finally the dried RNA pellet was dissolved in 50 µL RNase free ddH₂O at 55°C for 10 min. The total RNA was stored at -20°C until use.

4.5.2 *In vitro* modification of nucleic acid

Standard molecular biology methods, such as purification, precipitation, electrophoresis of DNA or molecular cloning techniques were performed following the protocols described in Ausubel *et al.* (1987) and Sambrook *et al.* (1989). The concentration of nucleic acids was determined by photometric measurements using NanoDrop 2000 spectrophotometer (Life Technologies, Darmstadt, Germany).

4.5.2.1 Restriction of nucleic acid

The restriction of DNA was performed with type-II restriction endonucleases (NEB, Frankfurt, Germany) for 1-16 hours at enzyme specific temperatures. A standard reaction mix was set as the following:

X μ g	DNA
2 μ L	NEB buffer Cutsmart or 1-4
10 U	Restriction enzyme
Add ddH ₂ O to 20 μ L	

4.5.2.2 Ligation of DNA fragments

For the ligation of DNA fragments, T4 DNA ligase (NEB, Frankfurt, Germany) or Gibson assembly mix (kindly prepared by Petra Happel) was used. In the ligation reactions, 50 ng linearized vector was ligated with an insert in a molar ratio of 1:3 to 1:10. T4-ligation of DNA was incubated at 37°C for 1 hour while Gibson assembly was incubated at 50°C for at least 15 min.

Standard T4 ligation reaction:

X μ L	Vector (50 ng)
Y μ L	Insert (to vector 3:1-10:1)
2 μ L	T4 ligation buffer
1 μ L	T4 ligase
Add ddH ₂ O to 20 μ L	

Standard Gibson assembly reaction:

X μ L	Vector (50 ng)
Y μ L	Insert (to vector 3:1-10:1)
5 μ L	Gibson assembly mix
Add ddH ₂ O to 10 μ L	

4.5.2.3 Polymerase Chain Reaction (PCR)

To amplify DNA fragments for cloning or for analytical purposes, the polymerase chain reaction (PCR) was used (Mullis *et al.*, 1986). Depending on the application, different polymerases were employed. For amplification of DNA for cloning purposes Phusion DNA polymerase was used (Thermo Fisher Scientific, Dreieich, Germany). For Colony-PCR/screening on a large scale the BioMix Red (Bioline, Luckenwalde, Germany) was used which contains the Taq polymerase.

Typical settings for the individual polymerases are described below. The elongation time was chosen based on the expected fragment size and rate of synthesis by the polymerase used. PCR reactions were performed in a TProfessional standard gradient thermocycler (Biometra, Goettingen, Germany) or a peqSTAR 96 well gradient thermocycler (PEQLAB, Erlangen, Germany).

PCR setting with Phusion polymerase:

1 μ L	DNA template (50 ng)
10 μ L	5 \times Phusion HF Buffer
1 μ L	dNTPs (25 μ M, 1:1:1:1 ratio)
2.5 μ L	Forward Primer (10 μ M)
2.5 μ L	Reverse Primer (10 μ M)
1.5 μ L	DMSO
0.5 μ L	Phusion DNA Polymerase (2 U/ μ L)

Add ddH₂O to 50 μ L

Program: 98°C/1 min–[98°C/10 s–55–74°C/20 s–72°C/15 s/kb] \times 35–72°C/5 min

PCR setting with BioMix Red polymerase:

1 μ L	DNA template (50 ng) or cell lysate
0.5 μ L	Forward Primer (10 μ M)
0.5 μ L	Reverse Primer (10 μ M)
5 μ L	2 \times BioMix Red

Add ddH₂O to 10 μ L

Program: 94°C/2 min– [94°C/10 s–50–65°C/20 s–72°C/30 s/kb] \times 35–72°C/5 min

4.5.2.4 DNase-treatment of total RNA

For removal of residual DNA inside extracted RNA samples, the Ambion[®]TURBO DNafree[™] Kit (Thermo Scientific, Bonn, Germany) was used according to the manufacturer's instructions. In a 50 μ L reaction, 5 μ L 10 \times DNase buffer and 2 μ L DNase were added to 2 μ g of the extracted RNA and the sample was incubated at 37 °C for 30 min. Afterwards, 5 μ L inactivation buffer was added and the sample was incubated for 5 min at room temperature. Finally, the sample was centrifuged at 7500 rpm for 2 min and 40 μ L supernatant was transferred to a fresh 1.5 mL microcentrifuge tube.

4.5.2.5 cDNA synthesis

After isolation of RNA and DNase treatment (4.5.1.3 - 4.5.1.4), cDNA was synthesized using the

SuperScript™ III (Thermo Scientific, Bonn, Germany) according to the manufacturer's instructions. For one reaction, 1 µg total RNA was transcribed into cDNA using Oligo(dT)₂₀ primer in a total reaction volume of 20 µL. The synthesized cDNA was diluted with a ratio of 1:2 in RNase free water and stored at -20°C until use.

4.5.2.6 Quantitative real-time PCR

For quantitative reverse transcription PCR (qRT-PCR), cDNA prepared in Chapter 4.5.2.5 was used as template. The qRT-PCR was performed using Platinum™ SYBR™ Green qPCR SuperMix-UDG (Thermo Scientific, Bonn, Germany) according to the manufacturer's instructions. The reactions were performed on a Bio-Rad iCycler (Bio-Rad, Munich, Germany). The specificity of the reaction was ensured by melting curve calculations after the qPCR run. The determination of threshold cycles was performed with the Bio-Rad Software. Relative expression values were calculated with the $2^{-\Delta\Delta C_t}$ method (Livak and Schmittgen, 2001).

qRT-PCR reaction:

12.5 µL	2× SYBR green Supermix
1 µL	Diluted cDNA
1 µL	Forward Primer (10 µM)
1 µL	Reverse Primer (10 µM)
Add ddH ₂ O to 25 µL	
Program: 95°C/2 min– [95°C/30 s–62°C/30 s–72°C/30 s] × 45	

4.5.2.7 Site-directed mutagenesis

The site-directed mutagenesis was carried out with QuikChange Lightning Multi Site-Directed Mutagenesis Kit (Agilent, Waldbronn, Germany), which is used to introduce single or multiple site-specific mutations in double-stranded plasmids. The procedure was performed according to the manufacturer's instructions.

4.5.3 Separation and detection of nucleic acids

4.5.3.1 Agarose gel electrophoresis

For a size-specific separation of nucleic acids, agarose gel electrophoresis was performed. Due to its negative charge, DNA migrates towards the anode if an electric field is applied. Concentrations of agarose gels varied between 0.8% and 2% (w/v), depending on the size of the fragments to be separated. The respective amount of agarose was dissolved in 1× TAE buffer by boiling. After the

solution was cooled down to 60 °C, ethidium bromide (f. c. 0.25 µg/mL) was added. The gel was poured into an appropriate gel casting tray. After solidifying, the gel was transferred into a running gel chamber and covered with 1× TAE buffer, respectively. Samples were mixed with non-denaturing loading dye, loaded on the gel at the side of the cathode, and separated by applying a constant voltage of 90-120 V. DNA was visualized by UV irradiation at 254 nm on a UV table (2UV™ Transilluminator, UVP, Upland, CA, USA) and documented using the UV solo TS Imaging system (Biometra GmbH, Göttingen, Germany).

50× TAE buffer

2 M Tris base
2 M acetic acid
50 mM EDTA, pH 8.0
dissolve in ddH₂O

6× DNA loading dye

50 % (w/v) sucrose
0.1 % (v/v) bromophenol blue
dissolve in 1x TE buffer, sterile filtrate and store at 4 °C

1× TE buffer

10 mM Tris base
1 mM Na₂-EDTA 2H₂O
dissolve in ddH₂O, adjust pH to 8.0 with HCl and autoclave

4.5.3.2 Southern blot analysis

For southern analysis (Southern, 1975) 15 µL of genomic DNA, which was prepared as described in chapter 4.5.2.2 (Isolation of genomic DNA from *U. maydis*), was digested with the respective restriction enzymes overnight. Digested products were separated on a 1× TAE (0.8 %) agarose gel for 3 h at 90 V. After depurination with 0.25 M HCl for 15 min, which is a prerequisite for transfer of large DNA fragments, and subsequent neutralization with 0.4 M NaOH for 15 min, the DNA was transferred from the gel to a nylon membrane (Hybond-N+, GE Healthcare, Munich, Germany). The transfer was facilitated by a capillary blot with 0.4 M NaOH as transfer solution. Afterwards the membrane was placed into a hybridization tube, in which all subsequent steps were carried out. The membrane was pre-hybridized with 20 mL Southern hybridization buffer in a hybridization oven (HB-1000 Hybridizer, UVP) at 65°C for 30 min. Immobilized DNA was detected by DIG-labeled probes. To generate such probes, DNA fragments were labeled with PCR DIG Labeling Mix (Roche, Mannheim, Germany) according to the manufacturer's instructions. Probes were denatured at 95°C for 10 min and added to 20 mL pre-warmed Southern hybridization buffer (65°C). After pre-hybridization of the membrane with Southern hybridization buffer, the denatured probe

solution was added. Hybridization was performed at 65°C for at least 6 h. Afterwards the membrane was washed twice with Southern wash buffer at 65°C for 20 min. All subsequent steps were performed at room temperature. The membrane was washed once with DIG wash buffer for 5 min followed by a 30 min blocking step with DIG2 buffer. After blocking, 20 mL of the DIG antibody solution was added. Membrane and antibody solution were incubated for 30 min followed by two 15 min-washing steps in DIG wash buffer to remove residual antibody. The membrane was equilibrated in DIG3 buffer for 5 min, which was followed by incubation with CDP star solution for 5 min. DIG-labelled DNA fragments were visualized using X-ray films (CEA, Hamburg, Germany) and AGFA CP 1000 film processor (AGFA HealthCare, Mortsel, Belgium).

Na-phosphate buffer, 1 M (pH 7.0)	Solution 1: 1 M Na ₂ HPO ₄ Solution 2: 1 M NaH ₂ PO ₄ ·H ₂ O Add Solution 2 to Solution 1 until pH reaches 7.0 in ddH ₂ O
Southern hybridization buffer	0.5 M Na-phosphate buffer, pH 7.0 7% SDS dissolve in ddH ₂ O
Southern wash buffer	0.1 M 1 M Na-phosphate buffer, pH 7.0 1% SDS dissolve in ddH ₂ O
DIG1	0.1 M maleic acid 0.15 M NaCl dissolve in ddH ₂ O, adjust pH to 7.5 (NaOH)
DIG2	1% (w/v) skim milk powder in DIG1
DIG3	0.1 M Tris-HCl (pH 9.5) 0.1 M NaCl 50 mM MgCl ₂ dissolve in ddH ₂ O, adjust pH to 9.5 (Tris-HCl) and sterile-filtered
DIG antibody solution	Anti-DIG antibody 1:10,000 in DIG2
DIG wash buffer	0.3% (v/v) Tween-20 in DIG1
CDP-Star solution	CDP-Star 1:250 in DIG3

4.6 Protein methods and biochemical assays

4.6.1 Protein overexpression in *E. coli* and purification

For overexpression of Cmu1 and Aro7p, *E. coli* BL21 Star (DE3) strain (Thermo Fisher Scientific, Dreieich, Germany) was transformed with pET28a derived plasmid expressing respective proteins. Single colony of transformed *E. coli* cells was inoculated in LB medium in the presence of Kan (50 mg/mL) and 1.75% (w/v) lactose for auto-induction. The culture was incubated at 30°C for 16 h under constant shaking.

For overexpression of Cmi1, *E. coli* SHuffle® T7 strain (NEB, Frankfurt, Germany) was transformed with pET28a derived plasmid expressing Cmi1. Transformed *E. coli* cells were grown at 30°C in LB medium in the presence of Kan (50 mg/mL) to OD₆₀₀ of 0.6, followed by the addition of 0.5 mM IPTG. The culture was incubated at 16°C for 16 hours under constant shaking.

The cells were harvested by centrifugation at 4000 rpm for 20 min at 4°C, suspended in Lysis buffer and subsequently disrupted by sonication or French press. After centrifugation at 13000 rpm for 30 min at 4°C, the clarified supernatant was incubated with 0.5 mL equilibrated Ni-NTA agarose beads (Qiagen, Hilden, Germany) and kept constant rotated for 1 h at 4°C. After washing with 10 mL Lysis buffer, proteins were eluted using 3 mL Elution buffer. The eluted protein solution was concentrated with Amicon® Ultra Centrifugal Filter (10 kDa, Merck, Darmstadt, Germany) to 0.5 mL and subsequently applied to size exclusive chromatography (SEC). After SEC, proteins were eluted in SEC buffer. Fractions were analyzed using SDS polyacrylamide gel electrophoresis (SDS-PAGE). Protein containing fractions were pooled and concentrated up to a concentration fitting the experimental requirements. The concentrations of proteins were determined by NanoDrop spectrophotometer (Thermo Fisher Scientific, Dreieich, Germany).

For purification of Cmu1/Cmi1 complex, two proteins were produced and purified separately. The eluted solutions of each protein were mixed and incubated for 10 min at RT, followed by normal SEC purification procedure.

Lysis buffer	20 mM HEPES, pH 8.0
	250 mM NaCl
	20 mM KCl
	20 mM MgCl ₂
	40 mM imidazole

	dissolve in ddH ₂ O and filter-sterilize.
Elution buffer	20 mM HEPES, pH 8.0 250 mM NaCl 20 mM KCl 20 mM MgCl ₂ 500 mM imidazole dissolve in ddH ₂ O and filter-sterilize.
SEC buffer	20 mM HEPES, pH 7.5 200 mM NaCl 20 mM KCl 20 mM MgCl ₂ dissolve in ddH ₂ O and filter-sterilize.

4.6.2 Protein extraction from *S. cerevisiae*

Proteins from yeast strains in Y2H assays were prepared as previously described (Kushnirov, 2000). 1 mL overnight culture of yeast strain was pelleted by brief centrifugation at 10,000 rpm for 1 min. The pellet was resuspended in 100 μ L distilled water followed by the addition of 100 μ L 0.2 M NaOH. The suspension was incubated at room temperature for 10 min and pelleted by centrifugation at 4,000 rpm for 5 min. The pellet was resuspended in 50 μ L 1 \times Sample buffer, boiled for 10 min and centrifuged. The resulting supernatant was loaded onto SDS-PAGE gel.

4.6.3 Protein extraction from maize or tobacco

For extraction of proteins from plant materials, infected maize leaves or agroinfiltrated tobacco leaves were excised and frozen in liquid N₂. Subsequently, frozen materials were ground in liquid N₂ followed by the addition of HNN extraction buffer. After incubation on ice for 15 min, the sample was centrifuged at 16,000 g for 20 min at 4°C to remove the debris. The supernatant was tested by SDS-PAGE or subjected to further experiments.

HNN extraction buffer	50mM HEPES, pH7.5 150mM NaCl 50mM NaF 5mM EDTA 0.1% NP-40 1% polyvinylpyrrolidon (PVPP)
------------------------------	--

0.5% Sodium deoxycholate

1× cOmplete protease inhibitor cocktail (Roche)

Dissolve in ddH₂O

4.6.4 *In vitro* pull-down assay

For verification of the interaction between Cmu1 and Cmi1, *in vitro* pull-down was performed with Cmu1 secreted by *U. maydis* and Cmi1 expressed in tobacco via agroinfiltration. A *U. maydis* strain overexpressing Cmu1-HA₃ or Cmu1^{Δ117-140}-HA₃ was grown in CM liquid medium supplemented with 2% glucose. When OD₆₀₀ reached 0.8-1.0, the culture was harvested by centrifugation. The supernatant was concentrated using Amicon centrifugal filter unit (10 kDa) to 500 μL. Tobacco leaves were agroinfiltrated with *A. tumefaciens* strain GV3101 carrying pEZRK or pEZRK-Cmi1-His₆. Three day after infiltration, tobacco leaves were harvested and ground in liquid N₂. HNN extraction buffer was added to the ground powder and incubated for 15 min on ice. The sample was centrifuged at 16,000 g for 20 min at 4°C. 500 μL of the supernatant of plant lysate and the concentrated supernatant of *U. maydis* culture were mixed with 50 μL Ni-NTA agarose (Qiagen, Hilden, Germany). The mixture was incubated at 4°C for overnight under constant rotation. The beads were washed 3 times with the extraction buffer followed by the addition of 100 μL 1×Sample buffer and boiling for 10 min. After brief centrifugation, the supernatant was analyzed by SDS-PAGE and Western blot.

4.6.5 Co-immunoprecipitation of Cmu1-HA₃ followed by mass spectrometry

Infected maize leaves were harvested three day after infection with SG200Δcmu1-Cmu1-HA₃ and ground in liquid N₂. The ground powder (1 mL) was extracted with 3 mL HNN buffer and incubated on ice for 15 min. The sample was centrifuged at 16,000 g for 20 min at 4°C. The supernatant was mixed with 10 μL Anti-HA Magnetic Beads (Thermo Scientific, Bonn, Germany) and incubated at 4°C for 1 hour. The magnetic beads were immobilized using a magnetic rack to remove the supernatant and washed three times with 700 μL ABC buffer. 100 μL elution buffer I was added to the beads, vortexed and incubated at 27°C for 30 min under constant shaking. Proteins were eluted by centrifugation. 40 μL elution buffer II was added to the beads twice to further elute the protein by centrifugation. Three eluted fractions were combined and incubated at room temperature for overnight. Afterwards, iodoacetamid was added to the sample to the concentration of 27 mM, vortexed and incubated for 30 min in the dark. The peptides were purified using C18 Micro

SpinColumns (Harvard Apparatus, USA) according to the protocol of the manufacturer, resolved in 0.15% formic acid and 2% acetonitrile and applied to mass spectrometer.

ABC buffer	100 mM ammonium bicarbonate in ddH ₂ O
elution buffer I	1.6 M urea 100 mM ammonium bicarbonate 10 µg/mL trypsin dissolved in ddH ₂ O
elution buffer II	1.6 M urea 100 mM ammonium bicarbonate 1 mM TCEP dissolved in ddH ₂ O

4.6.6 SDS polyacrylamide gel electrophoresis (SDS-PAGE)

The separation of proteins was performed by SDS-PAGE according to Laemmli (1970). During SDS-PAGE, proteins were separated in an electric field according to their size. To achieve separation, proteins in 1× Sample buffer were denatured at 99 °C for 10 min. After denaturation, samples were loaded on a vertical SDS polyacrylamide gel composed of stacking and separation gel (Mini Protean System, Bio-Rad). As reference for the molecular weight of the separated proteins the PageRuler Prestained Protein ladder (ThermoFisher Scientific) was used.

4× Sample buffer	10 mL 1.5 M Tris-HCl pH 6.8 30 mL glycerin 6 mL 20 % SDS 5 mg bromophenol blue 3 g DTT (f. c. 400 mM) Fill up to 50 mL with ddH ₂ O
Stacking gel (5%)	0.5 mL 0.5 M Tris-HCl pH 6.8 0.333 mL 30 % Polyacrylamide (PAA) 20 µL 10 % SDS 20 µL 10 % Ammonium persulfate (APS) 2 µL Tetramethylethylenediamine (TEMED) 1.125 mL ddH ₂ O
Stacking gel (15 %)	1.25 mL 1.5 M Tris-HCl pH 8.8 2.49 mL 30 % Polyacrylamide (PAA) 50 µL 10 % SDS 1.17 mL ddH ₂ O 50 µL 10 % Ammonium persulfate (APS)

	5 μ L Tetramethylethylenediamine (TEMED)
SDS running buffer	25 mM Tris-HCl, pH 8.0 192 mM glycine 4 mM SDS dissolve in ddH ₂ O

4.6.7 Western blot

Proteins separated by SDS-PAGE were transferred to a PVDF nitrocellulose membrane by using the semi-dry Trans-Blot Turbo Transfer System (BioRad, Munich, Germany). The blotting procedure was performed according to the manufacturers' specifications using the Trans-Blot Turbo blotting apparatus as well as the membranes and protein blotting consumables provided for the system. The Bio-Rad preprogrammed protocol "Mixed MW (Turbo) for proteins with a molecular weight ranging from 5-150 kDa (7 min) was used by default. The Transfer was performed at 1.3 A, 25 V (one Mini format gel) or at 2.5 A, 25 V (two Mini format gels). After the transfer, the membrane was incubated in blocking solution for 1 hour at RT. The blocking solution was replaced with antibody solution containing the primary antibody. The membrane was incubated for approximately 16 hours at 4°C. Thereafter, the membrane was washed three times for 10 min with TBST buffer followed by incubation for 1 hour at RT in TBST buffer containing the secondary antibody. The antibodies used in this study are listed in Table 6. After three more washes with TBST buffer for 10 min each, the membrane was incubated for 5 min with ECL chemiluminescent detection reagent (GE Healthcare, Munich, Germany) or SuperSignal™ West Femto Maximum Sensitivity Substrate (Thermo Fisher Scientific, Dreieich, Germany). The blots were sealed in a plastic bag and developed using X-ray films (CEA, Hamburg, Germany) and the AGFA CP 1000 film processor (AGFA HealthCare, Mortsel, Belgium).

TBST	50 mM Tris-HCl, pH 7.5 150 mM NaCl 0.1 % (v/v) Tween 20 dissolve in ddH ₂ O
Blocking solution	5% (w/v) skim milk powder in TBST
Antibody solution	antibody diluted in Blocking solution

Table 6: Antibodies used in the study

Name	Source	Supplier	Working concentration
Monoclonal Anti-HA	Mouse	Sigma H9658	1:10,000
Polyclonal Anti-HA	Rabbit	Sigma H6908	1:10,000
Penta·His HRP Conjugate Kit	Mouse	QIAGEN 34460	1:10,000-30,000
c-Myc antibody	Rabbit	Sigma C3956	1:10,000
Anti-mouse IgG, HRP-linked Antibody	Horse	Cell Signaling Technology #7076	1:10,000
Anti-rabbit IgG, HRP-linked Antibody	Goat	Cell Signaling Technology #7074	1:10,000

4.6.8 Chorismate mutase assay

The CM activity of various CMs was determined with a previously described “online assay” (Kane et al., 1971; Sasso et al., 2005). The assay monitors the disappearance of the substrate chorismate at 274 nm (extinction efficiency $\epsilon_{274}=2630 \text{ M}^{-1}\cdot\text{cm}^{-1}$). Standard assays were performed at 30°C in 250 μL reaction buffer [40 mM Tris-HCl (pH 7.0), 100 mM NaCl]. For normal reaction, CM activity was measured with 100 ng of proteins and 0.5 mM chorismate. For K_m measurement, the concentration of chorismate varied from 0 to 3 mM. Initial velocity was calculated from the linear decrease of OD₂₇₄ in the first 10 min. The kinetic data were fit to Michaelis-Menten equation using SigmaPlot. The change of OD₂₇₄ of chorismate in the absence of CM during the time course was extracted as blanking procedure. The OD₂₇₄ was measured using TECAN Infinite 200 PRO plate reader (Tecan Trading AG, Switzerland).

4.7 Plant assays

4.7.1 *Z. mays* cultivars

For pathogenicity experiments of *U. maydis*, *Z. mays* cv. Early Golden Bantam (Old Seeds, Madison, WI, USA) was mainly used. The cultivar Gaspe Flint was only used for several experiments in chapter 2.1.1.

4.7.2 Cultivation of *Z. mays*

All corn plants were cultivated in a temperature controlled greenhouse with a light-dark cycle of 28 °C for 14 hours and 20 °C for 10 hours. During the day phase, the illumination intensity was at least 25 kLux - 30 kLux (with additional sunlight up to 90 kLux). Four corn grains were sowed per pot. EGB was grown in Fruhstorfer soil type “T” and watered once a day.

4.7.3 Infection of *Z. mays* with *U. maydis*

Pathogenicity assays were performed as previously described in Kämper *et al.*, 2006. For maize infections, cultures of *U. maydis* strains were grown to an OD₆₀₀ of 1.0 in YEPS_{light}, harvested by centrifugation at 3,500 g, 5 min at room temperature (Heraeus Multifuge 4 KR) and the OD₆₀₀ of each culture was adjusted in ddH₂O to 1.0. 1 mL of cell suspension was injected into 7-day-old or 14-day-old maize seedlings using a syringe. Disease symptoms were scored according to severity 12 dpi (Table 7) (Kämper *et al.*, 2006).

Table 7: Classification of symptoms of infected maize seedlings

Symptoms	Description
Chlorosis	Infected maize leaves display yellowish discoloration.
Ligula swelling	Only swellings are found on the ligula site and no tumor on the leaves.
Small tumors	Only little tumors (< 1 mm) are visible or very few tumors >1 mm.
Normal tumors	Most tumors visible are > 1 mm.
Heavy tumors	The plant displays changed growth axis, stunted growth or large tumor formed on the base of the stem.
Dead	The plant dies due to the infection with <i>U. maydis</i>

4.7.4 Cultivation of *N. benthamiana*

N. benthamiana seeds were sown in “Frühstorfer Pikiererde Typ T” soil and transplanted into single pots 7 days after germination. The plants were grown under controlled conditions in a PERCIVAL AR-95L3 phytochamber (Percival Scientific, USA) with a day phase at 21 °C with a 16 h light and 8 h night period.

4.7.5 Infiltration of *N. benthamiana* with *A. tumefaciens*

For transient expression of proteins, *A. tumefaciens* GV3101 strain carrying respective pEZRK plasmids was used to infiltrate leaves of 4-week-old *N. benthamiana*. GV3101 with pEZRK plasmids was grown in LB medium containing appropriate antibiotics to OD₆₀₀ of 1.0. After washing three times with distilled water, cell pellet was suspended in MES buffer (10 mM MES, 10 mM MgCl₂, 100 μM acetosyringone) to OD₆₀₀ of 0.25. The GV3101 cell suspension was infiltrated into the back side of leaves using 1 mL syringe without needle.

4.7.6 Biolistic transformation of maize leave cells

To transiently express proteins in maize cells, biolistic transformation was conducted with 1.6 μm gold particles (Biorad, Munich, Germany). Gold particles (60 mg) were resuspended in 1 mL ethanol and vortexed for 9 min. The gold suspension was spun for 1 min to remove ethanol. The gold particles were washed twice with 1 mL sterile distilled water. The gold particles were nicely resuspended in 50% glycerol by vortex. To label gold particles with plasmid DNA, 2-3 μg plasmid was mixed with 10 μL gold suspension and vortexed for 1 min. 20 μL of CaCl₂ (2.5 M) was added to the mixture and kept vortexed for 3 min. Subsequently, 10 μL of 0.1 M spermidine was added and continued vortexed for 1 min. The gold particles were washed with 1 mL of 70% ethanol and 1 mL of 100% ethanol, respectively. Finally, 40 μL of 100% ethanol was used to resuspend the gold particles coated with DNA. For biolistic transformation, 14-day-old maize leaves were excised and placed upside down on wet paper towels in a Petri dish. 20 μL of the coated gold suspension was applied to a carrier disk and dried for several minutes. The cartridge was assembled according to the manufacturer's instructions. The leaves were shoot with a pressure of 900 psi in a vacuum of 27 inches of mercury. The bombarded leaves were kept at room temperature for two days to allow the expression of respective proteins.

4.8 Live-cell imaging by laser-scanning confocal microscopy

Live-cell imaging was performed with a TCS SP5 confocal laser scanning microscope (Leica, Bensheim, Germany). The sfGFP and the chlorophyll were excited at 488 nm. Emission signals from sfGFP and chlorophyll were collected between 501-527 and 630-702 nm, respectively. Image processing was performed using the software Leica Application Suite (LAS, Leica, Bensheim, Germany).

4.9 Bioinformatics methods

U. maydis gene and protein sequences were obtained from the PEDANT 3 database (<http://http://pedant.helmholtz-muenchen.de/>). The prediction of SPs of secreted proteins was performed with SignalP 4.1 (<http://www.cbs.dtu.dk/services/SignalP/>). The prediction of non-classical secreted proteins was performed using the SecretomeP 2.0 Server (<http://www.cbs.dtu.dk/services/SecretomeP/>). The prediction of N-glycosylation sites was conducted with NetNGlyc 1.0 (<http://www.cbs.dtu.dk/services/NetNGlyc/>). Amino acid sequences were aligned with Clustal Omega (<http://www.ebi.ac.uk/Tools/msa/clustalo/>). The aligned sequences were displayed using ESPript 3.0 (<http://endscript.ibcp.fr/ESPrpt-/ESPrpt/index.php>). The virtual cloning of plasmids was performed using the “Clone Manager 9” software (Scientific & Educational Software, Denver, CO, USA).

References

- Aichinger, C., K. Hansson, H. Eichhorn, F. Lessing, G. Mannhaupt, W. Mewes, et al.** (2003). "Identification of plant-regulated genes in *Ustilago maydis* by enhancer-trapping mutagenesis." *Molecular Genetics and Genomics* **270**(4): 303-314.
- An, Q. L., K. Ehlers, K. H. Kogel, A. J. E. van Bel and R. Huckelhoven** (2006). "Multivesicular compartments proliferate in susceptible and resistant MLA12-barley leaves in response to infection by the biotrophic powdery mildew fungus." *New Phytol* **172**(3): 563-576.
- Asai, S. and K. Shirasu** (2015). "Plant cells under siege: plant immune system versus pathogen effectors." *Curr Opin Plant Biol* **28**: 1-8.
- Ausubel, F., R. Brent, R. Kingston, D. Moore, J. Seidman, J. Smith, et al.** (1987). *Current Protocols in Molecular Biology*. New York, Greene Pub. Associates and Wiley-Interscience.
- Banuett, F.** (1995). "Genetics of *Ustilago maydis*, a fungal pathogen that induces tumors in maize." *Annu Rev Genet* **29**: 179-208.
- Banuett, F. and I. Herskowitz** (1989). "Different alleles of *Ustilago maydis* are necessary for maintenance of filamentous growth but not for meiosis." *Proc. Natl. Acad. Sci. U.S.A.* **86**(15): 5878-5882.
- Banuett, F. and I. Herskowitz** (1994). "Identification of Fuz7, a *Ustilago-Maydis* Mek/Mapkk Homolog Required for a-Locus-Dependent and a-Locus-Independent Steps in the Fungal Life-Cycle." *Gene Dev* **8**(12): 1367-1378.
- Banuett, F. and I. Herskowitz** (1996). "Discrete developmental stages during teliospore formation in the corn smut fungus, *Ustilago maydis*." *Development* **122**(10): 2965-2976.
- Bekal, S., T. L. Niblack and K. N. Lambert** (2003). "A chorismate mutase from the soybean cyst nematode *Heterodera glycines* shows polymorphisms that correlate with virulence." *Mol Plant Microbe Interact* **16**(5): 439-446.
- Berens, M. L., H. M. Berry, A. Mine, C. T. Argueso and K. Tsuda** (2017). "Evolution of Hormone Signaling Networks in Plant Defense." *Annu Rev Phytopathol.*
- Bertini, L., C. Caporale, M. Testa, S. Proietti and C. Caruso** (2009). "Structural basis of the antifungal activity of wheat PR4 proteins." *Febs Letters* **583**(17): 2865-2871.
- Blondeau, K., F. Blaise, M. Graille, S. D. Kale, J. Linglin, B. Ollivier, et al.** (2015). "Crystal structure of the effector AvrLm4-7 of *Leptosphaeria maculans* reveals insights into its translocation into plant cells and recognition by resistance proteins." *Plant J* **83**(4): 610-624.
- Blume, B., T. Nurnberger, N. Nass and D. Scheel** (2000). "Receptor-mediated increase in cytoplasmic free calcium required for activation of pathogen defense in parsley." *Plant Cell* **12**(8): 1425-1440.
- Bohmer, M., T. Colby, C. Bohmer, A. Brautigam, J. Schmidt and M. Bolker** (2007). "Proteomic analysis of dimorphic transition in the phytopathogenic fungus *Ustilago maydis*." *Proteomics* **7**(5): 675-685.
- Bolker, M., M. Urban and R. Kahmann** (1992). "The a mating type locus of *U. maydis* specifies cell signaling components." *Cell* **68**(3): 441-450.
- Boller, T. and G. Felix** (2009). "A renaissance of elicitors: perception of microbe-associated molecular patterns and danger signals by pattern-recognition receptors." *Annu Rev Plant Biol* **60**: 379-406.
- Bomberger, J. M., D. P. MacEachran, B. A. Coutermarsh, S. Y. Ye, G. A. O'Toole and B. A. Stanton** (2009). "Long-Distance Delivery of Bacterial Virulence Factors by *Pseudomonas aeruginosa* Outer Membrane Vesicles." *Plos Pathog* **5** DOI: 10.1371/journal.ppat.1000382.

- Brachmann, A., G. Weinzierl, J. Kamper and R. Kahmann** (2001). "Identification of genes in the bW/bE regulatory cascade in *Ustilago maydis*." *Mol Microbiol* **42**(4): 1047-1063.
- Brefort, T., G. Doehlemann, A. Mendoza-Mendoza, S. Reissmann, A. Djamei and R. Kahmann** (2009). "Ustilago maydis as a Pathogen." *Annu Rev Phytopathol* **47**: 423-445.
- Brown, J. F. and I. W. Dawes** (1990). "Regulation of chorismate mutase in *Saccharomyces cerevisiae*." *Mol Gen Genet* **220**(2): 283-288.
- Brutus, A., F. Sicilia, A. Macone, F. Cervone and G. De Lorenzo** (2010). "A domain swap approach reveals a role of the plant wall-associated kinase 1 (WAK1) as a receptor of oligogalacturonides." *Proc. Natl. Acad. Sci. U.S.A.* **107**(20): 9452-9457.
- Bumann, D.** (2002). "Examination of Salmonella gene expression in an infected mammalian host using the green fluorescent protein and two-colour flow cytometry." *Mol Microbiol* **43**(5): 1269-1283.
- Calhoun, D. H., C. A. Bonner, W. Gu, G. Xie and R. A. Jensen** (2001). "The emerging periplasm-localized subclass of AroQ chorismate mutases, exemplified by those from *Salmonella typhimurium* and *Pseudomonas aeruginosa*." *Genome Biol* **2**(8): RESEARCH0030.
- Cao, Y., Y. Liang, K. Tanaka, C. T. Nguyen, R. P. Jedrzejczak, A. Joachimiak, et al.** (2014). "The kinase LYK5 is a major chitin receptor in Arabidopsis and forms a chitin-induced complex with related kinase CERK1." *Elife* **3** DOI: 10.7554/eLife.03766.
- Caporale, C., I. Di Berardino, L. Leonardi, L. Bertini, A. Cascone, V. Buonocore, et al.** (2004). "Wheat pathogenesis-related proteins of class 4 have ribonuclease activity." *Febs Letters* **575**(1-3): 71-76.
- Catanzariti, A. M., P. N. Dodds, T. Ve, B. Kobe, J. G. Ellis and B. J. Staskawicz** (2010). "The AvrM Effector from Flax Rust Has a Structured C-Terminal Domain and Interacts Directly with the M Resistance Protein." *Mol Plant Microbe In* **23**(1): 49-57.
- Chen, D. C., B. C. Yang and T. T. Kuo** (1992). "One-Step Transformation of Yeast in Stationary Phase." *Current Genetics* **21**(1): 83-84.
- Chisholm, S. T., G. Coaker, B. Day and B. J. Staskawicz** (2006). "Host-microbe interactions: shaping the evolution of the plant immune response." *Cell* **124**(4): 803-814.
- Choi, J., K. Tanaka, Y. Cao, Y. Qi, J. Qiu, Y. Liang, et al.** (2014). "Identification of a plant receptor for extracellular ATP." *Science* **343**(6168): 290-294.
- Chook, Y. M., H. M. Ke and W. N. Lipscomb** (1993). "Crystal-Structures of the Monofunctional Chorismate Mutase from *Bacillus-Subtilis* and Its Complex with a Transition-State Analog." *Proc. Natl. Acad. Sci. U.S.A.* **90**(18): 8600-8603.
- Christensen, J. J.** (1963). Corn smut caused by *Ustilago maydis*. *Monograph 2*. St. Paul (Minnesota), American Phytopathology Society: 1-40.
- Christopherson, R. I.** (1985). "Chorismate Mutase-Prephenate Dehydrogenase from *Escherichia-Coli* - Cooperative Effects and Inhibition by L-Tyrosine." *Arch Biochem Biophys* **240**(2): 646-654.
- Ciacchi, C., I. Russo, C. Bucci, P. Iovino, L. Pellegrini, I. Giangrieco, et al.** (2014). "The kiwi fruit peptide kissper displays anti-inflammatory and anti-oxidant effects in in-vitro and ex-vivo human intestinal models." *Clin Exp Immunol* **175**(3): 476-484.
- Ciardello, M. A., D. Meleleo, G. Saviano, R. Crescenzo, V. Carratore, L. Camardella, et al.** (2008). "Kissper, a kiwi fruit peptide with channel-like activity: Structural and functional features." *J Pept Sci* **14**(6): 742-754.
- Coaker, G., A. Falick and B. Staskawicz** (2005). "Activation of a phytopathogenic bacterial effector protein by a eukaryotic cyclophilin." *Science* **308**(5721): 548-550.
- Colquhoun, T. A., B. C. J. Schimmel, J. Y. Kim, D. Reinhardt, K. Cline and D. G. Clark** (2010). "A petunia chorismate mutase specialized for the production of floral volatiles." *Plant J*

- 61(1): 145-155.
- Couto, D. and C. Zipfel** (2016). "Regulation of pattern recognition receptor signalling in plants." *Nat Rev Immunol* **16**(9): 537-552.
- Dai, L. M., D. Wang, X. Q. Xie, C. H. Zhang, X. P. Wang, Y. Xu, et al.** (2016). "The Novel Gene VpPR4-1 from *Vitis pseudoreticulata* Increases Powdery Mildew Resistance in Transgenic *Vitis vinifera* L." *Frontiers in Plant Science* **7**.
- Dangl, J. L., D. M. Horvath and B. J. Staskawicz** (2013). "Pivoting the Plant Immune System from Dissection to Deployment." *Science* **341**(6147): 746-751.
- Daudi, A., Z. Cheng, J. A. O'Brien, N. Mammarella, S. Khan, F. M. Ausubel, et al.** (2012). "The apoplastic oxidative burst peroxidase in *Arabidopsis* is a major component of pattern-triggered immunity." *Plant Cell* **24**(1): 275-287.
- Davies, C. and S. P. Robinson** (2000). "Differential screening indicates a dramatic change in mRNA profiles during grape berry ripening. Cloning and characterization of cDNAs encoding putative cell wall and stress response proteins." *Plant Physiol* **122**(3): 803-812.
- de Guillen, K., D. Ortiz-Vallejo, J. Gracy, E. Fournier, T. Kroj and A. Padilla** (2015) "Structure Analysis Uncovers a Highly Diverse but Structurally Conserved Effector Family in Phytopathogenic Fungi." *Plos Pathog* **11**, e1005228 DOI: 10.1371/journal.ppat.1005228.
- de Jonge, R., H. P. van Esse, A. Kombrink, T. Shinya, Y. Desaki, R. Bours, et al.** (2010). "Conserved Fungal LysM Effector Ecp6 Prevents Chitin-Triggered Immunity in Plants." *Science* **329**(5994): 953-955.
- de Wit, P. J. G. M., R. Mehrabi, H. A. van den Burg and I. Stergiopoulos** (2009). "Fungal effector proteins: past, present and future." *Molecular Plant Pathology* **10**(6): 735-747.
- Dean, R., J. A. Van Kan, Z. A. Pretorius, K. E. Hammond-Kosack, A. Di Pietro, P. D. Spanu, et al.** (2012). "The Top 10 fungal pathogens in molecular plant pathology." *Mol Plant Pathol* **13**(4): 414-430.
- Dempsey, D. A., A. C. Vlot, M. C. Wildermuth and D. F. Klessig** (2011). "Salicylic Acid biosynthesis and metabolism." *Arabidopsis Book* **9**: e0156.
- Djamei, A. and R. Kahmann** (2012) "Ustilago maydis: Dissecting the Molecular Interface between Pathogen and Plant." *Plos Pathog* **8** DOI: 10.1371/journal.ppat.1002955.
- Djamei, A., K. Schipper, F. Rabe, A. Ghosh, V. Vincon, J. Kahnt, et al.** (2011). "Metabolic priming by a secreted fungal effector." *Nature* **478**(7369): 395-398.
- Dodds, P. N. and J. P. Rathjen** (2010). "Plant immunity: towards an integrated view of plant-pathogen interactions." *Nat Rev Genet* **11**(8): 539-548.
- Doehlemann, G. and C. Hemetsberger** (2013). "Apoplastic immunity and its suppression by filamentous plant pathogens." *New Phytol* **198**(4): 1001-1016.
- Doehlemann, G., S. Reissmann, D. Assmann, M. Fleckenstein and R. Kahmann** (2011). "Two linked genes encoding a secreted effector and a membrane protein are essential for Ustilago maydis-induced tumour formation." *Mol Microbiol* **81**(3): 751-766.
- Doehlemann, G., K. van der Linde, D. Assmann, D. Schwambach, A. Hof, A. Mohanty, et al.** (2009) "Pep1, a secreted effector protein of Ustilago maydis, is required for successful invasion of plant cells." *Plos Pathog* **5**, e1000290 DOI: 10.1371/journal.ppat.1000290.
- Dong, S. M., S. Raffaele and S. Kamoun** (2015). "The two-speed genomes of filamentous pathogens: waltz with plants." *Curr Opin Genet Dev* **35**: 57-65.
- Dopheide, T. A., B. E. Davidson and P. Crewther** (1972). "Chorismate Mutase-Prephenate Dehydratase from *Escherichia-Coli* K-12 .2. Kinetic Properties." *J Biol Chem* **247**(14): 4447-&.
- Doyle, E. A. and K. N. Lambert** (2003). "Meloidogyne javanica chorismate mutase 1 alters plant cell development." *Mol Plant Microbe Interact* **16**(2): 123-131.

- Draffehn, A. M., L. Li, N. Krezdorn, J. Ding, J. Lubeck, J. Strahwald, et al.** (2013). "Comparative transcript profiling by SuperSAGE identifies novel candidate genes for controlling potato quantitative resistance to late blight not compromised by late maturity." *Front Plant Sci* **4**: 423.
- Drakopoulou, E., J. Vizzavona, J. Neyton, V. Aniot, F. Bouet, H. Virelizier, et al.** (1998). "Consequence of the removal of evolutionary conserved disulfide bridges on the structure and function of charybdotoxin and evidence that particular cysteine spacings govern specific disulfide bond formation." *Biochemistry* **37**(5): 1292-1301.
- Duplessis, S., C. A. Cuomo, Y. C. Lin, A. Aerts, E. Tisserant, C. Veneault-Fourrey, et al.** (2011). "Obligate biotrophy features unraveled by the genomic analysis of rust fungi." *P Natl Acad Sci USA* **108**(22): 9166-9171.
- Dutheil, J. Y., G. Mannhaupt, G. Schweizer, C. M. K. Sieber, M. Munsterkotter, U. Guldener, et al.** (2016). "A Tale of Genome Compartmentalization: The Evolution of Virulence Clusters in Smut Fungi." *Genome Biol Evol* **8**(3): 681-704.
- Eberhard, J., M. Bischoff, H. R. Raesecke, N. Amrhein and J. Schmid** (1996a). "Isolation of a cDNA from tomato coding for an unregulated, cytosolic chorismate mutase." *Plant Molecular Biology* **31**(4): 917-922.
- Eberhard, J., T. T. Ehrler, P. Epple, G. Felix, H. R. Raesecke, N. Amrhein, et al.** (1996b). "Cytosolic and plastidic chorismate mutase isozymes from *Arabidopsis thaliana*: Molecular characterization and enzymatic properties." *Plant J* **10**(5): 815-821.
- El Kasmi, F. and M. T. Nishimura** (2016). "Structural insights into plant NLR immune receptor function." *Proc. Natl. Acad. Sci. U.S.A.*
- Englander, S. W.** (2006). "Hydrogen exchange and mass spectrometry: A historical perspective." *J Am Soc Mass Spectr* **17**(11): 1481-1489.
- Espadaler, J., E. Querol, F. X. Aviles and B. Oliva** (2006). "Identification of function-associated loop motifs and application to protein function prediction." *Bioinformatics* **22**(18): 2237-2243.
- Forrellad, M. A., L. I. Klepp, A. Gioffre, J. S. Y. Garcia, H. R. Morbidoni, M. D. Santangelo, et al.** (2013). "Virulence factors of the *Mycobacterium tuberculosis* complex." *Virulence* **4**(1): 3-66.
- Franceschetti, M., A. Maqbool, M. J. Jimenez-Dalmaroni, H. G. Pennington, S. Kamoun and M. J. Banfield** (2017). "Effectors of Filamentous Plant Pathogens: Commonalities amid Diversity." *Microbiol Mol Biol Rev* **81**(2).
- Friedrich, L., M. Moyer, E. Ward and J. Ryals** (1991). "Pathogenesis-related protein 4 is structurally homologous to the carboxy-terminal domains of hevein, Win-1 and Win-2." *Mol Gen Genet* **230**(1-2): 113-119.
- Gaffney, T., L. Friedrich, B. Vernooij, D. Negrotto, G. Nye, S. Uknes, et al.** (1993). "Requirement of Salicylic-Acid for the Induction of Systemic Acquired-Resistance." *Science* **261**(5122): 754-756.
- Gan, P., K. Ikeda, H. Irieda, M. Narusaka, R. J. O'Connell, Y. Narusaka, et al.** (2013). "Comparative genomic and transcriptomic analyses reveal the hemibiotrophic stage shift of *Colletotrichum* fungi." *New Phytol* **197**(4): 1236-1249.
- Gillissen, B., J. Bergemann, C. Sandmann, B. Schroeer, M. Bolker and R. Kahmann** (1992). "A two-component regulatory system for self/non-self recognition in *Ustilago maydis*." *Cell* **68**(4): 647-657.
- Gilroy, S., M. Bialasek, N. Suzuki, M. Gorecka, A. R. Devireddy, S. Karpinski, et al.** (2016). "ROS, Calcium, and Electric Signals: Key Mediators of Rapid Systemic Signaling in Plants." *Plant Physiol* **171**(3): 1606-1615.

- Glazebrook, J.** (2005). "Contrasting mechanisms of defense against biotrophic and necrotrophic pathogens." *Annu Rev Phytopathol* **43**: 205-227.
- Goers, S. K. and R. A. Jensen** (1984). "The differential allosteric regulation of two chorismate-mutase isoenzymes of *Nicotiana glauca*." *Planta* **162**(2): 117-124.
- Gomez-Gomez, L. and T. Boller** (2000). "FLS2: an LRR receptor-like kinase involved in the perception of the bacterial elicitor flagellin in *Arabidopsis*." *Mol Cell* **5**(6): 1003-1011.
- Gongora-Castillo, E., E. Ibarra-Laclette, D. L. Trejo-Saavedra and R. F. Rivera-Bustamante** (2012). "Transcriptome analysis of symptomatic and recovered leaves of geminivirus-infected pepper (*Capsicum annuum*)." *Virology* **9**.
- Grandaubert, J., R. G. T. Lowe, J. L. Soyer, C. L. Schoch, A. P. V. de Wouw, I. Fudal, et al.** (2014). "Transposable element-assisted evolution and adaptation to host plant within the *Leptosphaeria maculans*-*Leptosphaeria biglobosa* species complex of fungal pathogens." *Bmc Genomics* **15**.
- Guevara-Morato, M. A., M. G. de Lacoba, I. Garcia-Luque and M. T. Serra** (2010). "Characterization of a pathogenesis-related protein 4 (PR-4) induced in *Capsicum chinense* L3 plants with dual RNase and DNase activities." *J Exp Bot* **61**(12): 3259-3271.
- Guyon, K., C. Balague, D. Roby and S. Raffaele** (2014). "Secretome analysis reveals effector candidates associated with broad host range necrotrophy in the fungal plant pathogen *Sclerotinia sclerotiorum*." *Bmc Genomics* **15**.
- Hake, S. and J. Ross-Ibarra** (2015) "Genetic, evolutionary and plant breeding insights from the domestication of maize." *Elife* **4** DOI: 10.7554/eLife.05861.
- Hamiaux, C., R. Maddumage, M. J. Middleditch, R. Prakash, D. A. Brummell, E. N. Baker, et al.** (2014). "Crystal structure of kiwellin, a major cell-wall protein from kiwifruit." *J Struct Biol* **187**(3): 276-281.
- Hartmann, H. A., R. Kahmann and M. Bolker** (1996). "The pheromone response factor coordinates filamentous growth and pathogenicity in *Ustilago maydis*." *Embo J* **15**(7): 1632-1641.
- Hejgaard, J., S. Jacobsen, S. E. Bjorn and K. M. Kragh** (1992). "Antifungal Activity of Chitin-Binding Pr-4 Type Proteins from Barley-Grain and Stressed Leaf." *Febs Letters* **307**(3): 389-392.
- Helmstaedt, K., G. Heinrich, W. N. Lipscomb and G. H. Braus** (2002). "Refined molecular hinge between allosteric and catalytic domain determines allosteric regulation and stability of fungal chorismate mutase." *Proc. Natl. Acad. Sci. U.S.A.* **99**(10): 6631-6636.
- Helmstaedt, K., S. Krappmann and G. H. Braus** (2001). "Allosteric regulation of catalytic activity: *Escherichia coli* aspartate transcarbamoylase versus yeast chorismate mutase." *Microbiol Mol Biol Rev* **65**(3): 404-421, table of contents.
- Hemetsberger, C., C. Herrberger, B. Zechmann, M. Hillmer and G. Doehlemann** (2012) "The *Ustilago maydis* effector Pep1 suppresses plant immunity by inhibition of host peroxidase activity." *Plos Pathog* **8**, e1002684 DOI: 10.1371/journal.ppat.1002684
PPATHOGENS-D-11-02600 [pii].
- Holliday, R.** (1974). *Ustilago maydis*. *Bacteria, Bacteriophages, and Fungi*. R. C. King. Boston, MA, Springer US. **1**: 575-595.
- Huffaker, A., G. Pearce and C. A. Ryan** (2006). "An endogenous peptide signal in *Arabidopsis* activates components of the innate immune response." *Proc. Natl. Acad. Sci. U.S.A.* **103**(26): 10098-10103.
- Hwang, I. S., D. S. Choi, N. H. Kim, D. S. Kim and B. K. Hwang** (2014). "Pathogenesis-related protein 4b interacts with leucine-rich repeat protein 1 to suppress PR4b-triggered cell death and defense response in pepper." *Plant J* **77**(4): 521-533.

- Illergard, K., D. H. Ardell and A. Elofson** (2009). "Structure is three to ten times more conserved than sequence-A study of structural response in protein cores." *Proteins* **77**(3): 499-508.
- Jashni, M. K., R. Mehrabi, J. Collemare, C. H. Mesarich and P. J. de Wit** (2015). "The battle in the apoplast: further insights into the roles of proteases and their inhibitors in plant-pathogen interactions." *Front Plant Sci* **6**: 584.
- Jelenska, J., J. A. van Hal and J. T. Greenberg** (2010). "Pseudomonas syringae hijacks plant stress chaperone machinery for virulence." *Proc Natl Acad Sci U S A* **107**(29): 13177-13182.
- Jelenska, J., N. Yao, B. A. Vinatzer, C. M. Wright, J. L. Brodsky and J. T. Greenberg** (2007). "A J domain virulence effector of Pseudomonas syringae remodels host chloroplasts and suppresses defenses." *Current Biology* **17**(6): 499-508.
- Jones, J. D. and J. L. Dangl** (2006). "The plant immune system." *Nature* **444**(7117): 323-329.
- Jones, J. D., R. E. Vance and J. L. Dangl** (2016). "Intracellular innate immune surveillance devices in plants and animals." *Science* **354**(6316).
- Jones, J. T., C. Furlanetto, E. Bakker, B. Banks, V. Blok, Q. Chen, et al.** (2003). "Characterization of a chorismate mutase from the potato cyst nematode *Globodera pallida*." *Mol Plant Pathol* **4**(1): 43-50.
- Kämper, J.** (2004). "A PCR-based system for highly efficient generation of gene replacement mutants in *Ustilago maydis*." *Mol Genet Genomics* **271**(1): 103-110.
- Kämper, J., R. Kahmann, M. Bolker, L. J. Ma, T. Brefort, B. J. Saville, et al.** (2006). "Insights from the genome of the biotrophic fungal plant pathogen *Ustilago maydis*." *Nature* **444**(7115): 97-101.
- Kämper, J., M. Reichmann, T. Romeis, M. Bolker and R. Kahmann** (1995). "Multiallelic recognition: nonself-dependent dimerization of the bE and bW homeodomain proteins in *Ustilago maydis*." *Cell* **81**(1): 73-83.
- Kaffarnik, F., P. Muller, M. Leibundgut, R. Kahmann and M. Feldbrugge** (2003). "PKA and MAPK phosphorylation of Prf1 allows promoter discrimination in *Ustilago maydis*." *Embo J* **22**(21): 5817-5826.
- Kahmann, R., T. Romeis, M. Bolker and J. Kamper** (1995). "Control of mating and development in *Ustilago maydis*." *Curr Opin Genet Dev* **5**(5): 559-564.
- Kahmann, R. and J. Schirawski** (2007). Mating in the smut fungi: from a to b to the downstream cascades. *Sex in Fungi*. K. J. Heitman J, Taylor J, Casselton L. Washington, DC., American Society of Microbiology: 377-387.
- Kahmann, R., G. Steinberg, C. Basse, M. Feldbrügge and J. Kämper** (2000). *Ustilago maydis*, the Causative Agent of Corn Smut Disease. *Fungal Pathology*. J. W. Kronstad. Dordrecht, Springer Netherlands: 347-371.
- Kamoun, S.** (2006). "A catalogue of the effector secretome of plant pathogenic oomycetes." *Annu Rev Phytopathol* **44**: 41-60.
- Kane, J. F., S. L. Stenmark, D. H. Calhoun and R. A. Jensen** (1971). "Metabolic interlock. The role of the subordinate type of enzyme in the regulation of a complex pathway." *J Biol Chem* **246**(13): 4308-4316.
- Katsir, L. and O. Bahar** (2017) "Bacterial outer membrane vesicles at the plant-pathogen interface." *Plos Pathog* **13** DOI: 10.1371/journal.ppat.1006306.
- Kazan, K. and R. Lyons** (2014). "Intervention of Phytohormone Pathways by Pathogen Effectors." *Plant Cell* **26**(6): 2285-2309.
- Keon, J. P. R., G. A. White and J. A. Hargreaves** (1991). "Isolation, Characterization and Sequence of a Gene Conferring Resistance to the Systemic Fungicide Carboxin from the Maize Smut Pathogen, *Ustilago-Maydis*." *Current Genetics* **19**(6): 475-481.
- Kim, N. H. and B. K. Hwang** (2015). "Pepper pathogenesis-related protein 4c is a plasma

- membrane-localized cysteine protease inhibitor that is required for plant cell death and defense signaling." *Plant J* **81**(1): 81-94.
- Kobayashi, M., I. Ohura, K. Kawakita, N. Yokota, M. Fujiwara, K. Shimamoto, et al.** (2007). "Calcium-dependent protein kinases regulate the production of reactive oxygen species by potato NADPH oxidase." *Plant Cell* **19**(3): 1065-1080.
- Kohler, A. C., L. H. Chen, N. Hurlburt, A. Salvucci, B. Schwessinger, A. J. Fisher, et al.** (2016). "Structural Analysis of an Avr4 Effector Ortholog Offers Insight into Chitin Binding and Recognition by the Cf-4 Receptor." *Plant Cell* **28**(8): 1945-1965.
- Konermann, L., J. X. Pan and Y. H. Liu** (2011). "Hydrogen exchange mass spectrometry for studying protein structure and dynamics." *Chem Soc Rev* **40**(3): 1224-1234.
- Kong, G. H., Y. Zhao, M. F. Jing, J. Huang, J. Yang, Y. Q. Xia, et al.** (2015) "The Activation of Phytophthora Effector Avr3b by Plant Cyclophilin is Required for the Nudix Hydrolase Activity of Avr3b." *Plos Pathog* **11** DOI: 10.1371/journal.ppat.1005139.
- Kovtun, Y., W. L. Chiu, G. Tena and J. Sheen** (2000). "Functional analysis of oxidative stress-activated mitogen-activated protein kinase cascade in plants." *Proc. Natl. Acad. Sci. U.S.A.* **97**(6): 2940-2945.
- Kradolfer, P., J. Zeyer, G. Miozzari and R. Huetter** (1977). "Dominant Regulatory Mutants in Chorismate Mutase of Saccharomyces-Cerevisiae." *Fems Microbiol Lett* **2**(4): 211-216.
- Kronstad, J. W. and S. A. Leong** (1990). "The B-Mating-Type Locus of Ustilago-Maydis Contains Variable and Constant Regions." *Gene Dev* **4**(8): 1384-1395.
- Kuehn, M. J. and N. C. Kesty** (2005). "Bacterial outer membrane vesicles and the host-pathogen interaction." *Gene Dev* **19**(22): 2645-2655.
- Kushnirov, V. V.** (2000). "Rapid and reliable protein extraction from yeast." *Yeast* **16**(9): 857-860.
- Laemmli, U. K.** (1970). "Cleavage of structural proteins during the assembly of the head of bacteriophage T4." *Nature* **227**(5259): 680-685.
- Lanver, D., M. Tollot, G. Schweizer, L. Lo Presti, S. Reissmann, L. S. Ma, et al.** (2017). "Ustilago maydis effectors and their impact on virulence." *Nat Rev Microbiol* **15**(7): 409-421.
- Le Roux, C., G. Huet, A. Jauneau, L. Camborde, D. Tremousaygue, A. Kraut, et al.** (2015). "A receptor pair with an integrated decoy converts pathogen disabling of transcription factors to immunity." *Cell* **161**(5): 1074-1088.
- Lecourieux, D., C. Mazars, N. Pauly, R. Ranjeva and A. Pugin** (2002). "Analysis and effects of cytosolic free calcium increases in response to elicitors in Nicotiana plumbaginifolia cells." *Plant Cell* **14**(10): 2627-2641.
- Lee, A. Y., P. A. Karplus, B. Ganem and J. Clardy** (1995). "Atomic structure of the buried catalytic pocket of Escherichia coli chorismate mutase." *J Am Chem Soc* **117**(12): 3627-3628.
- Lee, J., L. Eschen-Lippold, I. Lassowskat, C. Bottcher and D. Scheel** (2015). "Cellular reprogramming through mitogen-activated protein kinases." *Front Plant Sci* **6**: 940.
- Letunic, I. and P. Bork** (2016). "Interactive tree of life (iTOL) v3: an online tool for the display and annotation of phylogenetic and other trees." *Nucleic Acids Res* **44**(W1): W242-W245.
- Liu, T. L., T. Q. Song, X. Zhang, H. B. Yuan, L. M. Su, W. L. Li, et al.** (2014). "Unconventionally secreted effectors of two filamentous pathogens target plant salicylate biosynthesis." *Nat Commun* **5**.
- Liu, T. L., W. W. Ye, Y. Y. Ru, X. Y. Yang, B. A. Gu, K. Tao, et al.** (2011). "Two Host Cytoplasmic Effectors Are Required for Pathogenesis of Phytophthora sojae by Suppression of Host Defenses." *Plant Physiol* **155**(1): 490-501.
- Liu, Z. H., J. D. Faris, R. P. Oliver, K. C. Tan, P. S. Solomon, M. C. McDonald, et al.** (2009)

- "SnTox3 Acts in Effector Triggered Susceptibility to Induce Disease on Wheat Carrying the Snn3 Gene." *Plos Pathog* **5** DOI: 10.1371/journal.ppat.1000581.
- Lo Presti, L. and R. Kahmann** (2017). "How filamentous plant pathogen effectors are translocated to host cells." *Curr Opin Plant Biol* **38**: 19-24.
- Lo Presti, L., D. Lanver, G. Schweizer, S. Tanaka, L. Liang, M. Tollot, et al.** (2015). "Fungal effectors and plant susceptibility." *Annu Rev Plant Biol* **66**: 513-545.
- Lo Presti, L., B. Zechmann, J. Kumlehn, L. Liang, D. Lanver, S. Tanaka, et al.** (2017). "An assay for entry of secreted fungal effectors into plant cells." *New Phytol* **213**(2): 956-964.
- Lobstein, J., C. A. Emrich, C. Jeans, M. Faulkner, P. Riggs and M. Berkmen** (2012). "SHuffle, a novel Escherichia coli protein expression strain capable of correctly folding disulfide bonded proteins in its cytoplasm." *Microb Cell Fact* **11**.
- Luna, E., V. Pastor, J. Robert, V. Flors, B. Mauch-Mani and J. Ton** (2011). "Callose deposition: a multifaceted plant defense response." *Mol Plant Microbe Interact* **24**(2): 183-193.
- Ma, Z. C., T. Q. Song, L. Zhu, W. W. Ye, Y. Wang, Y. Y. Shao, et al.** (2015). "A Phytophthora sojae Glycoside Hydrolase 12 Protein Is a Major Virulence Factor during Soybean Infection and Is Recognized as a PAMP." *Plant Cell* **27**(7): 2057-2072.
- Macho, A. P. and C. Zipfel** (2014). "Plant PRRs and the activation of innate immune signaling." *Mol Cell* **54**(2): 263-272.
- Maeda, H. and N. Dudareva** (2012). "The Shikimate Pathway and Aromatic Amino Acid Biosynthesis in Plants." *Annual Review of Plant Biology* **63**(1): 73-105.
- Manning, V. A., S. M. Hamilton, P. A. Karplus and L. M. Ciuffetti** (2008). "The Arg-Gly-Asp-containing, solvent-exposed loop of Ptr ToxA is required for internalization." *Mol Plant Microbe Interact* **21**(3): 315-325.
- Martin, F., A. Kohler, C. Murat, C. Veneault-Fourrey and D. S. Hibbett** (2016). "Unearthing the roots of ectomycorrhizal symbioses." *Nat Rev Microbiol* **14**(12): 760-773.
- Mazars, C., P. Thuleau, O. Lamotte and S. Bourque** (2010). "Cross-Talk between ROS and Calcium in Regulation of Nuclear Activities." *Molecular Plant* **3**(4): 706-718.
- Meinhardt, S. W., W. J. Cheng, C. Y. Kwon, C. M. Donohue and J. B. Rasmussen** (2002). "Role of the arginyl-glycyl-aspartic motif in the action of Ptr ToxA produced by Pyrenophora tritici-repentis." *Plant Physiol* **130**(3): 1545-1551.
- Mendoza-Mendoza, A., P. Berndt, A. Djamei, C. Weise, U. Linne, M. Marahiel, et al.** (2009). "Physical-chemical plant-derived signals induce differentiation in Ustilago maydis." *Mol Microbiol* **71**(4): 895-911.
- Mentlak, T. A., A. Kombrink, T. Shinya, L. S. Ryder, I. Otomo, H. Saitoh, et al.** (2012). "Effector-Mediated Suppression of Chitin-Triggered Immunity by Magnaporthe oryzae Is Necessary for Rice Blast Disease." *Plant Cell* **24**(1): 322-335.
- Miya, A., P. Albert, T. Shinya, Y. Desaki, K. Ichimura, K. Shirasu, et al.** (2007). "CERK1, a LysM receptor kinase, is essential for chitin elicitor signaling in Arabidopsis." *Proc. Natl. Acad. Sci. U.S.A.* **104**(49): 19613-19618.
- Mobley, E. M., B. N. Kunkel and B. Keith** (1999). "Identification, characterization and comparative analysis of a novel chorismate mutase gene in Arabidopsis thaliana." *Gene* **240**(1): 115-123.
- Mosquera, G., M. C. Giraldo, C. H. Khang, S. Coughlan and B. Valent** (2009). "Interaction Transcriptome Analysis Identifies Magnaporthe oryzae BAS1-4 as Biotrophy-Associated Secreted Proteins in Rice Blast Disease." *Plant Cell* **21**(4): 1273-1290.
- Mueller, A. N., S. Ziemann, S. Treitschke, D. Assmann and G. Doehlemann** (2013). "Compatibility in the Ustilago maydis-Maize Interaction Requires Inhibition of Host Cysteine Proteases by the Fungal Effector Pit2." *Plos Pathog* **9** DOI:

- 10.1371/journal.ppat.1003177.
- Mukamolova, G. V., O. A. Turapov, K. Kazarian, M. Telkov, A. S. Kaprelyants, D. B. Kell, et al.** (2002a). "The rpf gene of *Micrococcus luteus* encodes an essential secreted growth factor." *Mol Microbiol* **46**(3): 611-621.
- Mukamolova, G. V., O. A. Turapov, D. I. Young, A. S. Kaprelyants, D. B. Kell and M. Young** (2002b). "A family of autocrine growth factors in *Mycobacterium tuberculosis*." *Mol Microbiol* **46**(3): 623-635.
- Muller, P., G. Weinzierl, A. Brachmann, M. Feldbrugge and R. Kahmann** (2003). "Mating and pathogenic development of the Smut fungus *Ustilago maydis* are regulated by one mitogen-activated protein kinase cascade." *Eukaryot Cell* **2**(6): 1187-1199.
- Nyarko, A., K. K. Singarapu, M. Figueroa, V. A. Manning, I. Pandelova, T. J. Wolpert, et al.** (2014). "Solution NMR Structures of *Pyrenophora tritici-repentis* ToxB and Its Inactive Homolog Reveal Potential Determinants of Toxin Activity." *J Biol Chem* **289**(37): 25946-25956.
- O'Brien, J. A., A. Daudi, P. Finch, V. S. Butt, J. P. Whitelegge, P. Souda, et al.** (2012). "A peroxidase-dependent apoplastic oxidative burst in cultured *Arabidopsis* cells functions in MAMP-elicited defense." *Plant Physiol* **158**(4): 2013-2027.
- Ogino, H., T. Uchiho, J. Yokoo, R. Kobayashi, R. Ichise and H. Ishikawa** (2001). "Role of intermolecular disulfide bonds of the organic solvent-stable PST-01 protease in its organic solvent stability." *Appl Environ Microb* **67**(2): 942-947.
- Okvist, M., R. Dey, S. Sasso, E. Grahn, P. Kast and U. Krengel** (2006). "1.6 Å crystal structure of the secreted chorismate mutase from *Mycobacterium tuberculosis*: novel fold topology revealed." *J Mol Biol* **357**(5): 1483-1499.
- Papaleo, E., G. Saladino, M. Lambrugh, K. Lindorff-Larsen, F. L. Gervasio and R. Nussinov** (2016). "The Role of Protein Loops and Linkers in Conformational Dynamics and Allostery." *Chem Rev* **116**(11): 6391-6423.
- Parlange, F., G. Daverdin, I. Fudal, M. L. Kuhn, M. H. Balesdent, F. Blaise, et al.** (2009). "*Leptosphaeria maculans* avirulence gene AvrLm4-7 confers a dual recognition specificity by the Rlm4 and Rlm7 resistance genes of oilseed rape, and circumvents Rlm4-mediated recognition through a single amino acid change." *Mol Microbiol* **71**(4): 851-863.
- Pedelacq, J. D., S. Cabantous, T. Tran, T. C. Terwilliger and G. S. Waldo** (2006). "Engineering and characterization of a superfolder green fluorescent protein." *Nat Biotechnol* **24**(1): 79-88.
- Pei, Z. M., Y. Murata, G. Benning, S. Thomine, B. Klusener, G. J. Allen, et al.** (2000). "Calcium channels activated by hydrogen peroxide mediate abscisic acid signalling in guard cells." *Nature* **406**(6797): 731-734.
- Petre, B. and S. Kamoun** (2014) "How Do Filamentous Pathogens Deliver Effector Proteins into Plant Cells?" *Plos Biol* **12** DOI: 10.1371/journal.pbio.1001801.
- Phan, H. T. T., K. Rybak, E. Furuki, S. Breen, P. S. Solomon, R. P. Oliver, et al.** (2016). "Differential effector gene expression underpins epistasis in a plant fungal disease." *Plant J* **87**(4): 343-354.
- Pieterse, C. M., D. Van der Does, C. Zamioudis, A. Leon-Reyes and S. C. Van Wees** (2012). "Hormonal modulation of plant immunity." *Annu Rev Cell Dev Biol* **28**: 489-521.
- Plett, J. M., Y. Daguerre, S. Wittulsky, A. Vayssieres, A. Deveau, S. J. Melton, et al.** (2014a). "Effector MiSSP7 of the mutualistic fungus *Laccaria bicolor* stabilizes the *Populus* JAZ6 protein and represses jasmonic acid (JA) responsive genes." *Proc. Natl. Acad. Sci. U.S.A.* **111**(22): 8299-8304.
- Plett, J. M., A. Khachane, M. Ouassou, B. Sundberg, A. Kohler and F. Martin** (2014b).

- "Ethylene and jasmonic acid act as negative modulators during mutualistic symbiosis between *Laccaria bicolor* and *Populus* roots." *New Phytol* **202**(1): 270-286.
- Ponstein, A. S., S. A. Brevloemans, M. B. Selabuurlage, P. J. M. Vandanelzen, L. S. Melchers and B. J. C. Cornelissen** (1994). "A Novel Pathogen-Inducible and Wound-Inducible Tobacco (*Nicotiana-Tabacum*) Protein with Antifungal Activity." *Plant Physiol* **104**(1): 109-118.
- Prakash, P., B. Aruna, A. A. Sardesai and S. E. Hasnain** (2005). "Purified recombinant hypothetical protein coded by open reading frame Rv1885c of *Mycobacterium tuberculosis* exhibits a monofunctional AroQ class of periplasmic chorismate mutase activity." *J Biol Chem* **280**(20): 19641-19648.
- Puhalla, J. E.** (1969). "The formation of diploids of *Ustilago maydis* on agar medium." *Phytopathology* **59**(11): 1771-1772.
- Qamra, R., P. Prakash, B. Aruna, S. E. Hasnain and S. C. Mande** (2006). "The 2.15 Å crystal structure of *Mycobacterium tuberculosis* chorismate mutase reveals an unexpected gene duplication and suggests a role in host-pathogen interactions." *Biochemistry* **45**(23): 6997-7005.
- Qi, Z., R. Verma, C. Gehring, Y. Yamaguchi, Y. Zhao, C. A. Ryan, et al.** (2010). "Ca²⁺ signaling by plant *Arabidopsis thaliana* Pep peptides depends on AtPepR1, a receptor with guanylyl cyclase activity, and cGMP-activated Ca²⁺ channels." *Proc. Natl. Acad. Sci. U.S.A.* **107**(49): 21193-21198.
- Raab-Traub, N. and D. P. Dittmer** (2017). "Viral effects on the content and function of extracellular vesicles." *Nat Rev Microbiol* **15**(9): 559-572.
- Rabe, F., Z. Ajami-Rashidi, G. Doehlemann, R. Kahmann and A. Djamei** (2013). "Degradation of the plant defence hormone salicylic acid by the biotrophic fungus *Ustilago maydis*." *Mol Microbiol* **89**(1): 179-188.
- Raffaele, S. and S. Kamoun** (2012). "Genome evolution in filamentous plant pathogens: why bigger can be better." *Nat Rev Microbiol* **10**(6): 417-430.
- Rafiqi, M., P. H. Gan, M. Ravensdale, G. J. Lawrence, J. G. Ellis, D. A. Jones, et al.** (2010). "Internalization of flax rust avirulence proteins into flax and tobacco cells can occur in the absence of the pathogen." *Plant Cell* **22**(6): 2017-2032.
- Ramachandran, S. R., C. T. Yin, J. Kud, K. Tanaka, A. K. Mahoney, F. M. Xiao, et al.** (2017). "Effectors from Wheat Rust Fungi Suppress Multiple Plant Defense Responses." *Phytopathology* **107**(1): 75-83.
- Ranf, S., N. Gisch, M. Schaffer, T. Illig, L. Westphal, Y. A. Knirel, et al.** (2015). "A lectin S-domain receptor kinase mediates lipopolysaccharide sensing in *Arabidopsis thaliana*." *Nat Immunol* **16**(4): 426-433.
- Redkar, A., R. Hoser, L. Schilling, B. Zechmann, M. Krzymowska, V. Walbot, et al.** (2015). "A Secreted Effector Protein of *Ustilago maydis* Guides Maize Leaf Cells to Form Tumors." *Plant Cell* **27**(4): 1332-1351.
- Reinbothe, C., B. Ortel, B. Parthier and S. Reinbothe** (1994). "Cytosolic and Plastid Forms of 5-Enolpyruvylshikimate-3-Phosphate Synthase in *Euglena-Gracilis* Are Differentially Expressed during Light-Induced Chloroplast Development." *Molecular & General Genetics* **245**(5): 616-622.
- Robert, X. and P. Gouet** (2014). "Deciphering key features in protein structures with the new ENDscript server." *Nucleic Acids Res* **42**(W1): W320-W324.
- Rodrigues, M. L., E. S. Nakayasu, D. L. Oliveira, L. Nimrichter, J. D. Nosanchuk, I. C. Almeida, et al.** (2008). "Extracellular vesicles produced by *Cryptococcus neoformans* contain protein components associated with virulence." *Eukaryot Cell* **7**(1): 58-67.

- Rodriguez-Herva, J. J., P. Gonzalez-Melendi, R. Cuartas-Lanza, M. Antunez-Lamas, I. Rio-Alvarez, Z. Li, et al.** (2012). "A bacterial cysteine protease effector protein interferes with photosynthesis to suppress plant innate immune responses." *Cell Microbiol* **14**(5): 669-681.
- Rooney, H. C. E., J. W. van 't Klooster, R. A. L. van der Hoorn, M. H. A. J. Joosten, J. D. G. Jones and P. J. G. M. de Wit** (2005). "Cladosporium Avr2 inhibits tomato Rcr3 protease required for Cf-2-dependent disease resistance." *Science* **308**(5729): 1783-1786.
- Rovenich, H., J. C. Boshoven and B. P. H. J. Thomma** (2014). "Filamentous pathogen effector functions: of pathogens, hosts and microbiomes." *Curr Opin Plant Biol* **20**: 96-103.
- Rowell, J. B.** (1955). "Segregation of Sex Factors in a Diploid Line of Ustilago zeae Induced by Alpha Radiation." *Science* **121**(3139): 304-306.
- Sambrook, J., E. F. Fritsch and T. Maniatis** (1989). *Molecular cloning: a laboratory manual*. New York, Cold spring harbor laboratory press.
- Sanchez-Vallet, A., J. R. Mesters and B. P. H. J. Thomma** (2015). "The battle for chitin recognition in plant-microbe interactions." *Fems Microbiol Rev* **39**(2): 171-183.
- Sanchez-Vallet, A., R. Saleem-Batcha, A. Kombrink, G. Hansen, D. J. Valkenburg, B. P. H. J. Thomma, et al.** (2013) "Fungal effector Ecp6 outcompetes host immune receptor for chitin binding through intrachain LysM dimerization." *Elife* **2** DOI: 10.7554/eLife.00790.
- Santhanam, P. and B. P. H. J. Thomma** (2013). "Verticillium dahliae Sge1 Differentially Regulates Expression of Candidate Effector Genes." *Mol Plant Microbe In* **26**(2): 249-256.
- Sarris, P. F., Z. Duxbury, S. U. Huh, Y. Ma, C. Segonzac, J. Sklenar, et al.** (2015). "A Plant Immune Receptor Detects Pathogen Effectors that Target WRKY Transcription Factors." *Cell* **161**(5): 1089-1100.
- Sasso, S., M. Okvist, K. Roderer, M. Gamper, G. Codoni, U. Krengel, et al.** (2009). "Structure and function of a complex between chorismate mutase and DAHP synthase: efficiency boost for the junior partner." *Embo J* **28**(14): 2128-2142.
- Sasso, S., C. Ramakrishnan, M. Gamper, D. Hilvert and P. Kast** (2005). "Characterization of the secreted chorismate mutase from the pathogen Mycobacterium tuberculosis." *FEBS J* **272**(2): 375-389.
- Scherer, M., K. Heimel, V. Starke and J. Kamper** (2006). "The Clp1 protein is required for clamp formation and pathogenic development of Ustilago maydis." *Plant Cell* **18**(9): 2388-2401.
- Schmidheini, T., H. U. Mosch, J. N. Evans and G. Braus** (1990). "Yeast allosteric chorismate mutase is locked in the activated state by a single amino acid substitution." *Biochemistry* **29**(15): 3660-3668.
- Schnappauf, G., S. Krappmann and G. H. Braus** (1998). "Tyrosine and tryptophan act through the same binding site at the dimer interface of yeast chorismate mutase." *J Biol Chem* **273**(27): 17012-17017.
- Schornack, S., M. van Damme, T. O. Bozkurt, L. M. Cano, M. Smoker, M. Thines, et al.** (2010a). "Ancient class of translocated oomycete effectors targets the host nucleus." *Proc. Natl. Acad. Sci. U.S.A.* **107**(40): 17421-17426.
- Schornack, S., M. van Damme, T. O. Bozkurt, L. M. Cano, M. Smoker, M. Thines, et al.** (2010b). "Ancient class of translocated oomycete effectors targets the host nucleus." *Proc. Natl. Acad. Sci. U.S.A.* **107**(40): 17421-17426.
- Schulz, B., F. Banuett, M. Dahl, R. Schlesinger, W. Schafer, T. Martin, et al.** (1990). "The B-Alleles of U-Maydis, Whose Combinations Program Pathogenic Development, Code for Polypeptides Containing a Homeodomain-Related Motif." *Cell* **60**(2): 295-306.
- Schuster, M., G. Schweizer and R. Kahmann** (2017). "Comparative analyses of secreted proteins in plant pathogenic smut fungi and related basidiomycetes." *Fungal Genet Biol*.
- Schuster, M., G. Schweizer, S. Reissmann and R. Kahmann** (2016). "Genome editing in

- Ustilago maydis using the CRISPR-Cas system." *Fungal Genet Biol* **89**: 3-9.
- Sevier, C. S. and C. A. Kaiser** (2002). "Formation and transfer of disulphide bonds in living cells." *Nat Rev Mol Cell Biol* **3**(11): 836-847.
- Sievers, F., A. Wilm, D. Dineen, T. J. Gibson, K. Karplus, W. Z. Li, et al.** (2011). "Fast, scalable generation of high-quality protein multiple sequence alignments using Clustal Omega." *Mol Syst Biol* **7**.
- Skibbe, D. S., G. Doehlemann, J. Fernandes and V. Walbot** (2010). "Maize tumors caused by Ustilago maydis require organ-specific genes in host and pathogen." *Science* **328**(5974): 89-92.
- Snetselaar, K. M., M. Bolker and R. Kahmann** (1996). "Ustilago maydis mating hyphae orient their growth toward pheromone sources." *Fungal Genetics and Biology* **20**(4): 299-312.
- Snetselaar, K. M. and C. W. Mims** (1993). "Infection of Maize Stigmas by Ustilago-Maydis - Light and Electron-Microscopy." *Phytopathology* **83**(8): 843-850.
- Snetselaar, K. M. and C. W. Mims** (1994). "Light and Electron-Microscopy of Ustilago-Maydis Hyphae in Maize." *Mycol Res* **98**: 347-355.
- Sommer, S. and L. Heide** (1998). "Expression of bacterial chorismate pyruvate-lyase in tobacco: Evidence for the presence of chorismate in the plant cytosol." *Plant Cell Physiol* **39**(11): 1240-1244.
- Soyer, J. L., M. El Ghalid, N. Glaser, B. Ollivier, J. Linglin, J. Grandaubert, et al.** (2014). "Epigenetic Control of Effector Gene Expression in the Plant Pathogenic Fungus Leptosphaeria maculans." *Plos Genet* **10** DOI: 10.1371/journal.pgen.1004227.
- Soyer, J. L., A. Hamiot, B. Ollivier, M. H. Balesdent, T. Rouxel and I. Fudal** (2015). "The APSES transcription factor LmStuA is required for sporulation, pathogenic development and effector gene expression in Leptosphaeria maculans." *Molecular Plant Pathology* **16**(9): 1000-1005.
- Spellig, T., A. Bottin and R. Kahmann** (1996). "Green fluorescent protein (GFP) as a new vital marker in the phytopathogenic fungus Ustilago maydis." *Molecular & General Genetics* **252**(5): 503-509.
- Stanford, A., M. Bevan and D. Northcote** (1989). "Differential Expression within a Family of Novel Wound-Induced Genes in Potato." *Molecular & General Genetics* **215**(2): 200-208.
- Steinberg, G., M. Schliwa, C. Lehmler, M. Bolker, R. Kahmann and J. R. McIntosh** (1998). "Kinesin from the plant pathogenic fungus Ustilago maydis is involved in vacuole formation and cytoplasmic migration." *J Cell Sci* **111** (Pt 15): 2235-2246.
- Stergiopoulos, I., J. Collemare, R. Mehrabi and P. J. G. M. De Wit** (2013). "Phytotoxic secondary metabolites and peptides produced by plant pathogenic Dothideomycete fungi." *Fems Microbiol Rev* **37**(1): 67-93.
- Strable, J. and M. J. Scanlon** (2009). "Maize (Zea mays): a model organism for basic and applied research in plant biology." *Cold Spring Harb Protoc* **2009**(10): pdb emo132.
- Strater, N., K. Hakansson, G. Schnappauf, G. Braus and W. N. Lipscomb** (1996). "Crystal structure of the T state of allosteric yeast chorismate mutase and comparison with the R state." *Proc. Natl. Acad. Sci. U.S.A.* **93**(8): 3330-3334.
- Svensson, B., I. Svendsen, P. Hojrup, P. Roepstorff, S. Ludvigsen and F. M. Poulsen** (1992). "Primary structure of barwin: a barley seed protein closely related to the C-terminal domain of proteins encoded by wound-induced plant genes." *Biochemistry* **31**(37): 8767-8770.
- Szempruch, A. J., S. E. Sykes, R. Kieft, L. Dennison, A. C. Becker, A. Gartrell, et al.** (2016). "Extracellular Vesicles from Trypanosoma brucei Mediate Virulence Factor Transfer and Cause Host Anemia." *Cell* **164**(1-2): 246-257.
- Takai, S., S. A. Hines, T. Sekizaki, V. M. Nicholson, D. A. Alperin, M. Osaki, et al.** (2000).

- "DNA sequence and comparison of virulence plasmids from *Rhodococcus equi* ATCC 33701 and 103." *Infect Immun* **68**(12): 6840-6847.
- Tamburrini, M., I. Cerasuolo, V. Carratore, A. A. Stanziola, S. Zofra, L. Romano, et al.** (2005). "Kiwellin, a novel protein from kiwi fruit. Purification, biochemical characterization and identification as an allergen*." *Protein J* **24**(7-8): 423-429.
- Tanaka, S., T. Brefort, N. Neidig, A. Djamei, J. Kahnt, W. Vermerris, et al.** (2014) "A secreted *Ustilago maydis* effector promotes virulence by targeting anthocyanin biosynthesis in maize." *Elife* **3** DOI: 10.7554/eLife.01355.
- Tanaka, S., X. Han and R. Kahmann** (2015). "Microbial effectors target multiple steps in the salicylic acid production and signaling pathway." *Front Plant Sci* **6**: 349.
- Tollot, M., D. Assmann, C. Becker, J. Altmüller, J. Y. Dutheil, C. E. Wegner, et al.** (2016) "The WOPR Protein Ros1 Is a Master Regulator of Sporogenesis and Late Effector Gene Expression in the Maize Pathogen *Ustilago maydis*." *Plos Pathog* **12**, e1005697 DOI: 10.1371/journal.ppat.1005697.
- Toruno, T. Y., I. Stergiopoulos and G. Coaker** (2016). "Plant-Pathogen Effectors: Cellular Probes Interfering with Plant Defenses in Spatial and Temporal Manners." *Annu Rev Phytopathol* **54**: 419-441.
- Trueheart, J. and I. Herskowitz** (1992). "The *a* Locus Governs Cytoduction in *Ustilago-Maydis*." *Journal of Bacteriology* **174**(23): 7831-7833.
- Tuppo, L., I. Giangrieco, P. Palazzo, M. L. Bernardi, E. Scala, V. Carratore, et al.** (2008). "Kiwellin, a modular protein from green and gold kiwi fruits: evidence of in vivo and in vitro processing and IgE binding." *J Agric Food Chem* **56**(10): 3812-3817.
- Tyler, B. M., S. D. Kale, Q. Wang, K. Tao, H. R. Clark, K. Drews, et al.** (2013). "Microbe-independent entry of oomycete RxLR effectors and fungal RxLR-like effectors into plant and animal cells is specific and reproducible." *Mol Plant Microbe Interact* **26**(6): 611-616.
- Tzin, V. and G. Galili** (2010). "New Insights into the Shikimate and Aromatic Amino Acids Biosynthesis Pathways in Plants." *Molecular Plant* **3**(6): 956-972.
- van den Burg, H. A., S. J. Harrison, M. H. A. J. Joosten, J. Vervoort and P. J. G. M. de Wit** (2006). "Cladosporium fulvum Avr4 protects fungal cell walls against hydrolysis by plant chitinases accumulating during infection." *Mol Plant Microbe In* **19**(12): 1420-1430.
- van den Burg, H. A., N. Westerink, K. J. Francoijs, R. Roth, E. Woestenenk, S. Boeren, et al.** (2003). "Natural disulfide bond-disrupted mutants of AVR4 of the tomato pathogen *Cladosporium fulvum* are sensitive to proteolysis, circumvent Cf-4-mediated resistance, but retain their chitin binding ability." *J Biol Chem* **278**(30): 27340-27346.
- van der Hoorn, R. A. and S. Kamoun** (2008). "From Guard to Decoy: a new model for perception of plant pathogen effectors." *Plant Cell* **20**(8): 2009-2017.
- van Esse, H. P., M. D. Bolton, I. Stergiopoulos, P. J. G. M. de Wit and B. P. H. J. Thomma** (2007). "The chitin-binding *Cladosporium fulvum* effector protein Avr4 is a virulence factor." *Mol Plant Microbe In* **20**(9): 1092-1101.
- van Esse, H. P., J. W. van't Klooster, M. D. Bolton, K. A. Yadeta, P. van Baarlen, S. Boeren, et al.** (2008). "The *Cladosporium fulvum* virulence protein Avr2 inhibits host proteases required for basal defense." *Plant Cell* **20**(7): 1948-1963.
- van Wees, S. C. M. and J. Glazebrook** (2003). "Loss of non-host resistance of *Arabidopsis NahG* to *Pseudomonas syringae* pv. phaseolicola is due to degradation products of salicylic acid." *Plant J* **33**(4): 733-742.
- Vanholme, B., P. Kast, A. Haegeman, J. Jacob, W. Grunewald and G. Gheysen** (2009). "Structural and functional investigation of a secreted chorismate mutase from the plant-parasitic nematode *Heterodera schachtii* in the context of related enzymes from diverse

- origins." *Mol Plant Pathol* **10**(2): 189-200.
- Ve, T., S. J. Williams, A. M. Catanzariti, M. Rafiqi, M. Rahman, J. G. Ellis, et al.** (2013). "Structures of the flax-rust effector AvrM reveal insights into the molecular basis of plant-cell entry and effector-triggered immunity." *Proc. Natl. Acad. Sci. U.S.A.* **110**(43): 17594-17599.
- Vlot, A. C., D. A. Dempsey and D. F. Klessig** (2009). "Salicylic Acid, a Multifaceted Hormone to Combat Disease." *Annu Rev Phytopathol* **47**: 177-206.
- Wales, T. E. and J. R. Engen** (2006). "Hydrogen exchange mass spectrometry for the analysis of protein dynamics." *Mass Spectrom Rev* **25**(1): 158-170.
- Wang, C. I. A., G. Guncar, J. K. Forwood, T. Teh, A. M. Catanzariti, G. J. Lawrence, et al.** (2007). "Crystal structures of flax rust avirulence proteins AvrL567-A and -D reveal details of the structural basis for flax disease resistance specificity." *Plant Cell* **19**(9): 2898-2912.
- Wawra, S., A. Djamei, I. Albert, T. Nurnberger, R. Kahmann and P. van West** (2013). "In vitro translocation experiments with RxLR-reporter fusion proteins of Avr1b from *Phytophthora sojae* and AVR3a from *Phytophthora infestans* fail to demonstrate specific autonomous uptake in plant and animal cells." *Mol Plant Microbe Interact* **26**(5): 528-536.
- Webby, C. J., W. T. Jiao, R. D. Hutton, N. J. Blackmore, H. M. Baker, E. N. Baker, et al.** (2010). "Synergistic Allosteric Regulation, a Sophisticated Regulatory Network for the Control of Aromatic Amino Acid Biosynthesis in *Mycobacterium tuberculosis*." *J Biol Chem* **285**(40): 30567-30576.
- Westfall, C. S., A. Xu and J. M. Jez** (2014). "Structural evolution of differential amino acid effector regulation in plant chorismate mutases." *J Biol Chem* **289**(41): 28619-28628.
- Whisson, S. C., P. C. Boevink, L. Moleleki, A. O. Avrova, J. G. Morales, E. M. Gilroy, et al.** (2007). "A translocation signal for delivery of oomycete effector proteins into host plant cells." *Nature* **450**(7166): 115-118.
- Wiker, H. G. and M. Harboe** (1992). "The Antigen-85 Complex - a Major Secretion Product of *Mycobacterium-Tuberculosis*." *Microbiol Rev* **56**(4): 648-661.
- Williams, S. J., K. H. Sohn, L. Wan, M. Bernoux, P. F. Sarris, C. Segonzac, et al.** (2014). "Structural basis for assembly and function of a heterodimeric plant immune receptor." *Science* **344**(6181): 299-303.
- Willmann, R., H. M. Lajunen, G. Erbs, M. A. Newman, D. Kolb, K. Tsuda, et al.** (2011). "Arabidopsis lysin-motif proteins LYM1 LYM3 CERK1 mediate bacterial peptidoglycan sensing and immunity to bacterial infection." *Proc. Natl. Acad. Sci. U.S.A.* **108**(49): 19824-19829.
- Xue, Y. and W. N. Lipscomb** (1995). "Location of the active site of allosteric chorismate mutase from *Saccharomyces cerevisiae*, and comments on the catalytic and regulatory mechanisms." *Proc. Natl. Acad. Sci. U.S.A.* **92**(23): 10595-10598.
- Xue, Y. F., W. N. Lipscomb, R. Graf, G. Schnappauf and G. Braus** (1994). "The Crystal-Structure of Allosteric Chorismate Mutase at 2.2-Angstrom Resolution." *Proc. Natl. Acad. Sci. U.S.A.* **91**(23): 10814-10818.
- Yamaguchi, Y., A. Huffaker, A. C. Bryan, F. E. Tax and C. A. Ryan** (2010). "PEPR2 is a second receptor for the Pep1 and Pep2 peptides and contributes to defense responses in *Arabidopsis*." *Plant Cell* **22**(2): 508-522.
- Yamaguchi, Y., G. Pearce and C. A. Ryan** (2006). "The cell surface leucine-rich repeat receptor for AtPep1, an endogenous peptide elicitor in *Arabidopsis*, is functional in transgenic tobacco cells." *Proc. Natl. Acad. Sci. U.S.A.* **103**(26): 10104-10109.
- Yamamoto, S., M. Katagiri, H. Maeno and O. Hayaishi** (1965). "Salicylate Hydroxylase a Monooxygenase Requiring Flavin Adenine Dinucleotide .I. Purification General

- Properties." *J Biol Chem* **240**(8): 3408-&.
- Yu, X. L., J. L. Tang, Q. Q. Wang, W. W. Ye, K. Tao, S. Y. Duan, et al.** (2012). "The RxLR effector Avh241 from *Phytophthora sojae* requires plasma membrane localization to induce plant cell death." *New Phytol* **196**(1): 247-260.
- Zhang, M. X., Q. Li, T. L. Liu, L. Liu, D. Y. Shen, Y. Zhu, et al.** (2015). "Two Cytoplasmic Effectors of *Phytophthora sojae* Regulate Plant Cell Death via Interactions with Plant Catalases." *Plant Physiol* **167**(1): 164-175.
- Zhang, Z. M., X. Zhang, Z. R. Zhou, H. Y. Hu, M. L. Liu, B. Zhou, et al.** (2013). "Solution structure of the *Magnaporthe oryzae* avirulence protein AvrPiz-t." *J Biomol Nmr* **55**(2): 219-223.
- Zipfel, C.** (2014). "Plant pattern-recognition receptors." *Trends Immunol* **35**(7): 345-351.
- Zipfel, C., G. Kunze, D. Chinchilla, A. Caniard, J. D. Jones, T. Boller, et al.** (2006). "Perception of the bacterial PAMP EF-Tu by the receptor EFR restricts *Agrobacterium*-mediated transformation." *Cell* **125**(4): 749-760.
- Zuccaro, A., U. Lahrmann, U. Guldener, G. Langen, S. Pfiffi, D. Biedenkopf, et al.** (2011) "Endophytic Life Strategies Decoded by Genome and Transcriptome Analyses of the Mutualistic Root Symbiont *Piriformospora indica*." *Plos Pathog* **7** DOI: 10.1371/journal.ppat.1002290.
- Zuccaro, A., U. Lahrmann and G. Langen** (2014). "Broad compatibility in fungal root symbioses." *Curr Opin Plant Biol* **20**: 135-145.

Acknowledgements

Several days later it will be four years since I came to Germany. During the past four years, there are a lot of people to whom I am pleased to express my sincere gratitude.

First and foremost, I would like to thank my supervisor Prof. Dr. Regine Kahmann for providing me the opportunity to pursue my PhD in her research group. I am so deeply impressed by her immense knowledge about *Ustilago maydis*. Her enthusiasm and motivation in science is truly valuable on my road to become a scientist. It is her guidance, patience and encouragements which helped me throughout my PhD research and writing this thesis.

I would especially like to thank Dr. Gert Bange for his excellent cooperation in structural biology, for his constant support being my second supervisor and my Thesis Advisory Committee member and for his willingness to be in my examination committee.

I am deeply grateful to Prof. Dr. Michael Bölker for his constructive discussions and suggestions during the Thesis Advisory Committee meetings. My sincere thanks also go to my examination committee members Prof. Dr. Alfred Batschauer and Prof. Dr. Hans-Ulrich Mösch for their time to review my thesis.

Many thanks to Dr. Jan Schuhmacher and Dr. Wieland Steinchen from Bange lab for their valuable work on solving the crystal structure of Cmu1 and mapping the interaction interface between Cmu1 and Cmi1, respectively.

I would also like to acknowledge Dr. Timo Glatter for his exceptional collaboration in Mass spectrometry & Proteomics, which identified Cmi1, the interaction partner of Cmu1.

My thanks go to all the people in the Kahmann lab, present and past, for a nice working atmosphere, lively discussions, assistance and all events in and outside the lab. I would like to thank my former colleagues Dr. Armin Djamei and Dr. Anupama Ghosh for their previous work on the Cmu1 project. I am sincerely grateful to Dr. Stefanie Reißmann for her continuous advice and support in my project, encouragements and suggestions when I felt frustrated and translation of the summary of the thesis into German.

I am grateful to the China Scholarship Council (CSC) for funding my PhD study in Germany.

Most of all, I am deeply indebted to my family and friends. Especially I would like to thank my wife Huili Yu for her accompany and support all the time.

03.10.2017, Marburg

Curriculum Vitae

Xiaowei Han

Born on September 21st, 1987 in Weifang, China

Education

- 2006-2010 Bachelor of Agriculture, Northwest A&F University, Yangling, China
Thesis (supervised by Prof. Dr. Yongchun Niu, Chinese Academy of Agricultural Sciences, Beijing, China):
“Preliminary study of the antagonism of endophytic fungi from cucurbitaceous plants against *Sclerotinia sclerotiorum* and *Fusarium oxysporum* f.sp. *cucumerinum*.”
- 2010-2013 Master of Science, Shandong University, Jinan, China
Thesis (supervised by Prof. Dr. Yuemao Shen, Shandong University, Jinan, China):
“Insights into the regulatory role of TetR family in secondary metabolism of *Streptomyces* sp. LZ35”
- 2013-2017 Doctoral studies in Philipps-Universität Marburg
Thesis (supervised by Prof. Dr. Regine Kahmann, Max-Planck-Institute for Terrestrial Microbiology):
“Structure-function analysis of Cmu1, the secreted chorismate mutase in *Ustilago maydis*”

Appendix

Table 8: CMs that are used in the construction of the phylogenetic tree

Protein	Accession	Protein	Accession
AtCM1	NP_566846.1	FGRAMPH1_01T22073	EYB23440.1
AtCM2	NP_196648.1	FGRAMPH1_01T26701	EYB31241.1
AtCM3	NP_177096.1	LACBIDRAFT_177156	XP_001875866.1
ZmCM1	NP_001145983.1	LACBIDRAFT_317179	XP_001878810.1
ZmCM2	NP_001130752.1	Rv1885c	WP_003899064.1
ZmCM3	XP_008678594.1	Rv0948c	COW87243.1
Aro7p	NP_015385.1	PchB	CAA57968.1
UmAro7	XP_011390701.1	*AroQ	WP_003114063.1
UmCmu1	XP_011391476.1	PheA	AAT51335.1
UhCmu1	CCF49464.1	AroH	WP_009967606.1
SrCmu1	CBQ69595.1	PICM	WP_023482655.1
SsCmu1	CDW96772.1	TtCM	WP_011172959.1
UbCmu1	SAM85328.1	STM14_1531	WP_000617985.1
SS1G_14320	XP_001584707.1	EcCM	WP_000200120.1
SS1G_08569	XP_001590829.1	Mi-CM-1	AAR37372.1
PGTG_07564	XP_003326586.2	Mi-CM-2	AAR37373.1
PGTG_19827	XP_003338235.1	Gp-CM-1	CAD29887.1
MELLADRAFT_74217	XP_007406326.1	Hg-CM-1	AAY42590.1
MELLADRAFT_101066	XP_007403571.1	Hs-CM-1	ABA06538.1